Evaluation and neurocomputational modelling of visual adaptation to optically induced distortions

Dissertation

der Mathematisch-Naturwissenschaftlichen Fakultät
der Eberhard Karls Universität Tübingen
zur Erlangung des Grades eines
Doktors der Naturwissenschaften
(Dr. rer. nat.)

vorgelegt von
Selam W. Habtegiorgis
aus Addis Ababa, Äthiopien

Tübingen
2018

Gedruckt mit Genehmigung der Mathematisch-Naturwissenschaftlichen Fakultät der Eberhard Karls Universität Tübingen.

Tag der mündlichen Qualifikation: 22.02.2019

Dekan:	Prof. Dr. Wolfgang Rosenstiel
1. Berichterstatter:	Prof. Dr. Felix A. Wichmann
2. Berichterstatter:	Prof. Dr. Siegfried Wahl

Contents

Acronyms list

ANOVA	Analysis of Variance
CRF	Classical receptive field
CPI	Cycle per image
FB	Feedback
FF	Feedforward
IT	Inferior temporal cortex
LGN	lateral geniculate nucleus
MA	Adaptation aftereffect
MAE	Motion aftereffect
MT	Middle temporal visual area
nCRF	Non-classical receptive field
PAL	Progressive additional lens
PSE	Point of subjective equality
RF	Receptive field
V1	Primary visual cortex
V2	Secondary visual cortex
V4	Fourth visual cortex

1 Introduction

1.1 Motivation

Vision impairment due to refractive errors is a significant worldwide health concern which affects individuals' well-being and puts a heavy economic burden on society in general [Contreras and Ackland, 2017]. There is an ever growing demand for optical solutions to combat the increasing trend in the prevalence of this problem. Age related vision problems, such as presbyopia, considerably contribute to this demand as their pervasiveness is inherently correlated to the ageing of the world's population [United Nations Population Division and Affairs, 2015]. Presbyopia is an inevitable vision problem wherein the crystalline lens of the eye loses its elasticity with ageing causing an inability to focus during near distance vision. This degrades the elderlies' quality of life by limiting their daily activities, e.g. difficulty of reading and navigation due to lack of clear vision for near distance obstacles. In 2020, presbyopia will affect 1.4 billion individuals and this estimate is expected to rise to 1.8 billion by the year 2050 [Holden et al., 2008]. Efficient optical solutions to correct presbyopia are therefore consequential for a huge portion of the world's population.

Progressive additive lenses (PALs) are one of the recurrently used modalities to correct for presbyopia [Meister and Fisher, 2008a,b]. The optical power of PALs continuously increases from the upper to the lower part of their surface providing a continuous field of corrected vision from far to near distances, respectively. However, the physical implementation of such progressive optical power results in geometrical distortions as inevitable artefacts [Sheedy et al., 2005]. Distortions are one of the causes for visual discomforts, such as apparent motion perception and spatial disorientation, experienced by novice PAL wearers [Meister and Fisher, 2008a; Sheedy and Andre, 2013; Johnson et al., 2007]. Some groups of PAL wearers successfully habituate to these optical elements wherein they no longer perceive any visual discomforts after prolonged usage. Nonetheless, the visual discomforts might persist in some other wearers and make it difficult for them to regularly use the optical elements [Alvarez et al., 2017]. As distortions are daily constraints when using PALs, fast and efficient habituation would increase the wearers' comfort and consequently overcome the related problems such as risk of fall in the elderly [Johnson et al., 2007; Sheedy and Andre, 2013]. A systematic solution, such as a customised training paradigm or designing habituation friendly PAL assisted by objective prediction of human performances, would thus have a significant role in facilitating the habituation process. Understanding of how vision processing beyond the optics of the eye underlies the habituation process is an important pillar for proposing such a solution.

A potential factor for optics induced perceptual discomforts is conflict of sensory

cues, specifically between the optically distorted visual input and inputs to other sensory systems unaffected by the distortions [Salomon et al., 2016]. Our brain integrates information from different sensory systems, e.g. motor and vision, for our successful interaction with the natural environment [Apps and Tsakiris, 2014]. Distortions alter several features of the visual input, e.g. motion and form features, conflicting with unaltered inputs to the motor system. During habituation, the brain seems to calibrate these conflicting cues. One of the possible means for such calibration is if the visual system adjusts its responses to compensate distortion induced changes before information from different sensory systems are integrated. Such response adjustments in correlation to changes in sensory inputs is called adaptation. However, if and how visual adaptation to distortion underlies habituation is not yet explored.

Complexity of features in the natural environment and the visual system organisation by itself necessitate a systematic approach of studying distortion induced adaptation and the underlying neural mechanisms. Behavioural studies, or psychophysical studies, are commonly used non-invasive approaches to probe visual adaptation. Previous classical studies often use simple artificial stimuli for investigating adaptation [Levinson and Sekuler, 1976; Stuit, 2009; Mather et al., 2008]. These classical approaches however do not always predict performances during natural viewing conditions [Ringach et al., 2002; David et al., 2004; Felsen and Dan, 2005]. Habituation is also a temporally dynamic process wherein perception gets better with experience. Previous behavioral studies have not assessed whether the long-term temporal dynamics of visual adaptation changes enabling habituation. Furthermore, the visual system is a complex system but its anatomy comprises orderly structured neural networks. Since this structural organisation is shaped by evolution, its orderliness may play a major functional role in enabling the visual system to efficiently perform in the natural environment. Understanding the relevance of anatomical implementation of neural mechanisms is thus critical to develop a model system that could successfully predict adaptation in a complex natural environment. Neural mechanisms underlying adaptation have been previously assessed with simplified models of the visual system [Clifford and Langley, 1996; van de Grind et al., 2003]. However, these models fail to predict adaptation at different time-scales [Mesik et al., 2013]. They also oversimplify the connections of the neural networks from the physiological realism and the possible effect of those simplification on the prediction performance of the models has not been assessed. Thus, comprehensive understanding of distortion adaptation benefits from probing the visual system using natural stimuli and modelling its organisation with an appropriate biological accuracy while keeping the implementation as simple as possible.

Inspired by the necessity of habituation, the present work is targeted to investigate the visual mechanisms underlying adaptation to distortions of PALs. Psychophysical

procedures are employed to investigate distortion induced visual adaptation and to probe the characteristics of the neural mechanisms underlying the adaptation process under natural viewing conditions. Furthermore, biologically plausible neural models are utilized to discern how the functional organisation of neurons enable the visual system to carry out a robust distortion adaptation in a natural environment. Prediction performance of different variants of the model with varying neural network complexity and temporal dynamics of operation were assessed. From the model simulations, major functional roles of the visual system's structural organisation was depicted and a psychophysically plausible model as an objective predictor of distortion adaptation was proposed. The outcomes would further contribute to suggest a solution for facilitating habituation.

The necessity of habituation to distortions is not restricted to PALs but to other daily used optical utilities, such as to distortions in virtual reality (VR) displays, as well [Barrett, 2004]. A thorough understanding about habituation to optical distortions will thus increase usability of VRs in variety of fields, including medicine, research, training, recreation and education [Bashiri et al., 2017; Keshner, 2004; Laver et al., 2012]. Optical distortions are also major artefacts in artificial sensory systems, like lens distortions in cameras of machine vision [Shih et al., 1995; Smith and Smith, 2005]. The natural environment comprises a broad spectrum of attributes which requires a robust computation of salient distortion information by the human visual system to adapt to it. Understanding the neural correlates of distortion adaptation in human vision will thereby elicit characteristic features of robust and flexible neural systems to be implemented in brain inspired artificial vision. Thus, the results of this research would be relevant to any natural or artificial sensory system.

In the upcoming subsections, basic theoretical concepts on information processing in the human visual system and examples of distortions in vision corrective optical elements are modularly presented.

1.2 The human visual system

1.2.1 The human eye

Human vision starts with light reflected from objects in the natural environment and coming through the sensory organ, the eye. The eye has multiple refractive units that focus the incoming light on the retina, Figure 1. The anterior part of the eye is called cornea and it is the main refractive component of the organ. The refracted light passes through an opening to the interior chamber of the eye known as the pupil. The pupil acts as an aperture and has an adjustable size to control the amount of light entering the eye. Light then passes through the crystalline lens which is a transmissive media composed of two refractive surfaces. The crystalline lens adjusts its thickness, thus its focal length, to precisely focus the light coming from different distances on the retina. Photosensitive receptors in the retina subsequently detect the photo signal and convert it into electrical signal to be processed in the brain for final perceptual interpretations. The photoreceptors preprocess the detected signal and send it to the brain via the optic nerve.

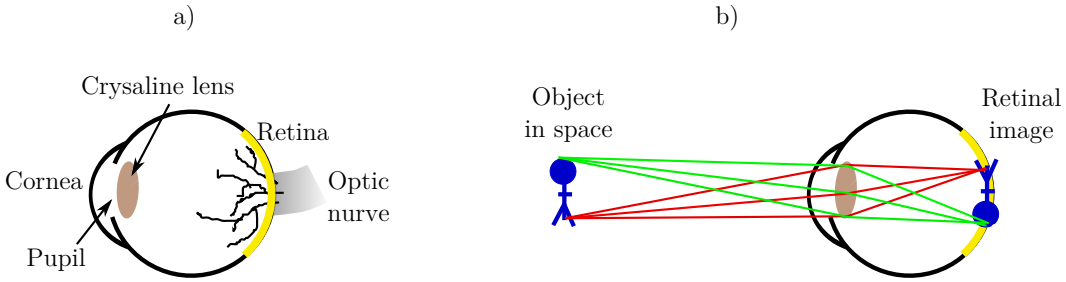

Figure 1: a) The human eye and its components b) Image formation in the human eye

1.2.2 Visual encoding in the brain

The electric signal from the photoreceptors in the eye is transmitted via the optic nerve to lateral geniculate nucleus (LGN) cells in the Thalamus, and then to the brain to be processed by a network of neurons as illustrated in Figure 2. The visual cortex is the posterior part of the brain responsible for encoding visual information.

The primate visual cortex comprises several parallel pathways dedicated to compute specific visual information [Livingstone and Hubel, 1987]. Information initially reaches the primary visual cortex (V1) and then bifurcates into different parallel streams. The dorsal and the ventral cortical pathways are the two extensively studied visual streams, see Figure 2 [Van Essen and Anderson, 1995; Van Essen and Maunsell, 1983]. After the V1, the dorsal (parietal) pathway comprises cortical areas such as the secondary visual cortex (V2), the medial temporal cortex (MT) and other areas. This pathway is dedicated to dominantly compute spatial information such as motion. Whereas, the

parallel ventral (temporal) stream consists of cortical areas such as V1, V2, fourth temporal cortex (V4) and extends to other cortical areas. This pathway mainly computes form information such as object orientation and size. The dominant feature selectivity of the two streams allows a simplified understanding of cortical processes, albeit some neurons within the aforementioned areas respond to both form and motion features [Barlow and Olshausen, 2004; Wilson and Wilkinson, 2002; Mather et al., 2012; Pavan et al., 2013].

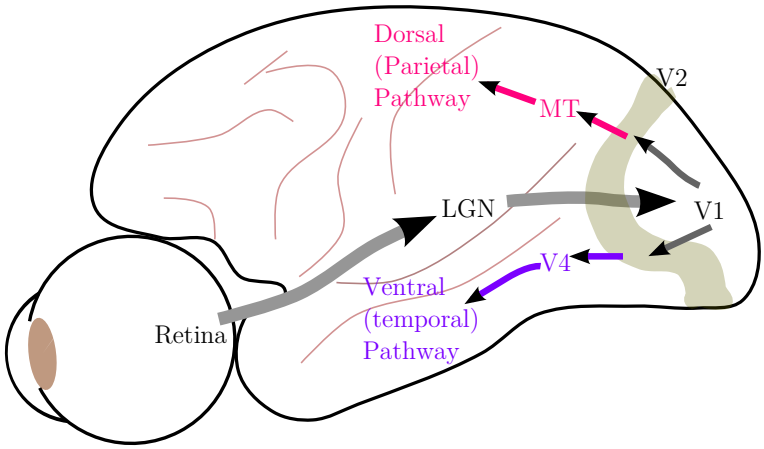

Figure 2: Overview of visual information processing from eye to the brain in different cortical pathways. Adapted from Kandel et.al. [Kandel et al., 2000].

Information is processed and transmitted within the different parts of the visual cortex as a form of an electric signal. The basic information processing units in the visual cortex are neurons. Neurons are cells which can encode an electric signal as a membrane potential formed by a difference in concentration of charged ions inside and outside of the cell. Ion channels in the neural membrane allow movement of ions in and out of the cell controlling the concentration gradient of charges. Neurons receive, process and further transmit electric signals. Synapses are connections between neurons where information is transmitted from a presynaptic neuron to a post synaptic neuron. This synaptic transmission can be either an electric or a chemical signal. When there is no synaptic input, the membrane potential of neurons is around $-65\,mV$ and is called resting potential [Purves D Fitzpatrick D, Hall WC, LaMantia A-S, et al., 2008]. In chemical synapses, chemicals called neurotransmitters are used for communication. Neurotransmitter synaptic inputs trigger opening or closing of ion channels which leads to a net flow of charge in or out of the cell. This changes the membrane potential. If the net charge flow increases the membrane potential to a level above a certain threshold, the neuron will release neurotransmitter at the synaptic terminal consequently affecting another neuron, thus transmitting information. Such synaptic input is called excitatory input. Whereas, if the input neurotransmitter triggers a net flow of charges which

decreases the membrane potential, it is less probable for the neuron to fire or to transmit information to another neuron. Consequently, such input is termed as inhibitory input.

Different cortical neurons are selective to distinct types of visual features, e.g. colour, motion directions, contour orientations, spatial dimensions, etc. Neurons respond to their preferred attribute when it occurs within a specific visual space in which they are sensitive to, commonly known as a classical receptive field (cRF) or simply receptive field (RF). This preferred visual space, the RF, can be classified as either retinotopic or spatiotopic based on the reference frame it uses to detect the stimulus [Gardner et al., 2008]. Neurons with retinotopic RFs respond only when the stimuli appear within specific location encoded relative to a reference point in the retinal plane, e.g. retinal center. Whereas, neurons with spatiotopic RFs respond to stimuli within specific area in space encoded relative to an extra-retinal-reference point, e.g. head center. Figure 3 illustrates responses of neurons entailing retinotopic and spatiotopic RFs. After information is detected by a neuron, it is processed and then transferred to another neuron with similar feature and visual space selectivity. Recurrent information processing and communication within a networked population of neurons tuned to similar visual attribute finally enables visual perception.

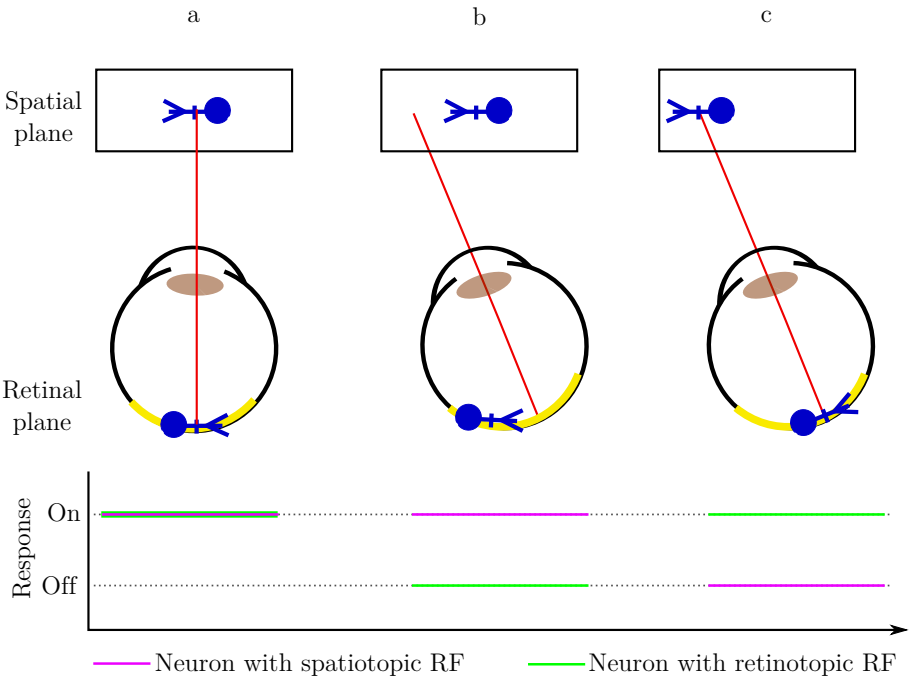

Figure 3: Illustration of spatiotopic and retinotopic encoding of visual stimulus. a) The spatial and retinal locations of the stimulus are in the preferred locations of spatiotopic and retinotopic neurons. b) An eye movement changes the retinal location of the stimulus while the spatial location is maintained. Thus only the neuron with spatiotopic RF responds to it. c) The spatial location of the stimulus is changed whereas the retinal location is within the RF of the retinotopic neuron. So, only the retinotopic neuron responds.

Cortical neurons are hierarchically organized, i.e. visual information passes through a layered topology of neural networks as illustrated in Figure 4. Neurons in lower cortical hierarchies dominantly entail small retinotopic RFs and encode simple stimuli features. In higher cortical areas, neurons exhibit larger RFs and their responses are retinal location invariant. This enables them to encode complex visual information by combining lower level neural responses in a wide range of visual and feature space. RFs of higher cortical areas are mostly spatiotopic since they also partake in contextual tasks involving information integration with other non-retinotopic sensory inputs, such as hearing, touch or motor system during movement planning [Groh et al., 2001; Jay and Sparks, 1984; Soechting and Flanders, 1992; Stricanne et al., 1996]. This hierarchical organization is a hallmark structure of information processing within the different areas of the visual system.

Neurons across the cortical hierarchies are intertwined with each other in a complex manner to encode relevant visual information. In addition to the already described feedforward (FF) connections which allow information flow from lower to higher cortical areas, neurons interact within layers via lateral connections and also from higher to lower cortical areas with feedback (FB) connections [Lamme and Roelfsema, 2000; Lamme et al., 1998]. Figure 4 illustrates such recurrent interactions within the hierarchically organised cortical neural networks. Neurons receive FF excitatory input, the yellow coloured inputs in Figure 4, through their cRFs whose size increases across the hierarchy as explained earlier. The FB and lateral information, the blue and the red inputs in Figure 4 respectively, are simultaneously received through a visual space commonly known as non-classical receptive fields (ncRFs) [Angelucci et al., 2002; Angelucci and Bullier, 2003; Sillito et al., 2006]. This ncRF has usually a larger dimension than the cRF [Angelucci and Bullier, 2003]. The lateral connections involve competitive interactions of neurons in the same hierarchical level which lead to response normalization by nearby neural responses. Inputs from lateral connections are inhibitory as they decrease the neural responses via normalization. Whereas, FB reentrant projection modulates the excitatory inputs with contextual information from higher cortical areas and is thus aptly named as modulatory input. FB modulation is selective in the feature domain, thus it has a consecutive impact on the competitive lateral interactions. Specifically, enhancement of a neural response by FB input will increase the normalization signal that is sent to other neurons within the same layer, thus decreases their responses. As a result, recurrent FF, FB and lateral interactions have fundamental roles in shaping neural response tuning across the cortical hierarchy.

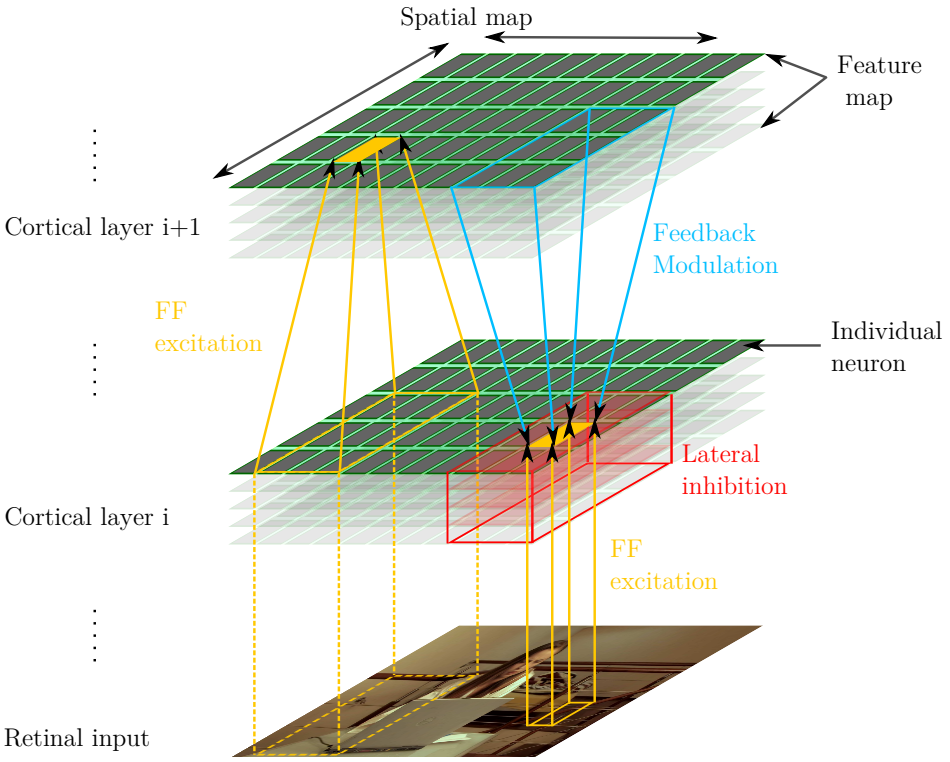

Figure 4: Illustration of visual information processing along the hierarchically organized cortical layers. Each square represents a single neuron. Neurons in each cortical layer are organized according to their selectivity in feature domain by the columns, and in spatial domain by the lateral dimensions. In this illustration, neurons in the same column thus process different features at the same location. The different cortical interactions, specifically FF, FB and lateral interactions are illustrated by the yellow, blue and red colours, respectively. Furthermore, the increase in receptive field size along the hierarchy is illustrated with the spatial dimensions of the FF input for the different layers.

1.2.3 Adaptation in the visual system

Adaptation is a process in which neurons adjust their sensitivity when they are continuously excited by their preferred stimulus attribute. Adaptation is a distinctive phenomenon throughout the hierarchy of the visual system. Perceptual stability is one of the main functional benefits of adaptation [Clifford et al., 2007; Webster, 2011, 2015]. For instance, we perceive optimally without being distracted by a continuously changing intensity of light throughout the day because neurons in the visual system continuously adjust their sensitivity in accordance to those changes through the process of adaptation.

Changes in synaptic inputs are sources of neural plasticity or response adjustments during adaptation [Abbott et al., 1997]. At the synapses, neurotransmitters are contained in vesicles at the presynaptic terminal in a limited amount [Hennig, 2013]. There are two types of vesicle pools, readily releasable pool and reserve pool [Hennig, 2013;

Abbott et al., 1997; Trommershäuser et al., 2003; Wölfel et al., 2007]. The readily releasable pools are usually located in the vicinity of the cell membrane ready to release neurotransmitters during excitation [Hennig, 2013; Wadel et al., 2007]. The reserve pools are kept on hold to refill empty releasable pools after transmitter release. The synaptic strength between neurons, i.e. the synaptic efficacy, depends on the amount of neurotransmitters available in the releasable pools. This amount is concurrently determined by the rate of how fast releasable pools are depleted and how fast they are replenished, with the latter process usually being slower. [Hennig, 2013; Wölfel et al., 2007]. During a continuous excitation of presynaptic neurons, its releasable pools will be depleted consequently decreasing the post synaptic neural response [Regehr, 2012; Hennig, 2013; Abbott et al., 1997; Tetzlaff et al., 2012]. In this manner, activity dependent short term synaptic depression underlies adaptation [Castellucci et al., 1970; Hawkins et al., 1993; Regehr, 2012; Zucker and Regehr, 2002]. If the excitation input is removed from the presynaptic neuron, the synaptic strength will slowly restore until the vesicles are fully replenished. During this time, adaptation induced neural response changes can be probed.

Concomitant to neural response changes, adaptation aftereffects are lingering perceptual modifications which occur when a stimulus of the same kind is reapplied after removal of an adaptation inducing stimulus. Adaptation aftereffects are common tools to investigate diverse properties of the underling neural mechanisms encoding and adapting to a specific visual feature [Blake and He, 2005]. For instance, since neurons are feature selective, adaptation aftereffects can be used to reveal plasticity in neurons encoding specific types of visual features [Webster, 2011, 2015]. Furthermore, inter-feature transferability of adaptation aftereffects, e.g. motion aftereffect from form features, indicates whether a specific feature is encoded within a specialized hierarchical pathway or distributed across different pathways. The cortical level of neural plasticity underlying adaptation to a specific feature can further be traced by testing retinal location invariance of the adaptation aftereffects, refer Figure 4. Retinotopic or spatiotopic nature of adaptation aftereffects can additionally predict the reference frames of neural RFs responsible for encoding specific stimuli. The temporal synaptic dynamics of the underlying mechanisms can as well be probed by testing how fast adaptation aftereffects can be induced or how long they can be retained. Thus, adaptation aftereffects are versatile tools to uncover different properties of the underlying neural mechanisms.

1.3 Refractive errors and optical elements as vision corrective modalities

To achieve clear visual perception, the optical components of the eye has to focus the light on the retina. Defects in any of these components degrades the quality of the retinal signal that is transmitted to the brain which consequently affect the final visual perception. These conditions are commonly known as refractive errors of the eye. Presbyopia is one type of such refractive errors wherein the crystalline lens loses its elasticity due to ageing and fails to focus light coming from near distances. Thus, additional lens power is needed to achieve clear near distance vision. Spectacle lenses, particularly progressive additional lenses (PALs), are one of the most commonly used modalities to provide for this additionally needed power.

PALs are multifocal lenses which have gradually increasing refractive power along their surface, Figure 5. The different parts of the lens are thus specialized to achieve clear vision at different distances as illustrated in Figure 5. The refractive power in the upper part of the lens, usually named distance zone, focuses light coming from far distances. The near zone is the lower part of the lens with additional power needed to refract light coming from near distances. The intermediate zone, with its gradually increasing power, is dedicated to intermediate distance vision and serves as a progressive corridor between the distance and near zones. Increasing the optical power along the progressive corridor results in inevitable unwanted optical properties, e.g. proportional increase of oblique cylindrical power or astigmatism in the perpendicular direction; the Minkwitz theorem [Sheedy et al., 2005]. As can be seen in Figure 3, the astigmatic effects are pushed towards the peripheral parts of PALs, i.e. the blending regions. These unwanted optical properties at the peripheries induce different artefacts such as geometric distortions.

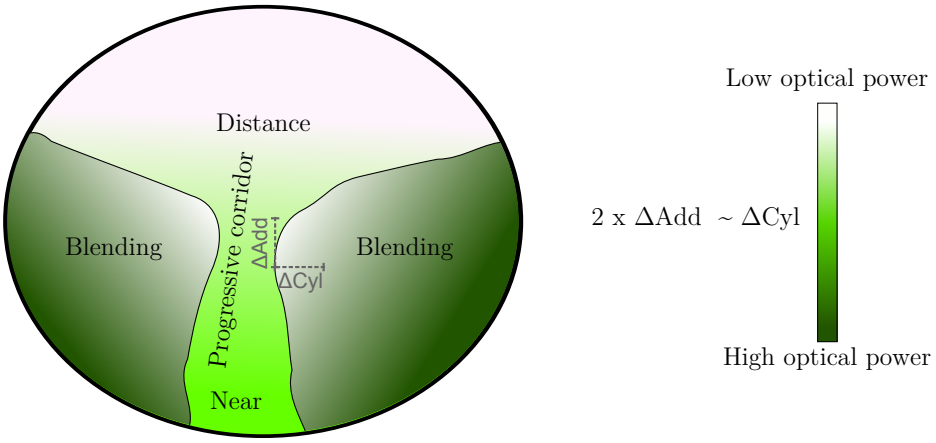

Figure 5: Illustration of optical power distribution along the surface of PALs. The addition power continuously increases from the distance to the near zone via the progressive corridor. This induces inevitable increase of cylinder power in the perpendicular direction, approximately at a double rate, causing oblique astigmatism in the blending regions [Sheedy et al., 2005].

1.3.1 Distortions as artefacts of PALs and the habituation process

To illustrate distortions induced by unwanted optical properties in the peripheral regions of PALs, Figure 6 shows an example of a ray tracing simulation of square grid imaged through a PAL using an in house ray tracer. As can be seen, the dots are displaced with spatially variable displacement vectors at the different parts of the lens. This results in different profiles of geometric distortions when considering shapes formed by the grid points. Specifically, in the peripheries, the points are displaced in the oblique directions wherein their global square profile is magnified obliquely and sheared from the vertical and horizontal directions leading to geometric skew distortions.

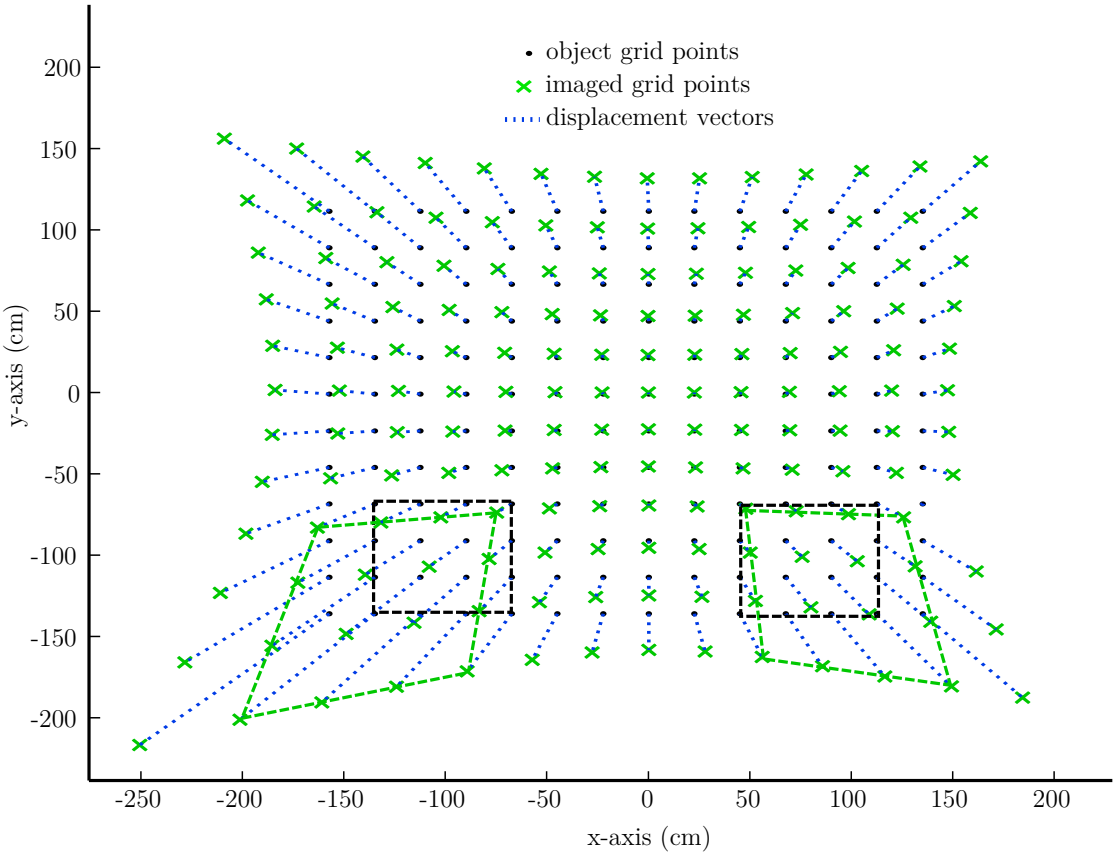

Figure 6: Distortions of grids imaged through PALs (a PAL design with no power in the distance zone and 2 Dioptre additional power in the near zone) using a ray tracing simulation. The black dots represent the object grid and the crosses represent the locations of the corresponding imaged grid points. The blue lines represent the displacement vectors of the imaged grid points relative to the original object grid points. Opposite skew distortions at the peripheries corresponds to the images of the square grid objects which are shown by connecting the locations of the dots and the crosses, respectively, to illustrate the distortion profiles of PALs in the blending regions.

Distortions are one of the potential causes for the difficulties encountered in habituating some novice wearers to their PALs. Novice PAL wearers often complain about visual discomforts such as blurred vision, perception of distorted scenes and apparent motion during dynamic vision which result in postural instabilities. The unwanted optical properties, e.g. skew distortions in the blending regions, are one of the candidate sources for these visual discomforts [Meister and Fisher, 2008a,b]. However, after habituation to PALs, wearers no longer perceive the distortions. This work explores how visual adaptation compensates for distortion induced alterations of features in the natural environment, and how this plays a role in the habituation process.

1.3.2 Distortion induced alterations in natural scene statistics

Statistical information of natural scenes is fundamentally important to understand the visual processing mechanism [Field, 1987; Gibson, 1966]. Here, natural image statistics is analysed to inspect features altered by distortions which need to be compensated by visual adaptation. Geometric skew distortions mimicking the profiles across the peripheries of PALs were simulated in natural image sequences. Statistics of form and motion features were quantified in distorted and undistorted natural image sequences to asses to which feature domain to probe visual adaptation.

Natural image sequences were taken from an open source movie as an example to the natural visual world [Baumann and Behnisch, 2010]. Two groups of oppositely skewed natural image sequences were prepared by geometrically shearing the images in the vertical and the horizontal directions as illustrated in Figure 7.

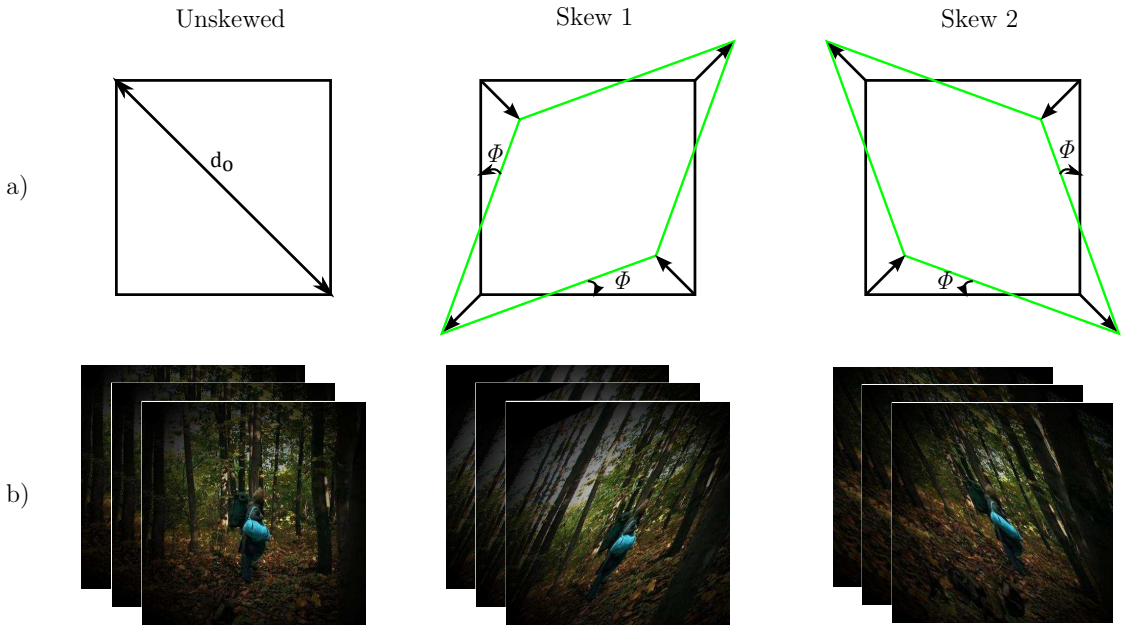

Figure 7: a) Illustration of skew geometrical distortion. b) Examples of unskewed natural image sequence group with its oppositely skewed counter groups at a shear angle of $|\phi| = 25\,°$.

Form statistics is computed in Matlab (Mathworks, MA, USA) in terms of the average orientation and spatial frequency distribution of the amplitude spectra from the different image sequence groups, see section 10.1.

Natural images feature a linear decrease of spectral amplitude when plotted against spatial frequency on a log-log scale [van der Schaaf and van Hateren, 1996; van Hateren and van der Schaaf, 1998]. Magnification of spatial dimension results in higher spectral amplitude distribution in low spatial frequencies which increases the slope of amplitude spectrum vs spatial frequency plot. To quantify the skew effect in dimension

symmetry of the natural images, the slope parameter was investigated for different orientations, which from here on is termed as oriented-slope. In undistorted image sequences, oriented-slope is distributed symmetrically in all orientations as can be inferred from Figure 8a. Due to oblique magnification in the skewed image sequences the oriented-slope value is biased to the magnification orientation.

Another characteristic form feature of natural images is the orientation statistics of their amplitude spectra which is mainly dominated by the cardinal axis. To assess the effect of skew on orientation statistics of the natural images, the weighted average of the spectral amplitude $A(\psi)$ was analysed for each orientation ψ. $A(\psi)$ was mainly distributed along the vertical and horizontal directions in the unskewed image sequences as presented in Figure 8b in line with existing literature [van der Schaaf and van Hateren, 1996; van Hateren and van der Schaaf, 1998]. Due to the image shear from the cardinal axis in the skewed image groups, the dominant orientations are shifted corresponding to the skew orientation.

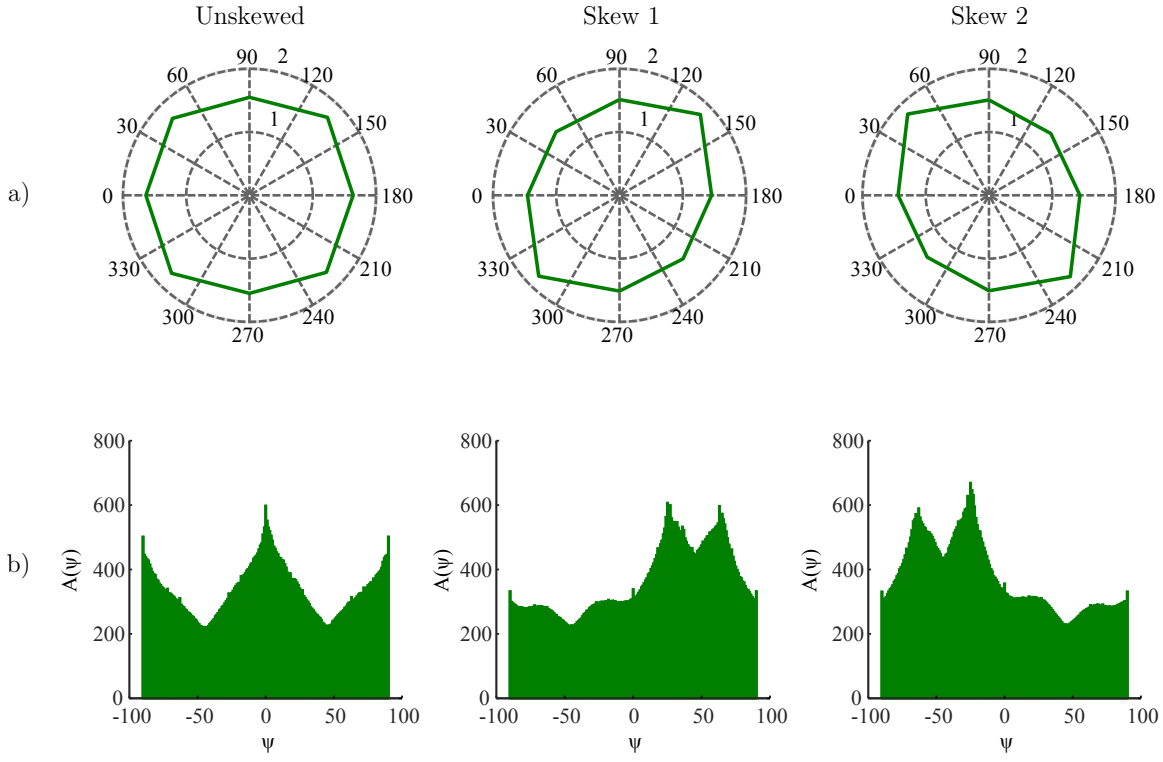

Figure 8: a) Dimension symmetry showed as oriented-slope; slope of amplitude spectrum vs. spatial frequency on a log-log scale in different orientations. High alpha value corresponds to larger amplitude spectra in lower than higher spatial frequencies, thus longer spatial dimensions. b) Contour orientations presented as amplitude spectrum versus Orientation.

Motion direction statistics is another feature which has to be taken into account when considering vision in a dynamic natural environment. Here, average motion direction statistics of optic flow fields from the three image sequences is examined.

Local motion direction was quantified by using biologically plausible correlation-based motion detection technique [Bayerl and Neumann, 2004; Reichardt, 1987], which was implemented in Matlab (Mathworks, MA, USA), see section 10.2.

The motion direction statistics of skewed and unskewed image sequences is shown in Figure 9. In undistorted stimuli, motion direction is dominant in the horizontal directions. Skew shifts these dominant motion directions to the oblique direction, either to upward or downward in correlation to the shearing direction.

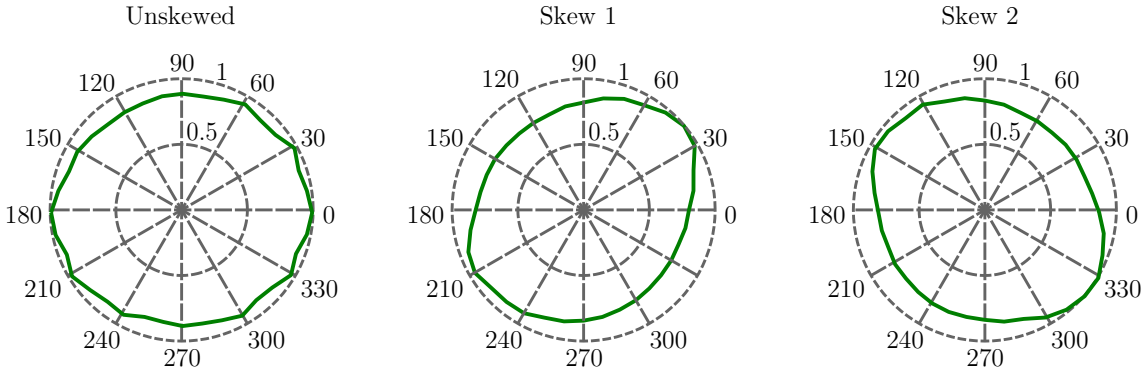

Figure 9: Normalized average motion energy vs. motion direction.

In sum, image skew alters form features, such as spatial dimension symmetry and orientation, as well as motion direction statistics of the natural environment. Thus, visual adaptation to these alterations is expected during exposure to skewed natural scenes. In the following sections, approaches to probe adaptation to these altered features and the underlying neural mechanisms will be introduced.

1.4 Psychophysical approaches to investigate adaptation aftereffects

Psychophysics is a non-invasive technique to examine internal brain functions by quantitatively analysing the relationship between a physical sensory input and a corresponding perceptual sensation as an output [Ehrenstein and Ehrenstein, 1999; Farell and Pelli, 1999; Pelli and Farell, 1995]. Its application is broad to assess the neural mechanisms involved in different sensory systems. In this thesis, psychophysical experiments are employed to investigate visual adaptation aftereffects.

There are different techniques for measuring perceptual responses in Psychophysics [Farell and Pelli, 1999]. The two main techniques used in this thesis involve adjustment and judgement tasks. For example, let us say we want to measure the oblique magnification level in a square object that is perceived as un-magnified in a psychophysical experiment, this parameter is from here on termed as point of subjective equality (PSE). In an adjustment psychophysical procedure, observers' will be presented with a randomly magnified stimulus and have a full control to adjust the magnification level until they perceive it undistorted or square. Then, they report the PSE level. Whereas in a judgement procedure, the experimenter will present a specific magnification level and observers will judge or identify what they have perceived, e.g. is the perceived oblique magnification in the left or right orientation? From a set of responses recorded at different magnification levels presented in a randomized order, the PSE is the magnification level at which the observer perceived left and right magnification equally likely, i.e. for each 50 percent response probability. This specific procedure is called constant stimulus procedure.

In general, adaptation aftereffects can be psychophysically tested by comparing the shift in observers' PSEs measured before and after exposure to adaptation inducing stimuli. As perceptual responses are results of population based neural responses, adaptation aftereffects can additionally indicate plasticity of neural mechanisms which partake in encoding of adaptation inducing and test stimuli.

Eye tracking can as well be incorporated in psychophysical procedures to address specific properties of adaptation aftereffects. In particular, an eye tracking technology allows the design of gaze contingent paradigms wherein adaptation aftereffects can be tested at a specific retinal location by tracking the gaze positions in real time. Thus, this technique is critically relevant to address retinal location invariance properties and reference frames of neural mechanisms underlying adaptation aftereffects.

1.5 Modelling the visual system

Neural models are simplified description of the visual system, its organisation and how its neural components dynamically change their responses to underlie a specific behaviourally relevant task, such as adaptation. Neural models are commonly used to give a compact summary of the complex visual information processing, to explain behavioural responses at neural levels and to provide objective prediction of human observer responses [Kay, 2017].

The level of abstraction considered when modelling the visual system has to be chosen carefully depending on the specific research question to be addressed [Nageswaran et al., 2010]. The abstraction levels can range from simple theoretical models to complex biophysical models. Theoretical models commonly employ high level mathematical principles to express visual system's processes and are used to infer statistics of the sensory data. Whereas, complex abstractions in biophysical models incorporate more detailed properties down to the cellular level; such as models of axons, dendrites and different ion channels as synaptic connections and detailed morphological, electrical, and molecular properties of neurons. Such models are targeted to investigate how neural firing properties depend on the different ionic channels. Biophysical models are more biologically accurate than theoretical models, albeit the computational cost they incur limits their size and complexity for their implementation. Thus, to design a specific model, appropriate abstraction has to be selected by compromising biological accuracy and computational cost, a notion depicted in Figure 10.

As illustrated in section 1.2, the visual system is orderly organised in a hierarchical manner with recurrent interactions. This orderliness may contain valuable clues about how the visual system efficiently performs behavioural tasks, specifically adaptation. In this work, a neural model for cortical motion processing was developed with an intermediate level of abstraction to investigate the functional role of recurrent interaction within the hierarchical cortex in the adaptation process. Model neural units compute motion direction in terms of dynamic membrane potential and transmit information via dynamic synapses. This is implemented without considering any molecular and cellular details.

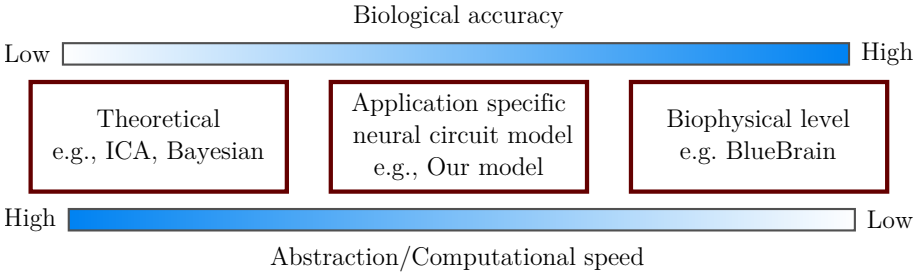

Figure 10: Modelling approaches of the visual system with different abstraction and accuracy levels (adapted from [Nageswaran et al., 2010]).

Our model is based on motion direction processing along hierarchically organized two cortical layers, specifically V1 and MT and extends the work of Bouecke and colleagues [Bouecke et al., 2011]. Each layer constitutes of neurons organized by their information selectivity in a 2D space and feature domain, in this case motion direction. Neural interactions in FF, FB and lateral connections are considered in the model.

Motion direction selective neurons are modelled as single compartment cell units. A circuit model of a single unit neural membrane is illustrated in Figure 11. The neural membrane is considered as an electric device featuring capacitance (c), resting potential (v) and a specific membrane conductance (g_{leak}). The membrane potential is used to quantify the neural responses. It is modelled as a dynamic state variable which adaptively changes with the membrane conductance as a function of excitatory and inhibitory presynaptic input currents and an intrinsic leaking current through the cell membrane. The membrane potential can thus be described by a dynamic equation as a function of the synaptic input currents and membrane conductance given by equation 1.

$$c \cdot \frac{d}{d_t} v(t) = (E_{leak} - v(t)) \cdot g_{leak} + (E_{ex} - v(t)) \cdot g_{ex} - (E_{in} + v(t)) \cdot g_{in} \qquad (1)$$

E_{leak} is the resting potential of the neuron, E_{ex} and E_{in} are the batteries driving the excitatory and inhibitory conductance, g_{ex} and g_{in}, respectively. '$\cdot$' represents a scalar multiplication.

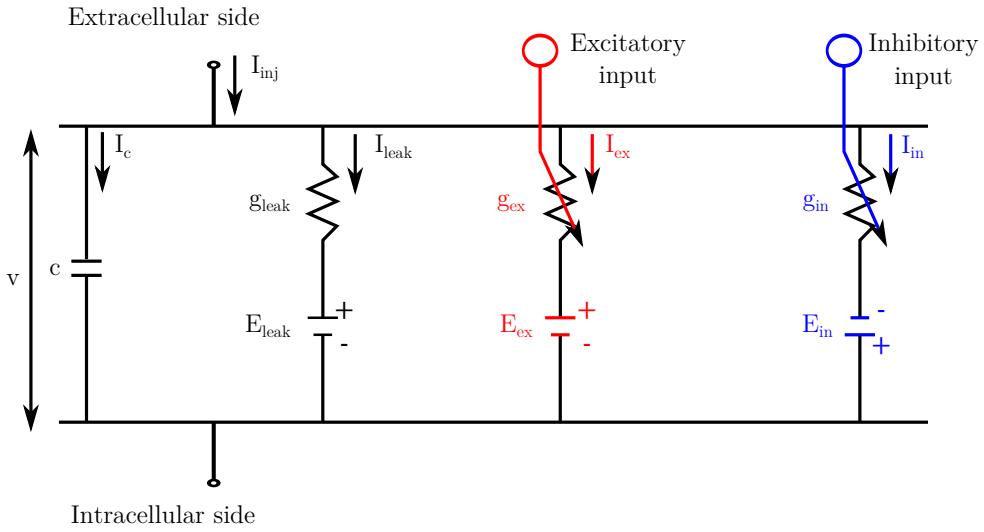

Figure 11: Circuit representation of a membrane potential in a model neuronal unit. The cell membrane is an insulator made from a phospholipid bilayer and separates the electrolytic media in the outside and inside of the cell giving rise to the membrane electric capacitance, c. The membrane potential, v, varies depending on a leaking conductance, g_{leak}, and excitatory and inhibitory conductance, g_{ex} and g_{in}, formed by opening and closing of ion channels which allow inward and outward flow of charged ions. (Adapted from Bouecke et al. [Bouecke et al., 2011]).

For parameter reduction purpose, by assuming $E_{leak} = 0$ and $E_{ex} = E_{in} = 1$ while maintaining the dynamics of the neural responses, equation 1 is simplified in our model to equation 2.

$$\tau \cdot \frac{d}{d_t} v(t) = -v(t) + (1 - v(t)) \cdot I_{ex} - (1 + v(t)) \cdot I_{in} \tag{2}$$

$\tau = \frac{c}{g_{leak}}$ is the membrane time constant, $I_{ex} = \frac{g_{ex}}{g_{leak}}$, and $I_{inh} = \frac{g_{in}}{g_{leak}}$.

In the model, biologically inspired short term depletion at excitatory synapses is additionally considered to realize adaptation and short term memory within the network. The excitatory synaptic efficacy, y, was considered as a probability of a presynaptic neuron affecting a post synaptic neuron and it is implemented as a multiplicative parameter in excitatory connections [Abbott et al., 1997]. The synaptic efficacy is represented as the quanta of the neurotransmitters in the releasable pool as a proportion of the total neurotransmitters' amount at the synaptic terminal, that is both in the reserve and releasable pool. Thus, y depends on the rate of depletion and replenishment processes as described in equation 3.

$$\tau_{syn} \cdot \frac{d}{d_t} y(t) = \alpha \cdot (1 - y(t)) - \beta \cdot y(t) \cdot v(t)_{presynaptic} \tag{3}$$

τ_{syn} is the time constant of the efficacy. The first term of the gating function represents the replenishment process and the second term represents the depletion process. α is the rate to replenish the release pool with transmitter by an amount that is proportional to the unexcited vesicles (reserve pool), $1 - y(t)$. The release process depletes the efficacy at a rate of β as a function of the presynaptic excitation level, $v(t)_{presynaptic}$.

Thus, the model employed in this thesis is a complex dynamic system encompassing multiple coupled differential equations of membrane potentials and synapses. It is well suited to investigate the network dynamics and biological neural response tuning properties during the adaptation process.

2 Objectives

The main objective of this thesis is to investigate how the adaptation partakes in the process of habituation to distortions of daily used optical elements like PALs. Psychophysical and neurocomputational modelling of the visual system were used for the investigation. The subsequent four sections are dedicated to these investigations.

With psychophysical studies, three main properties of distortion adaptation are investigated to predict and characterize the underlying neural mechanisms; its cortical origin, the reference frame in which it is achieved and its long-term temporal dynamics.

In section 3, a psychophysical study is performed to assess the cortical origin of distortion adaptation. As distortion affects multiple features of the natural environment, it is expected to trigger plasticity in different cortical areas. To reveal how distortion adaptation is spread in the visual system, the cortical origin of the plasticity is probed. This is particularly investigated in terms of the cortical level of distortion induced adaptation; i.e. if the underlying plasticity occurs in lower or higher cortical layers.

Section 4 presents psychophysical investigations aimed at revealing the reference frames of the adaptation process. The distortion profiles of PALs are distinct in different parts of the lens as illustrated in figure 7. Thus, during eye movements, commonly termed as saccades, the locations of the distortions continuously vary on the retinal plane although they still maintain their location in space, e.g. reference to the center of the head. This consequently disrupts the encoding and adaptation of the distortions in a retinal reference frame. Spatiotopic encoding is a possible way to achieve a robust adaptation irrespective of this retinal shifts. To systematically study this, the reference frames in which the visual system encodes distortions is assessed.

In section 5, the long term temporal dynamics of the adaptation process was investigated psychophysically. In the temporal domain, habituation is a dynamic process where PAL wearers get more comfortable with experience to their spectacles. Once habituated, wearers do not need a long adjustment time when donning their spectacles. A possible underlying factor for such fast adjustment is if previous visual experiences with the spectacles' distortions facilitates the ability to adapt fast in a long term. To systematically test this hypothesis, the long term experience dependent temporal dynamics of visual adaptation is investigated.

In section 6, combination of psychophysical and neurocomputational model approaches are employed to provide mechanistic explanation of how the visual system extracts distortion information from the complex natural input and adapts to it. A neural model of cortical motion processing is developed to investigate the functional role of recurrent bottom-up and top-down interactions within the hierarchical layers to achieve adaptation in the natural environment. In particular, their roles in neural

response tuning for encoding salient information from a noisy data and in mediating adaptation at different timescales through their synaptic dynamics is inspected.

3 Visual adaptation to distortions and cortical level of the underlying neural plasticity

Habtegiorgis, S. W., Rifai, K., Lappe, M., & Wahl, S. (2017). Adaptation to skew distortions of natural scenes and retinal specificity of its aftereffects. Frontiers in psychology, 8, 1158. doi: 10.3389/fpsyg.2017.01158.

3.1 Abstract

Image skew is one of the prominent distortions that exist in optical elements, such as in spectacle lenses. The present study evaluates adaptation to image skew in dynamic natural images. Moreover, the cortical levels involved in skew coding were probed using retinal specificity of skew adaptation aftereffects. Left and right skewed natural image sequences were shown to observers as adapting stimuli. The point of subjective equality (PSE), i.e. the skew amplitude in simple geometrical patterns that is perceived to be unskewed, was used to quantify the aftereffect of each adapting skew direction. The PSE shifted towards the adapting skew direction. Moreover, significant adaptation aftereffects were obtained not only at adapted, but also at non-adapted retinal locations during fixation. Skew adaptation information was transferred partially to non-adapted retinal locations. Thus, adaptation to skewed natural scenes induces coordinated plasticity in lower and higher cortical areas of the visual pathway.

3.2 Introduction

Spatial geometrical distortions often occur as artefacts in optical devices used in everyday life, such as spectacles and displays. Distortions alter many spatial features of a visual scene, including position information, form, or optic flow [Welch, 1969; Epstein, 1972; Vlaskamp et al., 2009]. They cause loss of visual constancy and disrupt stable visual perception [Welch, 1978].

Adaptation is a mechanism by which the visual system adjusts its response to stabilize perception when features are altered in the visual world [Clifford et al., 2007; Webster, 2015]. The visual system modifies its response when exposed to geometrical distortion of scenes [Regan and Hamstra, 1992; Suzuki et al., 2005]. Robust visual adaptation to geometric distortion of image size magnification induced by meridional magnifying lenses was previously demonstrated [Adams et al., 2001; Yehezkel et al., 2010]. Yet, the corresponding cortical origin of the plasticity during vision in distorted dynamic natural visual inputs is not well-explored. Specifically, contribution of higher cortical areas for the robust plasticity in distorted dynamic natural visual input has not been assessed.

Adaptation induces plasticity along the hierarchical visual stream; from lower to higher cortical levels [Helson, 1964; Webster, 2011]. Lower level cortical areas, such as V1, are retinotopically organized and the aftereffects of their plasticity can only be observed at the specific adapted retinal location [Hubel and Wiesel, 1968; Van Essen and Anderson, 1995; Clifford et al., 2000; Dickinson et al., 2010]. The receptive field size of neurons increases at higher levels enabling them to integrate the information over a wide range of the visual field [Gattass et al., 2005]. Thus, aftereffects originating from plasticity of higher cortical neurons can be transferred across different retinal locations. Retinal position invariance therefore allows identification of higher level distortion encoding mechanisms [Suzuki and Cavanagh, 1998; Zhao and Chubb, 2001; Afraz and Cavanagh, 2008].

Usually, the input to the visual system is rapidly changing natural image content. Natural images contain a great variety of visual features such as spatial frequency, luminance, contrast, orientation, texture, colour, or optic flow signals [Dong and Atick, 1995; Billock et al., 2001; Bex and Makous, 2002; Betsch et al., 2004; Bex et al., 2005, 2007, 2009]. Optically induced image modifications such as astigmatic blur and distortions of spectacles alter multiple features of the natural world; and the visual system adapts to them [Adams et al., 2001; Sawides et al., 2010; Yehezkel et al., 2010; Vinas et al., 2012, 2013]. Accordingly, plasticity of the visual system to optical modification of the dynamic natural environment might involve coordinated responses of several neural populations tuned to different stimuli features. These coordinated responses might not always be revealed by adaptation responses of specific groups of neurons to a selected stimulus feature under controlled experiments [Gallant et al., 1998; Ringach et al., 2002; David et al., 2004; Felsen and Dan, 2005]. Specifically, the study of the visual system's natural adaptation behavior, probably involving a diversity of neural populations, benefits from using scenes that mimic the dynamics of the natural environment.

In the present study, visual adaptation to skew distortion was studied systematically in psychophysical experiments with natural scenes. Adaptation to image skew is a prominent challenge in todays' natural visual world. Progressive additional lenses (PALs) are common spectacles inducing such a distortion as an inevitable artifact [Meister and Fisher, 2008a; Barbero and Portilla, 2015]. Some novice PAL wearers report prolonged discomfort to progressive additional lenses due to swim effect and spatial disorientations [Sheedy et al., 2005]. In this group of PAL wearers, lack of adaptation to image skew is a candidate source of the reported visual discomfort. The image skew is assumed to be one of the sources of visual discomfort and adaptation difficulty experienced by novice PAL wearers.

Skew geometrical distortion shears and unequally magnifies images in oblique me-

ridians [Fannin and Grosvenor, 1987]. Figure 12 shows an illustration of the distortion as well as examples of natural images and geometrical patterns. The shear and the magnification alters orientation and spatial frequency statistics of natural images, respectively. These alterations activate and change responses of lower level cortical areas [Field, 1987; Bao and Engel, 2012; Snowden et al., 2012; Dekel and Sagi, 2015]. The oblique magnification of image skew additionally modifies global form features, such as dimensional symmetry, of scenes. Encoding of dimensional symmetry as a global feature in simple geometrical patterns was suggested in prior studies [Regan and Hamstra, 1992; Suzuki et al., 2005]. Thus, image skew in natural scenes could activate neurons at various cortical levels along the visual pathway.

In the first experiment, adaptation to skew distortion in natural scenes was demonstrated. Subsequently, in a second experiment, retinal location specificity of the skew adaptation aftereffects was used to probe cortical levels involved in skew coding. Partial position invariance of the skew adaptation aftereffect was found. Aftereffects occurred at adapted and non-adapted retinal locations. Thus, visual adaptation to a skewed natural environment shows a new class of global adaptation to distortions mediated by coordinated plasticity of higher and lower cortical areas.

3.3 Experiment 1: Adaptation to image skew in natural scenes

The purpose of this experiment was to investigate if exposure to skewed natural scenes changes visual perception.

3.3.1 Materials and Methods

Adaptation was induced by presenting skewed natural image sequences to observers. Adaptation to skew was evaluated in a constant stimulus procedure. Psychometric curves of skew perception were computed after exposure to right and left skewed natural stimuli. The skew magnitude in the test stimuli that was perceived to be unskewed was used to measure adaptation effects.

Study Approval The study was approved by the Ethics Committee of the Medical Faculty of the Eberhard Karls University of Tübingen and the University Hospital.

Observers Ten observers, aged 18–40 years, participated in this psychophysical experiment. All but one observer were naïve about the purpose of the study. While taking part, all observers had normal or corrected to normal vision. Observers gave their informed written consent, in adherence to the Declaration of Helsinki, prior to participating in the experiment.

Set-Up The psychophysical procedure was designed and stimuli were generated in Matlab (Mathworks, MA, USA) using the PsychToolbox routines [Brainard, 1997] on an apple computer (Apple, USA). An LCD monitor (Benq corporate, USA) was used to display the stimuli at a screen resolution of $1,920 \times 1,080\, pixels$ (square pixels, with $0.31mm$ pixel pitch) and a screen refresh rate of $60Hz$.

The viewing distance was maintained at $57cm$ using a chin and head rest. At this observation distance, the whole screen subtended a visual angle (VA) of $55\,^\circ$ horizontally, and $33\,^\circ$ vertically. The stimuli were presented at the center of the screen in an otherwise completely darkened room and subtended a VA of $20\,^\circ$ both vertically and horizontally. Left, right and space keys of a keyboard were used to collect observer's responses during adaptation aftereffect measurements.

Stimuli The adapting stimuli were skewed natural image sequences (Figure 12b). Natural images were taken from an open source movie [Baumann and Behnisch, 2010]. Each natural image, sized $1,280 \times 720\, pixels$, was skewed in Matlab (Mathworks, MA, USA) by remapping the pixel positions of the undistorted image, x and y, into new distorted pixel positions, x_d and y_d, using the geometrical transformation matrix, M, equation 4 and 5.

$$\begin{bmatrix} x_d \\ y_d \end{bmatrix} = M * \begin{bmatrix} x \\ y \end{bmatrix} \tag{4}$$

$$M = \begin{bmatrix} 1 & -tan(\phi) \\ -tan(\phi) & 1 \end{bmatrix} \tag{5}$$

In Equation 5, ϕ is the shear angle in horizontal and vertical directions.

The inner $650 \times 650\, pixels$ of each distorted image were used cropping out the rest to remove sheared edges. Thus, the images subtended a VA of $20\,^\circ \times 20\,^\circ$ in horizontal and vertical directions. Boundary effects were further reduced by applying a Hanning window as a weighting function (see equation 6) [Harris, 1978]. This weighting function, w, had the same size as each image, $650 \times 650\, pixels$. Its intensity was 1 at the center and decreased radially outwards reaching zero at the boundaries (equation 6).

$$w(r) = \cos^2(\frac{\pi}{N}.r) \tag{6}$$

In equation 6, r is the radial distance of the pixel position from the center of the image and N was set to be equal to the image dimension, i.e., $650\, pixels$.

Two groups of adapting stimuli, containing oppositely skewed image sequences (left-skewed at $\phi = +25\,^\circ$ and right skewed at $\phi = -25\,^\circ$), were prepared as illustrated in Figure 12. The image content was identical in both distorted image sequences. Each

adapting image sequence consisted of 18,000 image frames. During adaptation, these image sequences were rendered at a rate of 20 frames per second, thus each image was refreshed three times when presented on the $60Hz$ display.

Plaid checkerboards, of the same dimension as the adapting images and distorted by different skew amplitude, were used as test stimuli to measure the adaptation aftereffect (Figure 12c).

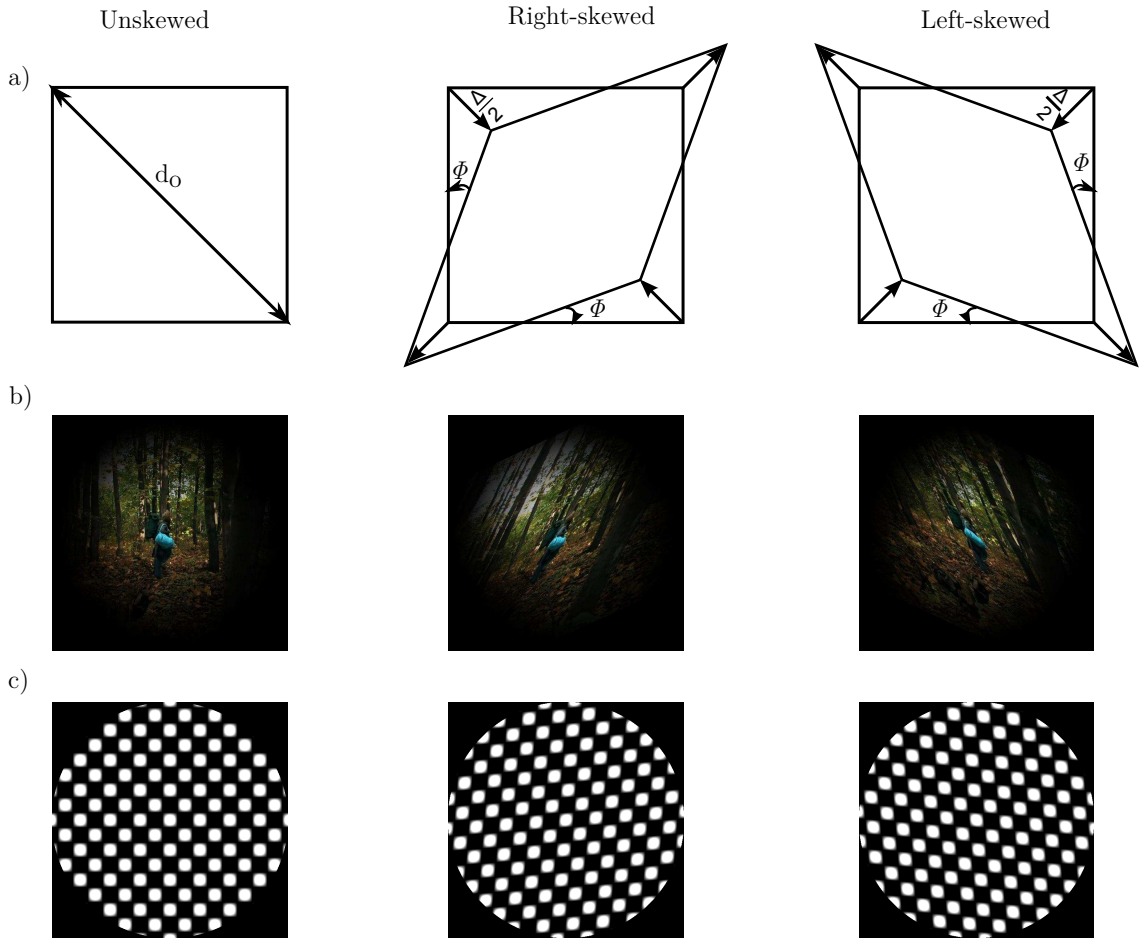

Figure 12: Example of an unskewed test plaid checkerboard stimulus with its skewed counterparts.

The skewed plaid checkerboard images were constructed by superimposing identical contrast sinusoidal gratings oriented at -45° to the right and $+45^\circ$ to the left. The dimensions of the squares' diagonals in the plaid correspond to the spatial wavelengths of the component gratings. The skew was induced by varying the wavelengths of the two component gratings, as in equation 7.

$$d_{right} = do - 1,\ d_{left} = do + 1 \tag{7}$$

d_{right} and d_{left} are the dimensions of the right and the left diagonals of the plaid

and corresponds to the wavelengths of the left and right oriented component gratings, respectively. Δ, in pixels, is the wavelength variation parameter to induce the skew in the plaids. When unskewed, i.e., $\Delta = 0$, the diagonals of the plaid squares have equal dimensions of $do = 40\,pixels$ subtending a VA of $1.24\,^{\circ}$. Non-zero Δ stretches the plaid diagonally and shears the zero-crossings of the squares in the plaid. Positive Δ corresponds to left skewed plaid and negative Δ to the right skewed plaid.

The skew amplitude was quantified by the magnification in oblique directions which is induced by either geometrically shearing or varying the diagonal dimensions, as presented in equation 8.

$$Skew_{amplitude}(\Delta \backslash \phi) = 1 - \frac{d_{right}}{d_{left}} = 1 - \frac{do - \Delta}{do + \Delta} = 1 - \frac{1 - \tan(\phi)}{1 + \tan(\phi)} \tag{8}$$

Procedure Before taking part in the psychophysical experiment, observers were informed about the procedure and trained on how to respond to the test stimuli using a keyboard. Viewing was monocular.

Adaptation was tested alternately to the oppositely skewed image sequences, first to the left-skewed then to the right-skewed natural image sequences. The adaptation aftereffect was tested after each adaptation using the method of constant stimuli. Ten amplitudes of skew were used for the test stimuli. Ten responses were recorded for each skew amplitude. In total, 100 responses were recorded to compute the psychometric curves of each adapting skew direction.

Observers fixated at the center of the screen. Each skewed adapting image sequence was shown first for $3\,minutes$ to induce adaptation and then for $15\,seconds$ after each test stimulus presentation to top up the adaptation. Test stimuli were presented for $2\,seconds$. The skew amplitude of the test stimuli was in a randomized order. After each test stimulus presentation, observers had to report whether the skew direction of the plaid checkerboard was to the right or to the left by pressing the right or the left key of a keyboard, respectively.

Statistical data analysis At each skew amplitude of the test stimuli, the percentage of leftward responses was computed. The percentage of leftward skew responses as a function of skew amplitude of test stimuli was then fitted with a cumulative Gaussian using Psignifit 4.0 software (asymptotes set free but assumed to be equal) [Schutt et al., 2016]. The point of subjective equality (PSE), i.e., the skew amplitude at 50 percent of leftward responses indicated the skew amplitude that was perceived as undistorted. The size of the adaptation aftereffect, ΔPSE, was evaluated as the difference between the PSE of the left-skew and the right-skew adaptations. The overall aftereffect was computed by averaging the ΔPSEs from all the observers. A paired sample t-test was

conducted on the $\Delta PSEs$ to evaluate the significance of the shift in perception due to exposure to skewed scenes.

3.3.2 Result

Figure 13a presents psychometric functions of the average response of all the observers. The percentage of leftward responses as function of the skew amplitude is shown. A negative skew amplitude corresponds to a right-skewed and a positive value to a left-skewed plaid checkerboard. All observers showed significant aftereffects with psychometric functions resembling the overall data. Thus, the PSE shifted to the direction of the adapting skew. After adaptation to right-skewed natural stimuli, observers perceived right-skewed plaid checkerboard as undistorted and vice versa. The magnitude of the PSE shift induced by left and right skew adaptations relative to the PSE measured in the training trials before any adaptation had comparable sizes ($p - value > 0.05$). The $\Delta PSEs$ measured after alternate adaptation to the right-skewed and left-skewed stimuli are significantly different form zero, $p - value < 0.01$. Overall subjects' average ΔPSE is shown in Figure 13b. In sum, an adaptation aftereffect was obtained after adaptation to skewed natural dynamic image sequences. The visual system continuously recalibrated its response after alternate adaptation to oppositely skewed dynamic natural stimuli. Thus, a robust and stimulus-independent plasticity of the visual system to skew distortions was demonstrated.

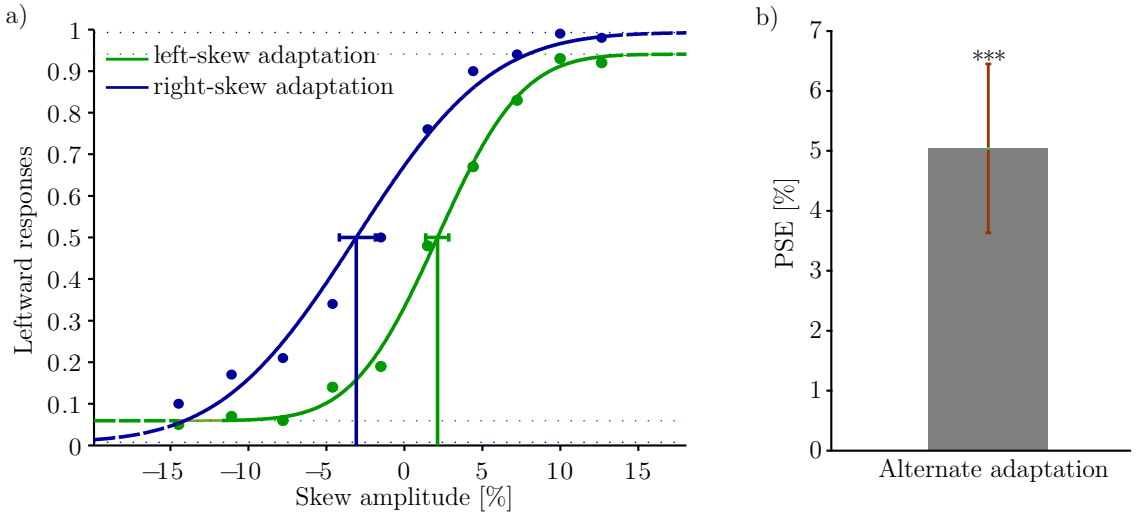

Figure 13: Adaptation aftereffects in response to skewed natural image sequences. Adaptation aftereffect is estimated by the PSE, the skew amplitude at which observers respond equally likely that the test plaid checkerboards are skewed to the right and to the left. (A) psychometric functions of the average response of all the observers. The gaussian fitted function, data points and the confidence intervals at PSE are shown in green for the left-skew adaptation aftereffects and in blue for the right skew adaptation aftereffects. (B) The overall ΔPSE of all the 10 observers after left and right skew adaptation. The error bar shows the standard error. *** t-Test result of $p < 0.05$.

3.4 Experiment 2: Retinal transfer of skew adaptation aftereffect

In this psychophysical experiment, we assessed whether higher level cortical areas contribute to the skew adaptation. Retinotopic and non-retinotopic adaptation conditions were tested wherein adaptation aftereffect was examined at adapted and non-adapted retinal locations during fixation, respectively.

3.4.1 Materials and Methods

As in experiment 1, skewed adaptation was induced by showing distorted natural image sequences to the observers. Aftereffects were then measured using an adjustment procedure wherein observers had control over the skew angle of the test stimulus to adjust it until it is perceived undistorted.

All the materials and methods were the same as in experiment 1, except the changes noted below.

Observers Ten participants partook in this psychophysical experiment. All but one participants were naïve about the purpose of the study. Participants gave their informed written consent, in adherence to the Declaration of Helsinki, prior to participating in the experiment.

Set-Up The stimuli were displayed on a ViewPixx/3D monitor at a resolution of $1,920 \times 1,080\, pixels$ and vertical refresh rate of $100\, Hz$ in an otherwise darkened room. A chin and head rest was used to maintain the viewing distance of $60\, cm$ at which the display subtended VA of 47° horizontally by 27° vertically. The lateral position of the stimuli was controlled gaze contingently by recording the right eye's position in real time at $1\, kHz$ sample rate with the Eyelink 1,000 Plus eye tracker (SR Research, Ltd., Ontario, Canada) and the Eyelink toolbox [Cornelissen et al., 2002]. Participants' response was recorded using the left, right and space keys of a keyboard.

Stimuli Adapting stimuli were natural image sequences as in experiment 1. Each image in the sequence subtended $13^\circ \times 13^\circ$ of VA at zero eccentricity. The test stimulus was a white cross image on a black background skewed at different angles by the transformation matrix in equation 5. The corresponding skew amplitude in the test stimulus at each skew angle, $Skew_{amplitude}(\phi)$, was computed using equation 8. The cross test stimulus was used since it is easily detectable in the periphery. At the 0 skew amplitude, the test stimuli subtended $9^\circ \times 9^\circ$ of VA when viewed at zero eccentricity.

Procedure Participants were informed about the procedure and trained on how to adjust a skewed cross until they perceive it undistorted while viewing was monocular and peripheral.

In both conditions, the retinotopic and the non-retinotopic condition, the perceptual shifts were inspected after alternate exposure to the oppositely skewed image sequences (Figure 3). To induce adaptation, observers watched left and right skewed image sequences each lasting $8\, minutes$, each followed by a test sequence. Aftereffects of each adapting skewed stimuli were assessed by an adjustment procedure. After each adaptation, the cross image skewed at a random angle between 3° and -3°, was presented on the screen. The observers' task was to adjust the skewed cross until it was perceived to be unskewed. The left and the right keys of a keyboard were used to increase or decrease the skew angle with a step size of 0.5° and the space key was used to confirm the perception of the undistorted cross. The skew angle, at which the cross was perceived as undistorted, was used to compute the skew amplitude at the PSE with equation 8. Fifteen trials of adjustment were performed in each aftereffect measurement step.

In both conditions, skewed adapting stimuli were presented in the upper-left visual field at 2° from the fixation dot (Figure 14). Gaze was fixed at the center of the screen throughout the experiment. Aftereffects were tested at adapted and non-adapted locations in the retinotopic and non-retinotopic condition, respectively (Figure 14). Performance asymmetries for visual tasks were previously reported between upper-lower as well as left-right visual fields [Karim and Kojima, 2010; Abrams et al., 2012; Matthews and Welch, 2015]. To reduce any bias from these asymmetries in the non-retinotopic condition, the transfer of adaptation was measured across left-right visual fields for half of the observers and across upper-lower visual fields for the other half.

Observers' gaze was tracked in real time during the whole adaptation measurement procedure. Whenever observers made an eye movement toward the stimuli, the stimuli vanished with a delay of less than 40 ms. This assured the presentation of the stimulus in the desired retinal location. Thus, in the nonretinotopic condition, the adapting and test stimuli did not overlap.

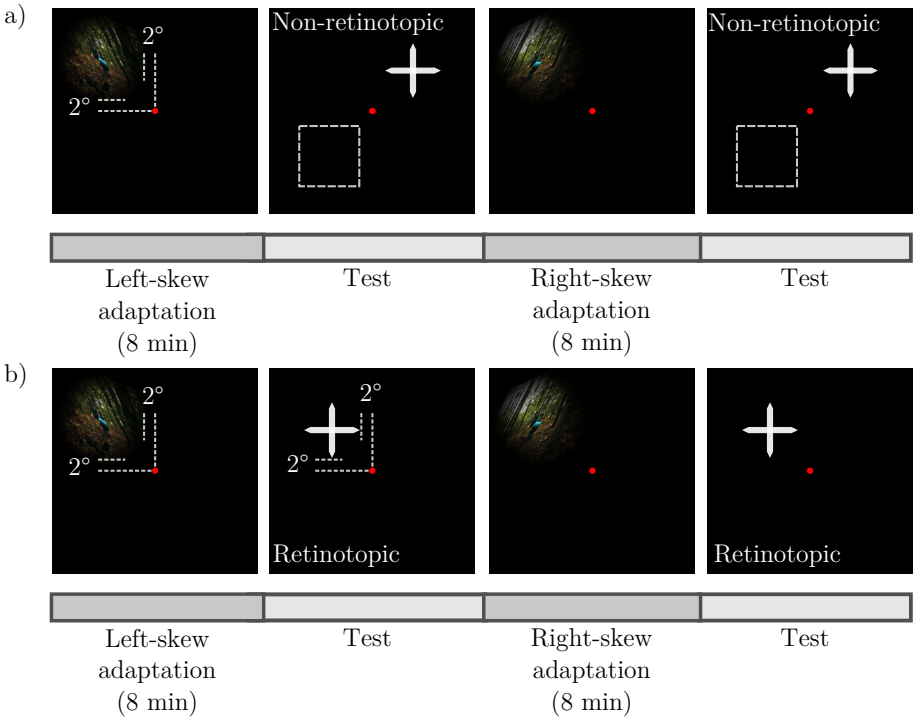

Figure 14: Scheme of experiment paradigm. Observers fixated centrally at the red dot and the aftereffect was measured in the upper-left visual field as the adapter in the retinotopic condition (a), or at a new location either in the upper-right or lower-left (the broken lines) visual field in the non-retinotopic condition (b).

Statistical data analysis For each observer, the PSEs of the left and right skew adaptations in the 15 adjustment trials were binned into three; i.e., trial 1 — trial 5 in bin 1, trial 6 — trial 10 in bin 2 and trial 11—trial 15 in bin 3 (equation 9).

$$PSE_{ave}(bin_i) = \frac{1}{5}\sum_{j=5i-4}^{5i} PSE(trial_j) \tag{9}$$

The magnitude of the aftereffect, ΔPSE, was computed by subtracting the averaged PSEs of the left and right skew adaptations in each bin.

$$\Delta PSE(bin_i) = PSE_{ave_left-skew}(bin_i) - PSE_{ave_right-skew}(bin_i) \tag{10}$$

For the non-retinotopic condition, the transferred adaptation to the new locations was quantified by ΔPSE in the first bin as percentage of the corresponding retinotopic first bin ΔPSE.

$$Transfered\,adaptation = \frac{\Delta PSE(bin_1)_{non-retinotopic}}{\Delta PSE(bin_1)_{retinotopic}} \times 100 \tag{11}$$

The overall average of the aftereffects' magnitude and the transfer was calculated. Paired-sample t-tests were performed to estimate significant differences of the overall averages from zero. An ANOVA was conducted to evaluate the influence of retinotopy and bin number, i.e. relative test time, on the magnitude of the aftereffect.

3.4.2 Result

The adaptation aftereffects of all the observers in each adaptation measurement condition is presented in Figure 15. A positive shift in PSE confirmed the aftereffect demonstrated in experiment 1 (Figure 15a). Moreover, as in experiment 1, the left and right skew adaptations induced comparable magnitude of PSE shift relative to the training PSE ($p > 0.05$). Aftereffect magnitudes in the first two bins were significantly different from zero for both retinotopic ($p(bin1) < 0.01$, $p(bin2) < 0.01$) and nonretinotopic ($p(bin1) < 0.01$, $p(bin2) < 0.04$) conditions. Albeit there was no significant main effect of the bin number, the magnitude showed a decreasing trend through the test trials [ANOVA:$F_{(59,2)} = 1.75$, $p > 0.2$]. The aftereffects of the two conditions are not significantly different from one another [ANOVA, $F_{(59,1)} = 1.53$, $p > 0.2$]. Thus, skew adaptation aftereffects at retinotopic and non-retinotopic locations had comparable sizes. Figure 15b shows the amount of adaptation transferred to the new retinal location. 86.5% of the adaptation was significantly transferred to an un-adapted retinal location ($p < 0.02$).

Therefore, at a fixed gaze, adaptation aftereffects of image skew can be observed at adapted and non-adapted retinal locations.

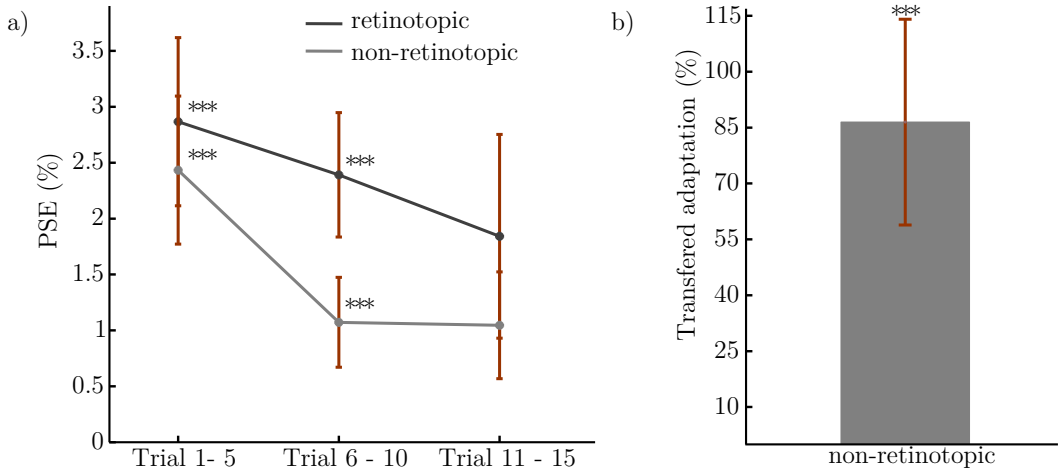

Figure 15: Skew adaptation aftereffects during fixed gaze, at retinotopic, and non-retinotopic locations. a) Overall Aftereffect magnitude. b) Overall transfer of adaptation: non-retinotopic aftereffects' magnitude as percentage of retinotopic aftereffect. The error bars show the standard errors. *** t-Test result of $p < 0.05$.

3.5 Discussion

In the present study, we demonstrated visual plasticity to skew distortions in natural scenes in two psychophysical experiments. In the first experiment, the general perceptual effect of exposure to image skew in natural scenes was revealed. The PSE of observers was shifting in the direction of the adapting skew direction, i.e., alternate adaptation to a left (positive) then a right (negative) skewed natural stimuli resulted in positive shift of the PSE. Thus, the visual system continuously recalibrated its response in correlation with the direction of the adapting skew irrespective of the stimuli image content. In the second experiment, to reveal the plasticity of higher cortical areas, retinal specificity of the skew adaptation aftereffect was inspected during fixation. At retinotopic and non-retinotopic locations, a positive shift of the PSE was observed as an adaptation aftereffect. More importantly, 86.5% of the adaptation effect was transferred to a new retinal location. Accordingly, during fixation, part of the skew adaptation effect was independent of the retinal location of the stimuli. This can be achieved only if neural mechanisms with large receptive field sizes partook in encoding of the skew information [Leopold et al., 2001; Zhao and Chubb, 2001; Afraz and Cavanagh, 2008]. Therefore, shift invariance of skew adaptation indicates plasticity of extrastriate higher level cortical areas in addition to retinotopically organized lower level cortical areas.

Aftereffects originate from response changes in specific neural populations tuned to the adapting stimuli attributes [Roach et al., 2008; Webster, 2015]. Thus, adjustments in neural substrates processing the altered features in the skewed natural images lead

to the measured aftereffect. Moreover, adaptation to attribute rich natural scenes activates several neural populations along the different visual cortical areas and might involve their dynamic interactions as well as coordinated responses [Berkley et al., 1994; Dakin et al., 1999; Smith et al., 2001; Poirier and Frost, 2005; Pavan et al., 2013].

Lower level contrast and contour orientation processing mechanisms in early stages of the visual system stream, such as simple cells in V1, exhibit fully retinotopic receptive fields [Hubel and Wiesel, 1968; Wilkinson et al., 1998; Zhao et al., 2011; Dickinson and Badcock, 2013]. These early stage visual processing mechanisms are well-tuned to orientation distribution of the contrast energy in natural scenes [Field, 1987; van Hateren and van der Schaaf, 1998; van der Schaaf and van Hateren, 1996]. They adjust their response depending on orientation statistics of the natural environment [Bao and Engel, 2012; Dekel and Sagi, 2015]. Skew distortion also alters the orientation statistics of images resulting in high contrast energy in the oblique direction which changes responses of the retinotopic orientation selective mechanisms. The induced lower level plasticity conceivably contributes to the adaptation aftereffect which was not transferred to the new retinal location.

In the visual processing stream, complex shape, and motion processing mechanisms in higher cortical areas feature large receptive field sizes [Van Essen and Anderson, 1995; Gattass et al., 2005; Suzuki et al., 2005; Mather et al., 2008]. Skew alters global form features, such as angles or points of high curvature, and dimensional symmetries. Area V2 contributes to angle information extraction by a linear combination of orientation selective V1 cells' outputs [Hegdé and Van Essen, 2000; Boynton and Hegdé, 2004; Ito and Komatsu, 2004]. Angle discrimination and judgment of the visual system is highly dependent on global geometry of the object containing them [Kennedy et al., 2006, 2008]. Curvatures and orientation flows of real and illusory contours also activate three dimensional and complex shape processing mechanisms in extra-striate cortical areas [Pasupathy and Connor, 1999, 2001; Li et al., 2008; Filangieri and Li, 2009]. Furthermore, higher cortical areas such as V4 and IT, encode complex geometric features including dimensional symmetry from global configurations of the oriented contours [Regan and Hamstra, 1992; Wilson and Wilkinson, 2002; Suzuki et al., 2005; Loffler, 2008]. Furthermore, even direct encoding of symmetry variations, including oblique magnification by skew, as a global feature was previously suggested [Regan and Hamstra, 1992; Suzuki et al., 2005]. Thus, the plasticity in the aforementioned higher level complex shape processing mechanisms potentially contributed to the reported shift invariant component of skew adaptation aftereffect. Further studies with series of dedicated experiments can reveal the exact origin of the higher level skew encoding from natural scenes.

Optical modifications of the visual world, such as astigmatic blur and distortions,

are daily life constraints in spectacle wearers [Fannin and Grosvenor, 1987; Meister and Fisher, 2008a]. Proper habituation is essential in challenging visual situations, such as vision in elderly, where mobility can be affected, e.g., in stepping and falling [Johnson et al., 2007]. Here, we showed adaptation to geometric distortions with ecological image content. Our methodology provides a tool to address the contribution of adaptation to distortion in real life scenarios, e.g., habituation to PALs.

In sum, the visual system is able to extract skew information from the dynamic natural environment and induce a robust stimulus-independent adaptation. Furthermore, plasticity of both lower and higher cortical areas account for skew adaptation in dynamic natural environment.

3.6 Author contributions

SH and KR designed the study. SH conducted the experiment, collected, and analysed the data. All authors interpreted the data, contributed intellectual content to the manuscript, and approved the final submission.

3.7 Funding

We acknowledge support by Deutsche Forschungsgemeinschaft and Open Access Publishing Fund of University of Tübingen.

4 Coordinate systems for visual encoding of distortions

Habtegiorgis, S. W., Rifai, K., & Wahl, S. (2018). Transsaccadic transfer of distortion adaptation in a natural environment. Journal of vision, 18(1), 13-13. doi: 10.1167/18.1.13.

4.1 Abstract

Spatially varying distortions in optical elements—for instance prisms and progressive power lenses—modulate the visual world disparately in different visual areas. Saccadic eye movements in such a complexly distorted environment thereby continuously alter the retinal location of the distortions. Yet the visual system achieves perceptual constancy by compensating for distortions irrespective of their retinal relocations at different fixations. Here, we assessed whether the visual system retains its plasticity to distortions across saccades to attain stability. Specifically, we tapped into reference frames of geometric skew-adaptation aftereffects to evaluate the transfer of retinotopic and spatiotopic distortion information across saccades. Adaptation to skew distortion of natural-image content was tested at retinotopic and spatiotopic locations after a saccade was executed between adaptation and test phases. The skew-adaptation information was partially transferred to a new fixation after a saccade. Significant adaptation aftereffects were obtained at both retinotopic and spatiotopic locations. Conceivably, spatiotopic information was used to counterbalance the saccadic retinal shifts of the distortions. Therefore, distortion processing in a natural visual world does not start anew at each fixation; rather, retinotopic and spatiotopic skew information acquired at previous fixations are preserved to mediate stable perception during eye movements.

4.2 Introduction

Images on the retina are not an exact replica of the visual world. Instead, they are often distorted by either inherent optical properties of the eye or magnification effects of spectacles worn to correct refractive errors [Fannin and Grosvenor, 1987]. In some cases, as in progressive addition lenses and prisms, the magnification axis varies across the surface of the spectacle [Meister and Fisher, 2008a]. Thus, the geometry of the distortions can even be complexly disparate in different parts of the visual field. On that condition, eye movements shift the retinal location of the distortions and disrupt retinotopic representations. Yet while people adapt to optical elements comprising spatially variable distortions, the visual system seems to compensate for the distortions

regardless of their continuous retinal shifts. How this perceptual constancy is attained during eye movements in complexly distorted dynamic natural visual inputs is not well explored. To reveal the underlying visual process, it is vital to assess if visual plasticity to distortion is transferred across saccades in different coordinate systems.

The visual system retains information of several visual features across a saccade based on their location in retinal and in some cases spatial reference frames [Galletti et al., 1993; Melcher and Morrone, 2003; Melcher, 2005, 2007; Zimmermann et al., 2013, 2016]. The retinotopic location of a stimulus brings perceptual advantages such as in tracking a moving object [Golomb and Kanwisher, 2012b; Howe et al., 2010]. Spatiotopic representation of specific visual features in extraretinal reference frames has been previously demonstrated [Andersen, 1997; Andersen et al., 1985; Burr and Morrone, 2011; Crespi et al., 2011; Zimmermann et al., 2013, 2016]. The visual system uses spatiotopic information to compensate for saccade associated retinal shifts. The spatiotopic location of a visual stimulus is therefore important information for successful interaction with the external world [Andersen, 1997; Burr and Morrone, 2011].

Examining the reference frames in which adaptation aftereffects occur is one of the approaches recurrently used to scrutinize transsaccadic transfer of visual information and the underlying coordinate system [Melcher, 2005, 2007; van Boxtel et al., 2008; Zimmermann et al., 2016]. By introducing an eye movement after adapter presentation and before test-stimulus presentation, it is possible to separately test if any adaptation is retained across a saccade in a retinotopic and a spatiotopic reference frame. In retinotopic adaptation, an aftereffect occurs at the adapted retinal location after an eye movement, whereas in spatiotopic adaptation, an aftereffect occurs at the adapted spatiotopic location though the retinal location is altered after the saccade.

The input to the visual cortex from the natural visual world comprises complex stimulus attributes which potentially excite interactions of different cortical levels [Betsch et al., 2004; Bex et al., 2005, 2007, 2009; Billock et al., 2001; Dong and Atick, 1995]. Although controlled studies with artificial stimuli elucidate feature-selective neural responses, they might not fully divulge how these mechanisms respond in a coordinated manner with other neural populations when stimulated by the rich natural-image content [David et al., 2004; Felsen and Dan, 2005; Ringach et al., 2002]. Studying visual plasticity to stimuli that resemble the natural world thus not only mirrors real-life visual circumstances but even asserts potential coordinated responses of different cortical areas.

Here, we evaluated whether distortion adaptation is transferred across fixations during eye movements in a distorted natural environment. Reference frames of geometrical skew-distortion adaptation were tested with natural-image contents. After a saccade, skew adaptation was partially transferred to a new fixation only at retinotopic

and spatiotopic locations. No aftereffect was obtained at a control location which was neither retinotopic nor spatiotopic. Thus, during eye movements in a skewed visual world, retinotopic as well as spatiotopic distortion information is conceivably used to mediate stable perception.

4.3 Materials and methods

Here, we assessed the coordinate frames in which skew-adaptation information was transferred across fixations. The measurements encompassed four conditions: no saccade, retinotopic, spatiotopic, and control.

4.3.1 Participants

In total, 12 observers participated in the study. All partook in the no-saccade adaptation condition, eight in the spatiotopic condition, and eight in the retinotopic and control conditions (four of whom also participated in the spatiotopic condition). All except one were unaware of the purpose of the study. Participants had normal or corrected-to-normal vision.

4.3.2 Study protocol

The ethics committee at the Medical Faculty of the Eberhard Karls University of Tübingen and the University Hospital approved the study. In adherence to the Declaration of Helsinki, participants' informed written consent was collected prior to their participation in the study.

4.3.3 Setup

Psychophysical experiments were designed and stimuli were generated in MATLAB (MathWorks, Natick, MA) using the PsychToolbox routines [Brainard, 1997] on an Apple computer (Apple Inc., Cupertino, CA). The stimuli were displayed on a ViewPixx/3D monitor (VPixx Technologies Inc., Saint-Bruno, Canada) at a resolution of $1,920 \times 1,080\,pixels$ and vertical refresh rate of $100\,Hz$ in an otherwise darkened room. A chin and head rest was used to maintain the viewing distance of $60\,cm$ at which the display subtended visual angles of approximately 47° horizontally $\times$ 27° vertically. The lateral position of the stimuli was controlled gaze contingently by recording the right eye's position in real time at a sample rate of $1\,kHz$ with the EyeLink 1000 Plus eye tracker (SR Research, Ontario, Canada) and the Eyelink toolbox [Cornelissen et al., 2002]. Participants' responses were recorded using the left, right, and space keys of a keyboard.

4.3.4 Stimuli

Geometrical transformation matrix M was used to skew images by a shear angle of ϕ, wherein the pixel positions x and y of the undistorted image were remapped to distorted positions x_d and y_d as in equation 4 and 5.

The adapting stimuli were skewed natural-image sequences. Two groups of oppositely skewed adapting stimuli were generated, containing left-skewed ($\phi = +25\,^\circ$) and right-skewed $\phi = -25\,^\circ$) natural-image sequences. Distortion information from sheared boundaries was removed by weighting each image with a Hanning window weighting function of the second order [Harris, 1978]. Each image subtended $10\,^\circ \times 10\,^\circ$ of visual angle at zero eccentricity. The image content was identical in the positive- and negative-skewed adapting image sequences. These image sequences were rendered at a rate of 20 frames/s. A white cross image on a black background, skewed at different angles, was used as a test stimulus to examine the aftereffect. At $0\,^\circ$ skew, the cross subtended $10\,^\circ \times 10\,^\circ$ of visual angle when viewed at zero eccentricity. Viewing was monocular with the right eye while the left eye was patched. Illustration of a skew geometrical distortion with examples of adapting and test stimuli are shown in Figure 16.

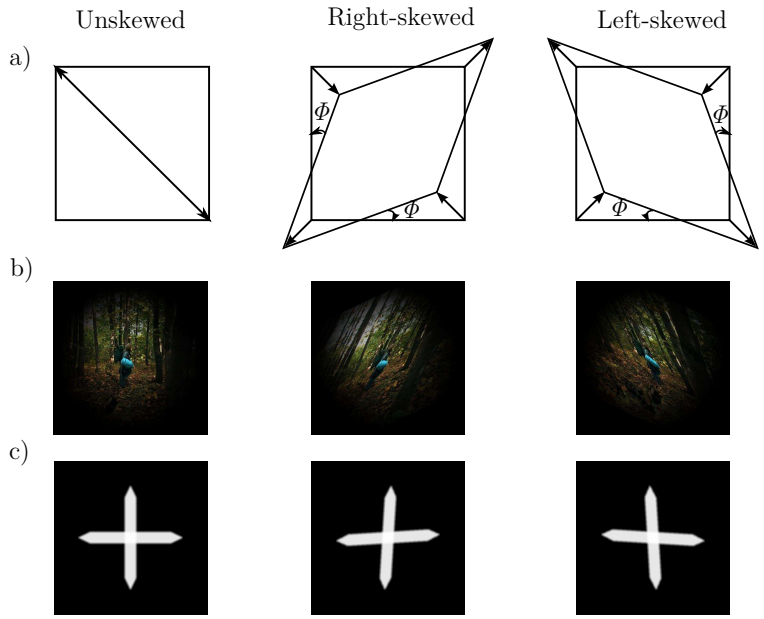

Figure 16: a) Sketch of skew geometrical distortion. b) Example of an unskewed natural image with its skewed counterparts from the adaptation image sequences. c) Example of an unskewed test cross stimulus with its skewed counterparts.

4.3.5 Procedure

Participants were informed about the procedure and trained on how to adjust a skewed cross until they perceive it to be undistorted.

In each condition, the baseline was first raised by exposure to a positively skewed image sequence for 8 *minutes*. Subsequently, the test stimulus appeared on the screen. The test stimulus was a cross skewed at a random angle between $3\,^\circ$ and $-3\,^\circ$. The observers' task was to adjust the skewed cross until it was perceived as undistorted, that is, until the two edges appeared perpendicular. The left and right keys of a keyboard were used to increase or decrease the skew angle with a step size of $0.5\,^\circ$, and the space key was used to confirm the perception of the undistorted cross. Then the negatively skewed image sequence was presented for another 8 *minutes*, followed by similar adjustment task. Fifteen trials of adjustment were performed in each aftereffect-measurement step. The point of subjective equality (PSE) was used as an aftereffect-measurement parameter. It was defined by the skew angle of the adjusted cross at which the subjective undistorted perpendicular cross was perceived.

In all conditions, skewed adapting stimuli were presented in the upper right visual field $2\,^\circ$ from the fixation dot. In the no-saccade condition, gaze position remained fixed throughout the adaptation-measurement procedure, as presented in Figure 17a. In all the other conditions, aftereffects were tested after a saccade, as shown in Figure 17b. Just after each adaptation and before the appearance of the test stimuli, observers made a saccade to a new fixation marker located $14\,^\circ$ to the left of the previous fixation marker. The transferred adaptation to the new fixation was measured at retinotopic, spatiotopic, or control null locations separately (Figure 17b). In the retinotopic condition, the spatial location of the test stimuli was altered, maintaining its retinal location as the adapting stimuli; whereas the spatiotopic condition was assessed by varying the retinal location of the test stimuli while preserving its spatial location as the adapting stimuli. The control measurement was performed at neither a retinal nor a spatial matching location, to make sure that the measured aftereffects were confined to retinotopic and spatiotopic locations.

Observers' gaze was tracked in real time during the whole measurement procedure. Around every fixation target, a circular boundary of radius $1\,^\circ$ was defined. Whenever gaze was positioned out of this circular boundary, the stimuli vanished from the screen gaze contingently. At the selected refresh rate of the screen and the sampling rate of the eye tracker, this was achieved in a delay of less than 40 *ms* [Saunders and Woods, 2014]. This assured exclusive presentation of the stimulus at the intended retinal and spatial position. Thus, in all nonretinotopic conditions, there was no retinal overlap of the adapting and test stimuli. Eye movements within a radius of $1\,^\circ$ from the fixation marker were ignored, to account for microscopic saccades during fixation.

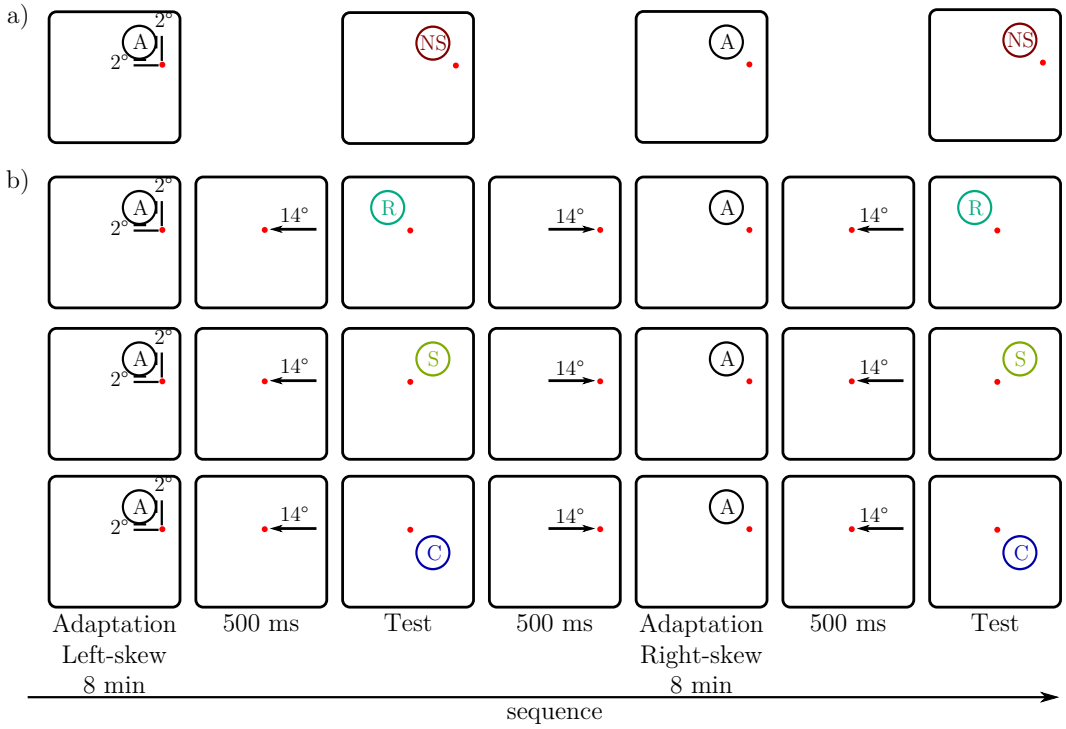

Figure 17: Scheme of experiment paradigm. a) No-saccade (NS) condition: Observers' gaze was fixed and the aftereffect was measured at the same location as the adapter (A). b) Transsaccadic transfer: Observers made a saccade of 14 ° amplitude after the presentation of the adapter (A). After 500 ms, the aftereffect was tested at the retinotopic (R) or spatiotopic (S) location of the adapter, in the retinotopic and spatiotopic condition, respectively. In the control condition (C), the aftereffect was measured at a novel unadapted location.

4.3.6 Data analysis

For every observer, the aftereffects measured in the 15 trials after each adaptation were binned into three by averaging Trials 1–5 into Bin 1, Trials 6–10 into Bin 2, and Trials 11–15 into Bin 3. The PSEs of the right skew-adaptation aftereffects in each bin were subtracted from those in the corresponding bin for the left skew-adaptation aftereffects to compute the aftereffect magnitude—the ΔPSE. In the retinotopic, spatiotopic, and control conditions, the transferred adaptation across saccade was quantified by the first-bin ΔPSE of each condition as a proportion of the first-bin ΔPSE of the no-saccade adaptation condition.

The overall data were computed by averaging the magnitudes of the aftereffects and the percentage values measured from all the observers. A t-test was performed on each aftereffect.

4.4 Results

The adaptation aftereffects of all the observers in each condition are presented in Figures 18 and 19. Figure 18 shows the shift in perception of an unskewed cross after alternate exposure to oppositely skewed image sequences measured in the no-saccade condition. During fixation, the adaptation aftereffect measured at the adapted retinal and spatial location showed a significant positive ΔPSE, decaying within the 15 test trials ($p_{trials1\text{–}5} < 0.01$, $p_{trials6\text{–}10} < 0.05$, $p_{trials11\text{–}15} > 0.05$). Thus, after exposure to skewed stimuli, observers perceived a cross that is skewed in the adapting skew direction to be unskewed.

Since the aftereffect decayed as the trials progressed, transfer of adaptation to a new fixation location was estimated by the magnitude of the aftereffects in the first five trials. The aftereffect magnitude measured in the saccadic conditions is shown in Figure 19a. In the saccade conditions, similar to the no-saccade condition, positive ΔPSE occurred in the retinotopic ($p_{trials1\text{–}5} < 0.05$) and spatiotopic ($p_{trials1\text{–}5} < 0.01$) conditions. No significant aftereffect was measured in the control condition at a location that was neither retinotopic nor spatiotopic ($p_{trials1\text{–}5} = 0.81$). After a saccade, 91% of the magnitude of adaptation was transferred to the retinotopic position and 82% to the spatiotopic position at a new fixation ($p < 0.01$ and $p < 0.05$, respectively). This is shown in Figure 4b. Thus, during eye movements, both spatiotopic and retinotopic mechanisms preserve distortion information acquired at previous gaze positions.

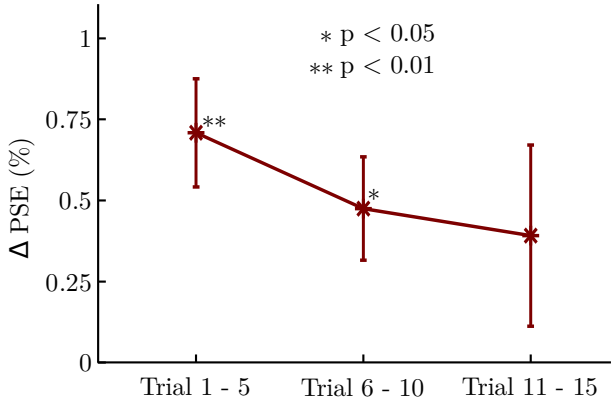

Figure 18: Skew-adaptation aftereffects during fixed gaze: Overall averages of aftereffect magnitude in the no-saccade (NS) condition.

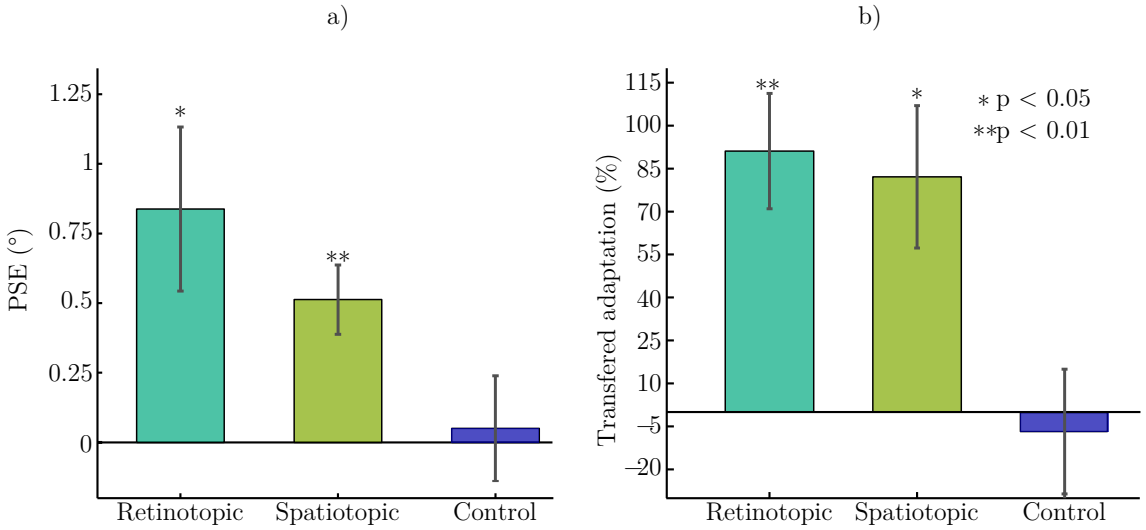

Figure 19: Skew-adaptation aftereffects after a saccade at retinotopic, spatiotopic, and control null locations. (a) Overall averages of aftereffect magnitude in the spatiotopic, retinotopic, and control adaptation conditions. (b) The overall transfer of adaptation across a saccade: Aftereffect magnitudes as percentage of the no-saccade adaptation aftereffect. Error bars show standard error.

4.5 Discussion

Reference frames of adaptation aftereffects were assessed to reveal the neural mechanisms that compensate for skew distortions in dynamic natural scenes during eye movements. While the gaze was varied between adaptation and test tasks, adaptation significantly transferred to retinotopic and spatiotopic locations but not to a null location-that is, neither retinotopic nor spatiotopic.

In this study, we elucidated that the visual system transfers retinotopic and spatiotopic skew distortion information across a saccade. Retinotopic and spatiotopic reference frames were decoupled by an eye movement just before the test task. Accordingly, retinotopic and spatiotopic effects were dissociated and measured at different positions. Partially transferred adaptation in a retinotopic as well as a spatiotopic reference frame was shown. In the retinotopic condition, the adaptation aftereffect was measured at an identical retinotopic position after a saccade. In the spatiotopic condition, the aftereffect was measured at a retinally novel but spatially constant location. Plasticity of neurons in higher cortical areas with large receptive field sizes leads to retinal-location-invariant aftereffects [Afraz and Cavanagh, 2008; Gattass et al., 2005; Leopold et al., 2001; Mather et al., 2008; Meng et al., 2006; Suzuki et al., 2005; Van Essen and Anderson, 1995; Zimmer and Kovacs, 2011]. Thus, general position invariance was excluded in a control condition. If the measured adaptation aftereffect at the spatiotopic position were a result of general position invariance, an aftereffect would

have occurred at a separate location as well [Ezzati et al., 2008; Mathot and Theeuwes, 2013; Zimmermann et al., 2016]. Accordingly, in our control condition the aftereffect was measured at a novel retinal location, which was neither retinotopically nor spatiotopically matched. No significant aftereffect was found. This ascertained that the measured significant spatiotopic effect did not originate from plasticity of position invariant mechanisms.

Spatiotopic transfer of visual information can be achieved by neurons either remapping the retinotopic organization of their receptive fields during a saccade [Duhamel et al., 1992; Nakamura and Colby, 2002; Kusunoki and Goldberg, 2003] or comprising receptive fields whose coordinate system is in extraretinal reference frames [D'Avossa et al., 2007; Duhamel et al., 1997; Galletti et al., 1993]. In the case of receptive-field remapping, saccadic eye movements trigger changes in the receptive- field location of neurons. If a stimulus initially appeared outside the neuron's receptive field and a saccade which will bring the stimulus into the receptive field is intended, the neuron changes its receptive-field location to the stimulus location before saccade execution. It starts firing at the initial gaze position and keeps this sensitivity after the saccade when the stimulus appears in its receptive field. Accordingly, the stimulus's spatial correspondence will be maintained. In purely spatiotopic neurons, on the other hand, receptive-field organization is based on an extraretinal reference frame and codes the visual stimulus with its location in space. Hence, the neurons keep responding to a preferred feature at any gaze position and retain information during eye movements as long as the stimulus is stationary in space.

Either one or both of the aforementioned spatiotopic mechanisms could account for the reported transfer of spatiotopic skew information across saccades. In a receptive-field remapping mechanism, skew-information- coding neurons should be sensitive to eye-movement- related signals, such as efference copy and proprioceptive information, to remap their receptive fields before the saccade [Andersen et al., 1985; Backus et al., 1999; Wexler et al., 2001; Wexler and Van Boxtel, 2005; Wolpert and Flanagan, 2001]. In the other case, neurons selective to the skew information would have pure spatiotopic receptive fields. This way, the same neurons process the skewed adapting and test stimuli before and after the saccade, respectively, by maintaining spatial correspondence.

In addition to stimulation of receptive-field remapping, eye-movement signals alter firing patterns of neurons in the cortical visual hierarchy [Andersen, 1997; Andersen et al., 1985; DeSouza et al., 2002; Trotter and Celebrini, 1999]. Gaze-contingent perceptual changes to distortions of a wedged prism have been previously demonstrated [Pick and Hay, 1966]. In the present study, the partial transfer of adaptation to a new gaze position might be explained by changes of neural mechanisms whose responses

are modulated by the gaze direction [Nishida et al., 2003; Parwaga et al., 2016].

Aftereffects originate from response changes in specific neural populations tuned to the adapting stimuli's attributes [Clifford et al., 2007; Roach et al., 2008; Webster, 2011, 2015]. Thus, adjustments in neural substrates processing the altered spatiotemporal features of the skewed natural-image content would have led to the measured aftereffects. These include neurons affected by skew effects such as tilt in contour orientations, dimension asymmetry due to oblique magnification, shift in the angle between the contours, and change in the distribution of motion signals in the direction of the skew.

Although studies argue that visual coding is purely retinotopic [Gardner et al., 2008; Golomb and Kanwisher, 2012a], spatiotopic adaptation at different visual areas has repeatedly been demonstrated in classical feature-selective adaptation paradigms [Melcher, 2005, 2007; Zimmermann et al., 2016]. Lower level contrast and contour-orientation processing mechanisms in early stages like V1 exhibit fully retinotopic reference frames [Bao and Engel, 2012; Dekel and Sagi, 2015; Dickinson and Badcock, 2013; Wilkinson et al., 1998; Zhao et al., 2011]. Electrophysiological and imaging studies have confirmed behavioral evidence on spatiotopic coding through receptive-field remapping in visual areas such as V2, V3, and V4 [Melcher, 2005; Nakamura and Colby, 2002; Zimmermann et al., 2016]. These areas are well suited to encode intermediate shape information, such as orientation, aspect ratio, symmetry, and angle [Boynton and Hegdé, 2004; Gegenfurtner et al., 1997; Hegdé and Van Essen, 2000; Ito and Komatsu, 2004; Laursen and Rasmussen, 1975; Loffler, 2008; Regan and Hamstra, 1992; Suzuki and Cavanagh, 1998; Wilson and Wilkinson, 2002; Zimmermann et al., 2016]. Moreover, motion processing neural mechanisms in MT^{+} exhibit pure spatiotopic receptive fields [Melcher and Morrone, 2003; Wexler et al., 2001]. Their possible interactions with form-processing mechanisms could contribute to the measured spatiotopic aftereffects [Pavan et al., 2013].

The present study extended these findings to a naturalistic stimulation of the visual system-that is, when the visual system is exposed to dynamic naturalimage content. Unlike classical feature-selective adaptation with artificial stimuli, such adaptation from a stimulus containing a variety of attributes potentially involves dynamic interactions between multiple levels in the hierarchy of the visual cortex and coordinated responses of several neural populations stimulated during adaptation [Berkley et al., 1994; Dakin et al., 1999; Pavan et al., 2013; Smith et al., 2001]. In line with the aforementioned feature-selective adaptation studies, our results assert spatiotopic as well as retinotopic visual-coding mechanisms during ecological viewing conditions. Furthermore, our methodology provides a tool to address the contribution of these mechanisms in real-life scenarios-for example, adaptation to optically induced distortions.

Therefore, during a saccade in a distorted natural environment, distortion processing does not start anew at every fixation. Rather, the visual system preserves distortion information acquired at previous fixations. This is specifically efficient in vision with progressive additional lenses, where the distortions are complexly distributed across the visual field. Specifically, during vision accompanying eye movements, spatiotopic mechanisms might facilitate habituation in this application scenario, since they retain the distortion's spatial layout of the spectacles though their retinal position is varied.

Keywords: visual adaptation, spatial distortions, transsaccadic adaptation, natural vision

4.6 Acknowledgments

We acknowledge support by Deutsche Forschungsgemeinschaft and Open Access Publishing Fund of University of Tübingen. Funding received from Eberhard-Karls-University Tübingen (ZUK 63) as part of the German Excellence initiative from the Federal Ministry of Education and Research (BMBF). This work was done in an industry on campus cooperation between the University of Tübingen and Carl Zeiss Vision International GmbH. S. W. Habtegiorgis is scientist at the University Tübingen; K. Rifai and S. Wahl are employed by Carl Zeiss Vision International GmbH and are scientists at the University Tübingen.
Commercial relationships: none.
Corresponding author: Selam W. Habtegiorgis.
Email: Selam-wondimu.habtegiorgis@uni-tuebingen.de.
Address: Institute for Ophthalmic Research, University of Tübingen, Tübingen, Germany

5 Long term temporal dynamics of visual adaptation to distortions

Habtegiorgis, S. W., Rifai, K., Lappe M., & Wahl, S. (2018). Experience dependent long-term facilitation of skew adaptation. Journal of vision,18(9):7, 1–11. doi: 10.1167/18.9.7.

5.1 Abstract

Adaptation to changes in the environment allows the visual system to achieve optimal perception in a continuously changing visual world. One particular example to recurrently encountered changes in everyday vision is geometrical distortions of the environment when wearing spectacles for vision correction, e.g. image shear by skew geometric distortions of in progressive additional lenses. For optimal visual performance, it would be beneficial if the visual system uses previous history of recurrent distortions and learns to adapt fast when they are reapplied, yet this has not been systematically shown. The present study evaluates experience dependent long-term facilitation of fast adaptation to image skew, i.e. a shear from the x and y- axis, using ecological stimuli. Immediate and long-term facilitation of fast adaptation induced by minutes time scales of extended skew exposures were tested. Fast adaptation was quantified via the magnitude of perceptual bias after a brief exposure to image skew in a constant stimulus procedure. Immediate facilitation was tested by comparing the magnitudes of fast adaptation that are measured on the same day before, i.e. baseline, and after extended skew exposure. The retention of the facilitation was evaluated by comparing the fast adaptation measured after, on average, 57 days of the previous extended skew exposure with the baseline. After one hour of skew exposure, the amount of fast adaptation significantly increased from the baseline measurement indicating immediate facilitation of the fast adaptation. This facilitation was retained at, on average, 57 days after the extended exposure. Thus, the results depicted experience dependent long-term facilitation of skew adaptation which potentially explains visual habituation to distortions of spectacles.

5.2 Introduction

Everyday vision constitutes a remarkably wide range of conditions, e.g. continuously varying luminance across a single day. For optimal functioning, it would be efficient if the visual system adjusts rapidly its responses to compensate for recurrent changes in the environment. The visual system might facilitate fast adaptation process to fre-

quently occurring alterations by using previous history of visual experiences. One real life scenario of such adaptation dynamics is how people habituate to unfamiliar image modifications introduced by new spectacle lenses. Distortion is one of the artefacts in spectacles which alters features of the visual world and induces loss of visual stability [Vlaskamp et al., 2009; Welch, 1969, 1978]. Skew geometrical distortion is an example of inevitable distortions in spectacles, such as progressive additional lenses (PALs) [Barbero and Portilla, 2015; Meister and Fisher, 2008a]. Image skew obliquely magnifies and shears images as illustrated in Figure 7 [Barbero and Portilla, 2015; Fannin and Grosvenor, 2013]. This manipulation alters multiple features, e.g. in orientation and dimension symmetry statistics of the natural environment, refer Figure 8. Lack of adaptation to such alterations potentially contribute to visual discomforts experienced by novice PAL wearers. Observers commonly report vanishing of the visual discomforts after wearing new spectacles continuously for a week or so. However, it is still unknown whether previous extended exposure to the distortions enables the visual system to adapt fast when the distortions are reapplied. To understand this temporal dynamics, it is vital to assess experience dependent long-term changes of the visual adaptation to such modifications.

Adaptation is a mechanism by which the visual system optimizes visual processing and attains perceptual stability in a continuously changing visual world [Clifford et al., 2007; Smithson and Zaidi, 2004; Webster, 2011; Welch, 1978]. Adaptation has been shown in a diversity of attributes, such as adaptation to colour [Belmore and Shevell, 2008, 2011; Delahunt et al., 2004; Eisner and Enoch, 1982; Neitz et al., 2002], contrast [Bao and Engel, 2012; Bao et al., 2013; Kwon et al., 2009], distortions and blur [Adams et al., 2001; Habtegiorgis et al., 2017; Yehezkel et al., 2010]. Adaptation effects are commonly shown as aftereffects that last on a seconds time scale after the adapting features are removed. However, exposure to some changes in the environment does not only induce momentary visual adjustments but also contributes to future visual experience. Experience dependent long-term facilitation of adaptation can be studied by testing the ability to adapt fast to features which have been adapted in previous sessions. This has been done by few studies that showed faster re-adaptation to blur after four hours of adaptation on the previous day [Yehezkel et al., 2010] and faster re-adaptation to colour after habitual wearing of coloured glasses for 14 months [Engel et al., 2016]. For such rapid re-adaptations, the visual system might need previous information about the alterations which increases its expectations or minimizes its insecurities for the risk of error driven fast adjustments [Todorovic et al., 2011; Wark et al., 2009].

The dynamics of adaptation also depend on the statistical distribution of features in the visual stimulus [Wark et al., 2009]. Particularly stimuli with higher order stat-

istics, such as natural images [Ruderman and Bialek, 1994], potentially affect the time course of adaptation [Wark et al., 2009]. In the daily visual world, the input to the visual system is rapidly changing natural image content. Natural images contain a great variety of visual attributes like spatial frequency, luminance, contrast, orientation, texture, colour, or optic flow signals [Betsch et al., 2004; Bex and Makous, 2002; Bex et al., 2005, 2007, 2009; Billock et al., 2001; Dong and Atick, 1995]. Adaptation to altered features in a dynamic natural environment might involve coordinated plasticity of several neural populations across multiple cortical areas, e.g. adaptation to skewed dynamic natural images [Habtegiorgis et al., 2017]. Due to the hierarchical and interactive nature of the visual system, these coordinated responses might not always be revealed by adaptation of a specific group of neurons to selected stimulus features under controlled experiments [David et al., 2004; Felsen and Dan, 2005; Gallant et al., 1998; Ringach et al., 2002]. Since, natural image content drives the visual system in its intended mode [Snow et al., 2017], visual stimuli that resemble the natural environment are important to comprehensively study the dynamics of the visual system's natural long-term adaptation process.

In the present study, psychophysics was conducted with natural scenes to systematically study the long-term dynamics of adaptation to skew distortion. Immediate visual adjustment after exposure to skewed natural scenes was behaviourally demonstrated in a previous study [Habtegiorgis et al., 2017]. To understand the long-term temporal dynamics of the habituation process to distortions of PALs, we examined if fast adaptation to skew distortion can be facilitated in the long-term by prior extended adaptation to the distortions. We measured fast adaptation via the amount of perceptual shift after a brief exposure to image skew. Long-term effects were measured by exposing participants to extended skew adaptation and then retesting the fast adaptation several weeks later. The results depicted that 1 hour of extended skew exposure facilitated fast adaptation, even when retested, on average, 57 days later. Thus, extended exposure to image skew facilitates adaptation whose long-term retention might enable fast and efficient re-adaptation when needed.

5.3 Materials and methods

Immediate and retained facilitation effects on fast skew adaptation (FA), induced by two extended skew exposure (EE) time scales, were tested. The entire experiment comprised five FA aftereffect measurement sessions and two EE sessions. The five FA aftereffect measurement sessions were: session 1.1, session 1.2, session 2.1, session 2.2 and session 3. The two EE sessions were session EE1 and session EE2.

FA was induced by a brief exposure to skewed natural image sequences. FA aftereffects were then measured in a constant stimulus procedure by the skew magnitude in

the test stimuli that subjectively appeared unskewed. During EE sessions, observers watched skewed natural image sequences for extended durations.

5.3.1 Study approval

The study was approved by the Ethics Committee of the Medical Faculty of the Eberhard Karls University of Tübingen and the University Hospital.

5.3.2 Observers

Ten naïve observers, between age of 18 to 40, participated in the study with a prior written consent in adherence to declaration of Helsinki. All observers took part in all sessions, except one observer who did not participate in session 1.2. All observers had normal or corrected to normal vision while taking part in the psychophysical measurements.

5.3.3 Set-up

The psychophysical procedure was designed and stimuli were generated in Matlab (Mathworks, MA, USA) using the PsychToolbox routines [Brainard, 1997] on an Apple computer (Apple, USA). The stimuli were displayed on an LCD monitor (Benq corporate, USA) at a screen resolution of $1920 \times 1080\, pixels$ (square pixels, with $0.31\, mm$ pixel pitch) and a screen refresh rate of $60\, Hz$. A chin and head rest was used to fix the viewing distance at $57\, cm$ at which the whole screen subtended a visual angle (VA) of $55\,^\circ$ horizontally, and $33\,^\circ$ vertically (pixel pitch of $0.031\,^\circ$ VA). During the experiment, viewing was monocular and stimuli were presented at the center of the screen in an otherwise completely darkened room. During aftereffect measurements, observers' responses were collected using the left and right keys of a keyboard.

5.3.4 Stimuli

The same adapting and test stimuli were used as in our previous adaptation study [Habtegiorgis et al., 2017]. Images were skewed by a shear angle of ϕ using a geometrical transformation matrix M, in equation 4 and 5, which remapped the pixel positions of the undistorted image, x and y, to distorted positions, x_d and y_d.

Natural images were taken from an open source movie [Baumann and Behnisch, 2010]. Three image sequences were prepared in this study, containing natural scenes that are unskewed at $\phi = 0\,^\circ$, right skewed a $\phi = -25\,^\circ$ and left skewed images $\phi = +25\,^\circ$. Sharp boundaries were blended by weighting each image with a Hanning window weighting function of the second order [Habtegiorgis et al., 2017; Harris, 1978]. Each image subtended $20\, degrees \times 20\, degrees$ at zero eccentricity. Figure 7 shows

an example of scenes from each image sequence. The left and right skewed stimuli were used as adapting stimuli whereas the unskewed image sequence was used as a de-adapting stimuli as will be explained in the procedure section. The content was similar in the three image sequences. Each image sequence was rendered at a rate of 20 frames per second.

Test stimuli were plaid checkerboards distorted at different skew amplitudes and comprising the same spatial dimension as the images in the adapting stimuli. The plaid checkerboards were prepared by superimposing identical contrast sinusoidal gratings oriented at $-45\,^{\circ}$ to the right and $+45\,^{\circ}$ to the left, refer Figure 20. The dimensions of the plaids' opposite diagonals were defined by the wavelengths of the component gratings in the corresponding directions, i.e. d_{right} and d_{left}, and had the same value $do = 1.24\,degrees$ of VA for a square plaid. Skew was induced by adding or subtracting Δ from the wavelengths the component gratings as in equation 7. Thus, plaids are skewed to the left when Δ is positive, and to the right when Δ is negative.

The unequal magnification factor in the oblique meridians, induced by either geometrically shearing or varying the diagonal dimensions, was used to quantify the skew amplitude as shown in equation 8.

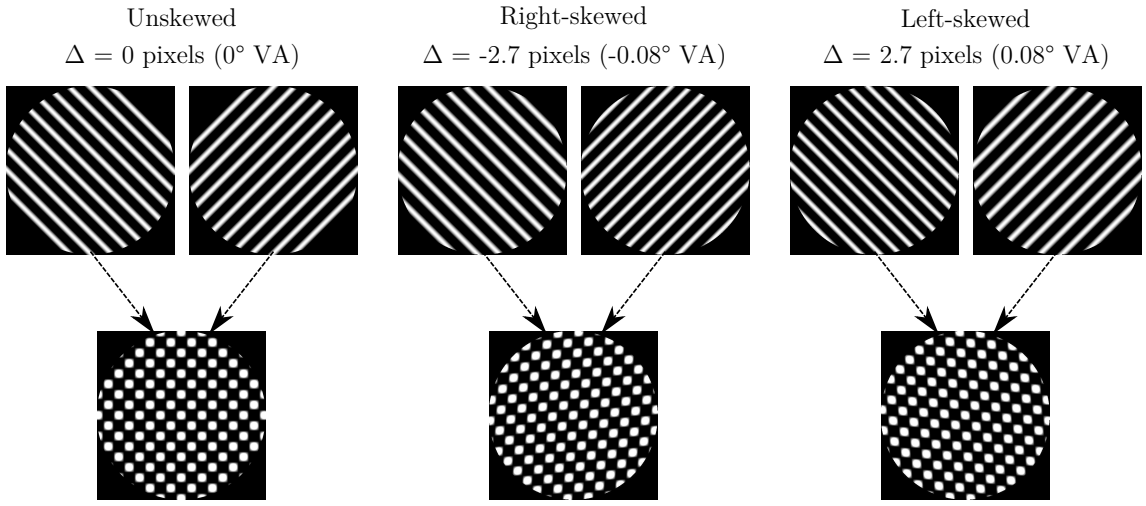

Figure 20: Examples of unskewed (at $\Delta = 0\,pixels$), left skewed (at $\Delta = 2.7\,pixels$ ($0.08\,degrees$ of VA)) and right skewed (at $\Delta = -2.7\,pixels$ ($-0.08\,degrees$ of VA)) plaid checkerboard test stimuli.

5.3.5 Procedure

All observers were trained on how to respond to the test stimuli and informed about the general measurement procedure.

Fast adaptation (FA) was evaluated five times on three measurement days with different skew EE durations, see Figure 21. On the first day of measurement, FA was

tested in session 1.1 and 1.2 respectively before and after EE1. FAs measured in session 1.1 and 1.2 were compared to test immediate facilitation induced by EE1, i.e. 30 minutes of extended exposure to each adapting image sequence. The second measurement was performed after, on average, 61 ± 1.3 days wherein FA was again tested in session 2.1 and session 2.2 respectively before and after EE2. Retained facilitation from EE1 was tested by comparing FA between session 1.2 and 2.1. Moreover comparison of FA between session 2.1 and 2.2 indicated immediate facilitation induced by EE2, i.e. 1 hour of extended exposure to each skewed adapting image sequence. Subsequently, after on average 57 ± 1 days, a retained facilitation from EE2 was tested by measuring FA in session 3.

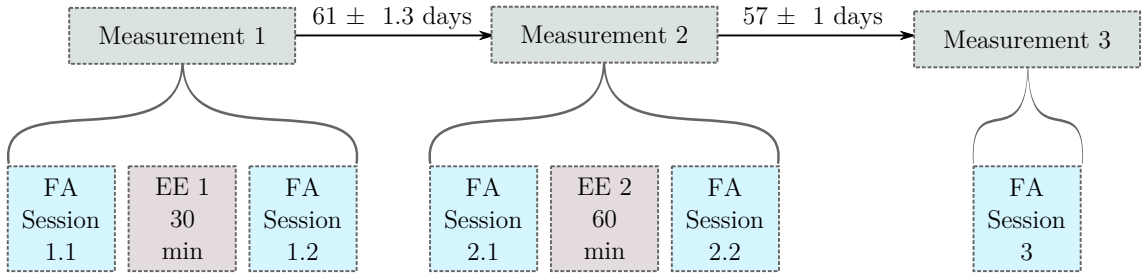

Figure 21: FA measurement paradigm to test long-term fast adaptation dynamics with time and experience. FA was evaluated five times. In session 1.1 and session 1.2, FA was measured before and after 30 minutes EE to each skew direction. On average, after 61 days, FA was again tested two times in session 2.1 and 2.2 before and after 60 minutes of skew exposure. After another, on average 57 days, FA was measured in session 3.

In FA measurement sessions, aftereffect was tested after a brief exposure to each skewed adapting stimulus with constant stimulus procedure as illustrated in Figure 22. Ten amplitudes of skew were used for the test stimuli. Observers fixated at the center of the screen. First the left skewed adapting stimuli were presented for 1 *second* followed by inter stimulus interval (ISI) of 0.25 *second* and another 0.25 *second* of test stimulus presentation. Then, observers had to respond whether the test stimulus was skewed to the left or to the right by pressing the left or the right key, respectively, within 1 *second* of response time (RT). During the ISI and RT, the screen was totally black. Afterwards, the unskewed stimuli were presented for 1 *second* followed by 0.25 *second* ISI. The undistorted stimuli were shown after each distortion FA to minimize a possible adaptation build up due to repeated exposure to the distorted stimuli and also to mimic alterations between distorted and undistorted natural environment that occurs in real world scenarios, e.g. during donning and removing of distortion inducing spectacles. Subsequently, the same steps were followed with the right skewed adapting stimuli, i.e. 1 *second* of right skew adaption, 0.25 *second* ISI, 0.25 *second* test stimulus presentation,

1 *second* RT, 1 *second* de-adaptation and then 0.25 *second* ISI. This cycle was repeated 80 times to collect 8 responses per each skew amplitude of the test stimuli. The presentation of the skew amplitude of the test stimuli was in a randomized order.

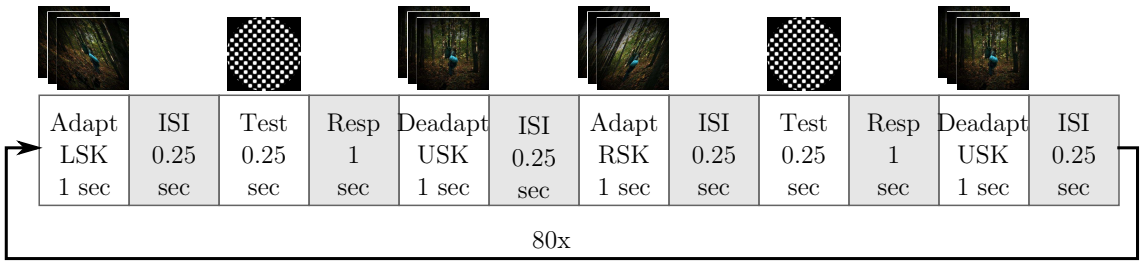

Figure 22: Scheme of FA measurement procedure. Aftereffect was tested alternately to the left skewed stimuli (LSK) and the right skewed stimuli (RSK) with constant stimulus procedure. The unskewed image sequences (USK) were presented after each adaptation as a de-adaptation to minimize a possible adaptation buildup.

5.3.6 Data analysis

Two psychometric curves of percentage of leftward responses were computed from the responses collected after left and right skew adaptations in each FA measurement session. Percentage of leftward response as a function of skew amplitude of the test stimuli was fitted with a cumulative Gaussian function using Psignifit 4.0 software (asymptotes set free but assumed to be equal) [Schutt et al., 2016]. The skew amplitude that was perceived as undistorted, the point of subjective equality (PSE), was indicated by the skew amplitude at 50 percent of leftward responses. On each measurement day, observers' PSE was tested before the adaptation sessions to test their un-adapted state responses. This un-adapted state PSE was subtracted from the PSEs of LSK and RSK FAs. Then, two parameters, i.e. $\sum PSE$ and ΔPSE, were computed from the FA PSEs as in equation 12 and equation 13. The ΔPSE quantifies the effect size and the$\sum PSE$ quantifies the direction bias of alternate LSK and RSK adaptations in FA sessions.

$$\Delta PSE = PSE_{LSK} - PSE_{RSK} \tag{12}$$

$$\sum PSE = PSE_{LSK} + PSE_{RSK} \tag{13}$$

The overall effects were calculated by averaging the $\sum PSE$s and ΔPSEs of all the observers in each session. A paired sample t-test was used to evaluate the significance of $\sum PSE$s and ΔPSEs due to the FAs and to compare the parameters between the different sessions.

5.4 Result

The overall observers' shift in perception due to the FA in each session is shown in Figure 23a in terms of averaged ΔPSE. In all the sessions, the PSE shifted towards the adapting skew direction. A significant positive ΔPSE was obtained in all the sessions, $p < 0.01$. The trend of this shift is the same as previously shown skew induced adaptation aftereffects [Habtegiorgis et al., 2017]. After exposure to left skewed natural stimuli, observers perceived left skewed checkerboards as unskewed and vice versa after right skew exposure. Comparing the FA magnitude between sessions, the ΔPSEs measured in session 1.1 and session 1.2 were not significantly different from one another. Similarly, the FA measured in session 1.2 and session 2.1 were not different from one another. The 30 minutes exposure in session 1 thereby did not induce any significant change in the FA dynamics that was retained for, on average, 61 days. However, after 1 hour of skew exposure, a significant increase in FA was obtained in session 2.2 relative to previous FA in session 2.1; $p < 0.001$. Thus, there was immediate facilitation due to the 1 hour skew exposure. Furthermore, this facilitation was retained for, on average, 57 days wherein the FA magnitude in session 3 was significantly higher than session 2.1 ($p < 0.01$) and session 1.1 ($p < 0.03$) and not different from session 2.2 ($p > 0.05$). The $\sum PSE$ was not significantly different from 0 ($p > 0.05$) in all the sessions. There was also no significant difference of $\sum PSE$s across sessions. Thus, no discernible direction bias was conceived from any of the FA and EE sessions. In the subsection 5.7, a plot is provided showing the raw PSE_{LSK} and PSE_{RSK} values of individual observers' and overall averages.

The corresponding long-term change in the psychometric curves of all observers' responses collected in session 1.1, session 2.1 and session 3 is shown in Figure 23b. To ease the realization of the amount of shift in responses in the different sessions, the curves from each session are calibrated in the x-axis by the PSE measured after the RSK adaptation. Thus, in each session, the amount of the perceptual shift after the alternate skew exposures is indicated by position of the LSK adaptation PSE relative to a common point 0. The FA induced shift in the psychometric curves was increasing depending on amount of previous skew experience. The psychometric curves clearly shows a larger shift of perception in session 3 than in session 2.1 relative to the baseline measurement in session 1.1.

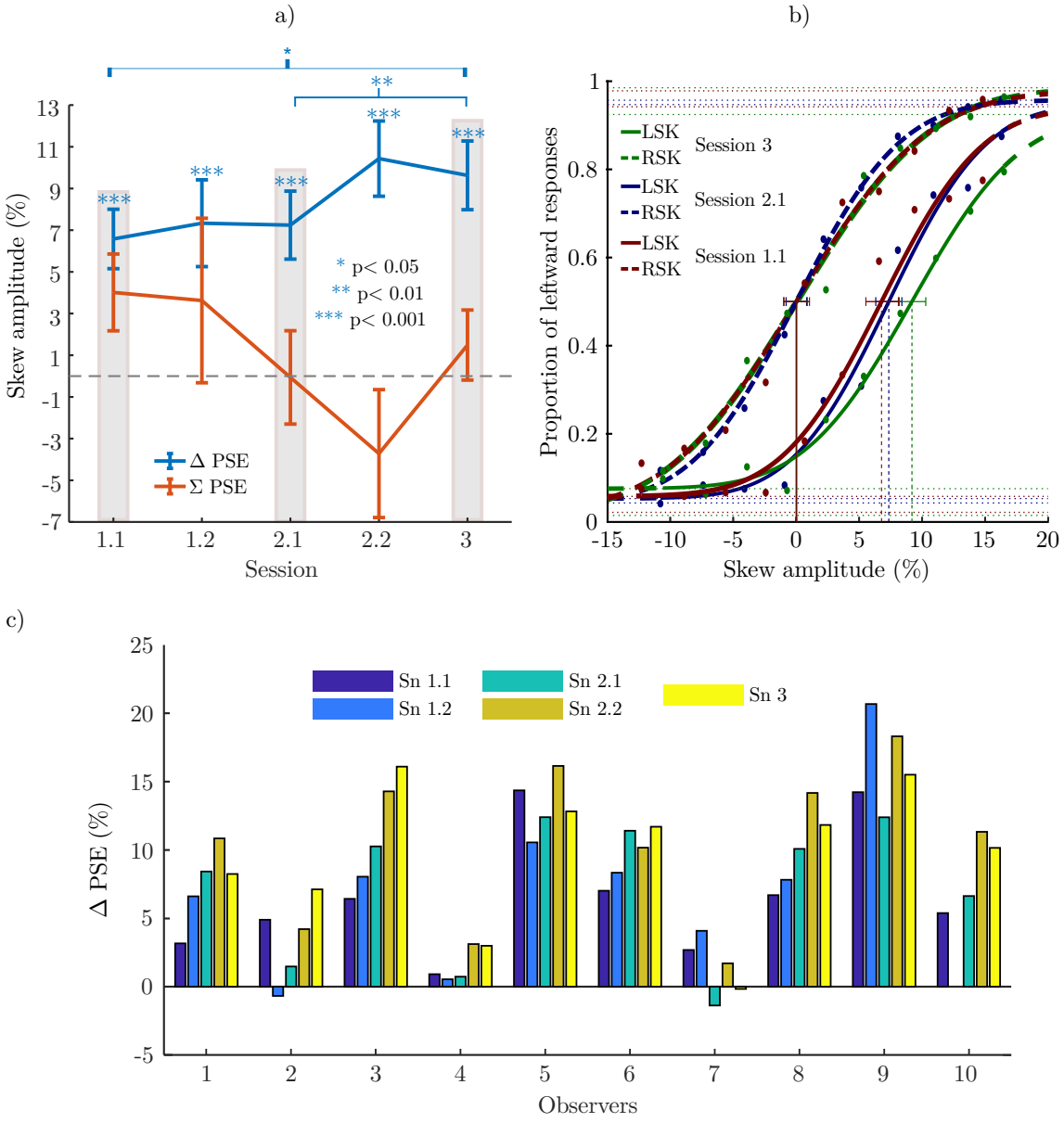

Figure 23: Time and experience dependent FA dynamics. FA is estimated by the ΔPSE after alternate brief exposure to left and right skewed natural image sequences. a) The overall FA in the five sessions: the averaged ΔPSEs and $\sum PSE$s from all the observers. The connecting line illustrates the trend of the ΔPSEs and $\sum PSE$s across the sessions. The error bars around the average represents the standard errors. The transparent bars show the data used to illustrate the long-term retention effect considered in Figure 23b. b) Long-term changes in the FA psychometric curves of all the observers' responses: measured at first day in session 1.1 (red), after 61 ± 1.3 days in session 2.1 (blue) and after another 57 ± 1 days in session 3 (green). For each session, the curves are calibrated in the x-axis to the RSK adaptation PSE. The Gaussian fitted function and the confidence intervals at PSE are shown by the broken lines for the RSK adaptation aftereffects and in solid lines for the LSK adaptation aftereffects. c) The individual observer's $\Delta PSEs$ in the five sessions.

In sum, after a brief exposure to skewed natural scenes, FA was observed. Furthermore, 1 hour of exposure to image skew induces facilitation in the FA dynamics which can be retained for over a month.

5.5 Discussion

In this study, experience dependent and long-term retained facilitation of skew adaptation was presented. Visual adaptation to geometrical skew distortion was induced in response to distorted natural image sequences. The adaptation aftereffect was tested via a skew identification in a simple geometrical pattern; specifically a checkerboard. In line with previous finding, oppositely skewed dynamic natural image sequences led to adaptation aftereffects in opposite directions [Habtegiorgis et al., 2017]. Facilitated fast adaptation was obtained after 1 hour of extended exposure to the skewed natural stimuli. A long-term retained facilitation was demonstrated after, on average, 57 days during which there was no skew exposure.

Previous studies have shown similar long-term effects in perceptual learning, depending on particular tasks and stimuli [Ball and Sekuler, 1987; Fahle, 2002; Fiorentini and Berardi, 1981; Gibson, 1969; Karni and Sagi, 1991; Redding et al., 2005; Sagi and Tanne, 1994]. However, in the paradigm followed in the present study, no feedback was given regarding a mistake or a correct response given by the observers. Thus, there was no opportunity of task related perceptual learning during aftereffect measurement. Therefore, extended exposure to skew geometric distortions in an hour time scale, induced visual adaptation and distortion information were retained long-term and facilitated future adaptations.

Adaptation is a mechanism that happens at several time scales. Adaptation to changes that occur frequently in the natural world is rapid to allow the visual system to operate in a wide range of conditions, such as to continuously varying luminance, contrast, colour and orientation. Adaptation to rare and subtle alterations, on the other hand, is rather slow, e.g. in adaptation to changes by wearing new glasses. It is commonly known that the visual system starts to adapt quicker after repeated exposure to these subtle changes. Experience dependent facilitation of adaptation to colour and blur features demonstrated these dynamics [Engel et al., 2016; Yehezkel et al., 2010]. Observers who wore coloured glasses for 14 months exhibited faster adaptation to colour changes than control groups. Four hours of extended exposure to blur also induced facilitation which was retained for a day. These results suggested that prior experience to recurrent alterations allows the visual system to adapt fast. Our study reveals a novel long-term plasticity of the visual system to geometrical distortion. We found a long-term facilitatory effects after 1 hour of skew exposure. Exposure duration of one hour is rather short compared to the other facilitation studies [Engel et al., 2016;

Yehezkel et al., 2010]. Moreover, the retention duration of this facilitation, i.e. on average for 57 days, was longer than previous long-term retention reports [Yehezkel et al., 2010]. Long-term effects of this form have not been reported so far and would thus point to a long retained learning component in adaptation.

We tested the long-term facilitation of skew adaptation sequentially for two time scales of extended exposure; first for 30 minutes and then for 1 hour. An immediate and retained facilitation effect was found almost two months after the 1 hour of exposure but not after the 30 minutes of exposure. The exposure time thereby has an effect on the facilitation. The 30 minutes of exposure might not have accumulated enough information about the skew to induce long-term facilitation. The long-term facilitated re-adaptations after 1 hour skew exposure in our study could have had two possible origins. The first possibility is that the 1 hour of exposure was enough per se to induce the retained facilitation. Second, some information might have been retained for two months after the prior 30 minutes exposure which was not enough to facilitate the adaptation but subsequently adds to the 1 hour exposure and contributes to the facilitation.

The facilitation of visual adaptation with extended exposure to the image skew might be governed by an inference process similar to the recently demonstrated effect of repeated donning and removing of colour filters [Engel et al., 2016; Grzywacz and de Juan, 2003; Kording et al., 2007; Wark et al., 2009]. In inference theory, the visual system adjusts its response to infer the environment under Bayesian decision making framework the parameters of which could be affected by previous stimulus history. Thus, according to the inference model of adaptation, previously acquired distortion information possibly increases the prior probability of the distorted scenes to re-occur or their likelihood which determines their detectability. If distorted scenes are recurrent, it would also be costly to the visual system to adapt slowly every time the distortions are reapplied. Moreover, to minimize the risk of error driven fluctuations in neural responses, optimum perceptual adjustments to some subtle or rare environmental alterations, like our skew distortions, might be rather slow [Todorovic et al., 2011; Wark et al., 2009]. However, extended exposure to the distortions could accumulate enough evidence about the distortions outweighing the risk of fast readjustments when the distortions reappear again. Accordingly, with past experience to the distortions, the visual system might have learned to re-adapt fast.

Physiologically, synaptic changes between neurons are one of the possible underling mechanisms for stimulus dependent sensory response changes, like adaptation [Castellucci et al., 1970; Thompson and Spencer, 1966]. Studies have suggested that short term adjustments operate upon presynaptic terminals through a reduction of effective neurotransmitter release [Hawkins et al., 1993] while long-term adjustments are pos-

sibly associated to structural changes in presynaptic terminals [Tetzlaff et al., 2012; Wang, 1993]. Exposure to a skewed natural environment affects multiple levels in the visual hierarchy [Habtegiorgis et al., 2017]. In line with the aforementioned studies, we suggest that the observed long-term facilitation of visual adaptation to image skew possibly constitutes long-term synaptic changes in the intra-cortical circuitry that encode features altered by the image skew, e.g. orientation, magnification or optic flow direction.

Habituation to progressive lenses might consist of oculomotor and visual components. Skew adaptation, although it simplifies the visual input, has been shown to mirror a variety of properties of the visual component of the habituation process. The current manuscript shows long-term retention of skew adaptation, as it occurs in a habituated progressive lens wearer. In contrast to skew adaptation in the present study, progressive lenses show a complex pattern of distortions. Skew produced by PALs is in opposite directions on the left and right side of the lens resulting in a different skew for each gaze direction. Parts of this complex adaptation are carried by a spatiotopic adaptation mechanism, retaining adaptation at a definite spatial location across saccades, and a retinotopic mechanism which has to adapt to specific distortions for different gaze directions [Habtegiorgis et al., 2018]. During habituation, fast adaptation is needed in these mechanisms, e.g. to skewed and unskewed environment during donning and removing of spectacles and to opposite skews during gazing through the opposite parts of PALs specifically in the retinotopic mechanism. Thus, the FA paradigm followed in the present study can be used as a valuable tool to systematically explore the ability of these mechanisms to handle habituation to complex distortions of PALs.

Distortion of the environment is a daily visual constraint in spectacle lens wearers. These modifications can be challenging in day to day living, e.g. when mobility is affected by distortion induced spatial disorientation [Johnson et al., 2007]. Proper and fast habituation is therefore essential to optical modifications. Here, we showed long-term facilitation of adaptation to skew geometrical distortions with ecologically valid stimuli. The reported adaptation dynamics could be one of the possible mechanisms to compensate for skew distortions commonly occurring in spectacles [Meister and Fisher, 2008a]. Our approach provides a new insight to address the habituation process to PALs.

To summarize, with extended exposure to skew geometric distortions in an hour time scale, adaptation can be facilitated in the long-term, enabling fast visual adjustments whenever the distortions are reapplied.

5.6 Acknowledgments

We acknowledge support by Deutsche Forschungsgemeinschaft and Open Access Publishing Fund of University of Tübingen. This project has received funding from Eberhard-Karls-University Tübingen (ZUK 63) as part of the German Excellence initiative from the Federal Ministry of Education and Research (BMBF), and from the European Union's Horizon 2020 research and innovation programme under the Marie Skłodowska-Curie grant agreement No 734227 – Platypus.

5.7 Supporting data

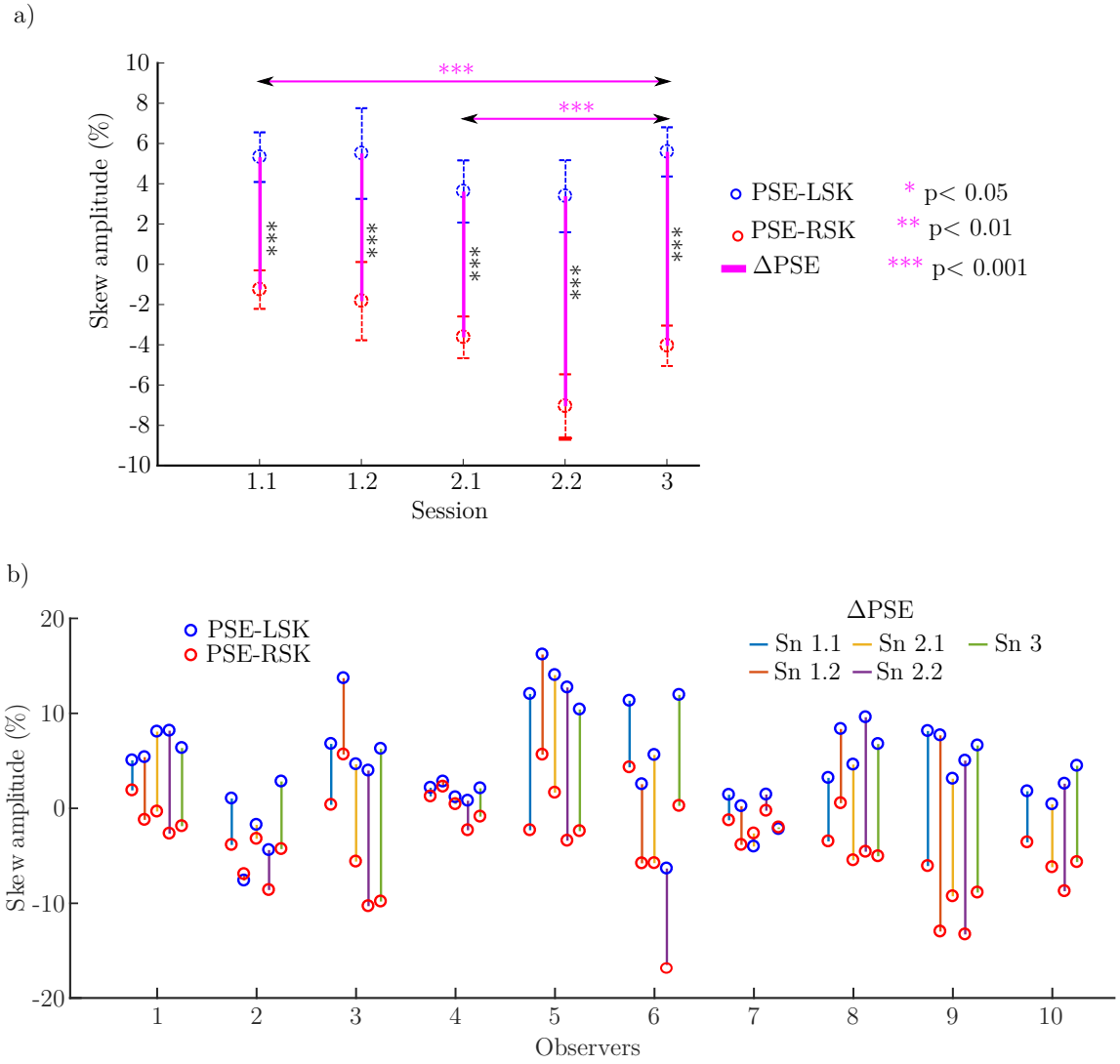

Figure 24: Figure. a) The overall data from all the observers in the five sessions: the averaged LSK and RSK PSEs are presented by the blue and red dots, respectively, with the standard errors of the average presented as the error bar around them. The pink line shows the adaptation effect size, ΔPSE, in each session. The facilitation effect can be seen as an increase in the ΔPSEthrough the sessions. b) Individual raw data from each observer in the five sessions. The LSK and RSK PSEs in each session are presented by the blue and red dots, respectively. For each observer, the $\Delta PSEs$ in the different sessions is shown by the different coloured lines between the LSK and RSK data points.

6 Functional role of cortical organisation in robust adaptation to distortions of natural scenes

Habtegiorgis, S. W., Jarvers, C., Rifai, K., Neumann H., & Wahl, S. (2019). The role of bottom-up and top-down cortical interactions in adaptation to natural scene statistics. Frontiers in neural circuits, 13, 9. doi: 10.3389/fncir.2019.00009.

6.1 Abstract

Adaptation is a mechanism by which cortical neurons adjust their responses according to recently viewed stimuli. Visual information is processed in a circuit formed by feedforward (FF) and feedback (FB) synaptic connections of neurons in different cortical layers. Here, the functional role of FF-FB streams and their synaptic dynamics in adaptation to natural stimuli is assessed in psychophysics and neural model. We propose a cortical model which predicts psychophysically observed motion adaptation aftereffects (MAE) after exposure to geometrically distorted natural image sequences. The model comprises direction selective neurons in V1 and MT connected by recurrent FF and FB dynamic synapses. Psychophysically plausible model MAEs were obtained from synaptic changes within neurons tuned to salient direction signals of the broadband natural input. It is conceived that, motion disambiguation by FF-FB interactions is critical to encode this salient information. Moreover, only FF-FB dynamic synapses operating at distinct rates predicted psychophysical MAEs at different adaptation timescales which could not be accounted for by single rate dynamic synapses in either of the streams. Recurrent FF-FB pathways thereby play a role during adaptation in a natural environment, specifically in inducing multilevel cortical plasticity to salient information and in mediating adaptation at different time-scales.

6.2 Introduction

Our visual perception is always affected by what we have observed in the past. For instance, after watching a moving entity after a prolonged amount of time, e.g. sea waves, stationary objects appear to move. Neurons in the visual system decrease their sensitivity after prolonged exposure to a specific type of visual input resulting in such concomitant perceptual modification for subsequently viewed stimulus [Blakemore and Campbell, 1969; Clifford et al., 2007; Fang et al., 2005; Mather et al., 1998]. This experience dependent change in the visual system is called adaptation. Adaptation has a key role for optimal and stable perception in a continuously changing natural environment [Clifford et al., 2000; Kohn, 2007; Webster, 2011, 2015].

The natural environment is characterized by large variations of several attributes [Betsch et al., 2004; Bex et al., 2005, 2007, 2009; Billock et al., 2001; Dong and Atick, 1995]. The design of the visual system is likely to mirror and efficiently compute the statistical properties of these attributes [Eckert and Zeil, 2001; Geisler, 2008; Kayser et al., 2004; Simoncelli, 2003; Snow et al., 2017]. Visual information is processed in a cortical circuit formed by synaptic organization of feedforward (FF) and feedback (FB) connections between different cortical areas [Mather et al., 2008; Rokszin et al., 2010; Sillito et al., 2006; Stuit, 2009]. One form of FF-FB recurrent interaction is a driving FF input from lower to higher cortical areas and a re-entrant modulatory FB enhancing the input signal matching to responses of higher cortical areas [Sillito et al., 2006; Friston and Büchel, 2000; Hupe et al., 2001]. The FB modulation acts as a prediction signal from higher to lower cortical areas and allows propagation of disambiguated signals through the network. This benefits to extract global salient information from a noisy input during response normalization process among a pool of neurons [Sillito et al., 2006; Friston and Büchel, 2000; Hupe et al., 2001]. Yet, the functional role of FF-FB recurrent interaction is not resolved for adaptation to features of the natural environment which are broadband and noisy.

Another unexplored functional relevance of reciprocal visual streams to adaptation is their synaptic dynamics. Activity dependent changes in synaptic inputs are one of the underlying mechanisms for adaptation [Abbott et al., 1997; Webster, 2015]. The visual system adapts to changes in the environment that last for a wide range of durations. How synaptic adaptations in the FF and FB connections mediate adaptation at different time-scales is an open question. Specifically, if synaptic adaptation at a single rate in either of the streams or at distinct rates in both streams underlie adaptation is yet unknown.

In the present study, we investigated the functional relevance of FF-FB cortical organization to the adaptation processes during natural viewing with psychophysical experiments and model simulations. Statistics of different features in the natural environment is often altered by geometric distortions of daily used optical elements. Two prominent examples of distorting optical elements are progressive addition lenses (PALs) and VR displays. The distortions in these optical elements introduce perceptual discomforts in a significant amount of wearers [Barrett, 2004; Bashiri et al., 2017; Johnson et al., 2007; Meister and Fisher, 2008a; Sheedy and Andre, 2013; Yao et al., 2014]. However, after prolonged use, wearers report vanishing of the side effects indicating adaptation [Alvarez et al., 2017; Barrett, 2004; Yao et al., 2014]. In this contribution, adaptation to distortion induced alterations is thereby used as a model system to address day to day visual experiences in a large number of populations who benefit from these optical elements [Aller, 2013; Bashiri et al., 2017; Holden et al.,

2008; Keshner, 2004; Laver et al., 2012; Meister and Fisher, 2008a].

Distortions prominently alter motion direction statistics of the natural visual input, e.g. skew geometric distortion in PALs [Meister and Fisher, 2008a]. Accurate motion perception has a key role in successful interaction with the dynamic natural world, be it in the inference of the direction of moving entities, or navigation through the environment. Its alteration by image skew is possibly one of the causes for the difficulties experienced by novice PAL wearers, like spatial disorientation during navigation [Johnson et al., 2007]. Visual adaptation to distortion induced alteration in motion direction statistics of the natural visual world is thus essential to successfully use such optical utilities. In this representative example, we assessed the functional role of recurrent streams to adaptation within motion processing cortical areas, in particular to aspects of neural response tuning and time-scales of adaptation.

We quantified motion direction statistics of skewed and un-skewed natural image sequences to assess the skew effect. Adaptation to skew induced motion alteration was probed in psychophysical experiments by persisting perceptual adjustments, i.e. motion direction adaptation aftereffects (MAE), after exposure to the skewed natural stimuli at different time-scales. Our model architecture is based on a biologically inspired model of recurrent visual motion processing in the dorsal pathway of the visual system, namely in V1 and MT, comprising FF-FB pathways and activity normalization in each model area [Bayerl and Neumann, 2004, 2007; Bouecke et al., 2011; Raudies and Neumann, 2010]. We suggest dynamic synapses within direction processing intracortical circuitry as adaptive mechanisms. Assessing neural responses across V1 and MT model units with and without FB stream, physiologically plausible response tuning was observed during and after adaptation only when FB was integrated. FF-FB interaction additionally leads to synaptic adaptation within neurons selective to a salient motion direction signal by enhancing it over the noisy natural input. Furthermore, comparing prediction performance of different variants of the suggested model, the psychophysically observed MAE at different time-scales are best predicted by distinct adaptive mechanisms in FF and FB streams than a single adaptive mechanism in either FF or FF-FB circuitry. In sum, recurrent bottom-up and top-down cortical streams are integral parts of adaptation in a natural environment and multiple dynamic synapses operating at different time scales within the reciprocal streams mediate temporal context dependency of this adaptation.

6.3 Results

6.3.1 Image skew alters motion direction statistics of natural image sequences

Natural image sequences were acquired from an open source movie as they are exemplary for everyday visual input. Opposite skew geometric distortions, i.e. up-skew (USK) and down-skew (DSK), were simulated in the images. The average motion direction statistics of the skewed and un-skewed image sequences were quantified by correlation based Reichardt motion detectors. Detailed descriptions of distortion simulation and motion detection are provided in the section 6.6 and section 10.2, respectively. As illustrated in Figure 25, motion direction signal statistics in the un-skewed image sequence is broad band but dominated by horizontal direction signals. In the skewed natural image sequences, the dominant signal is shifted in the skewing direction, i.e. to the positive in USK stimuli and to the negative in the DSK stimuli.

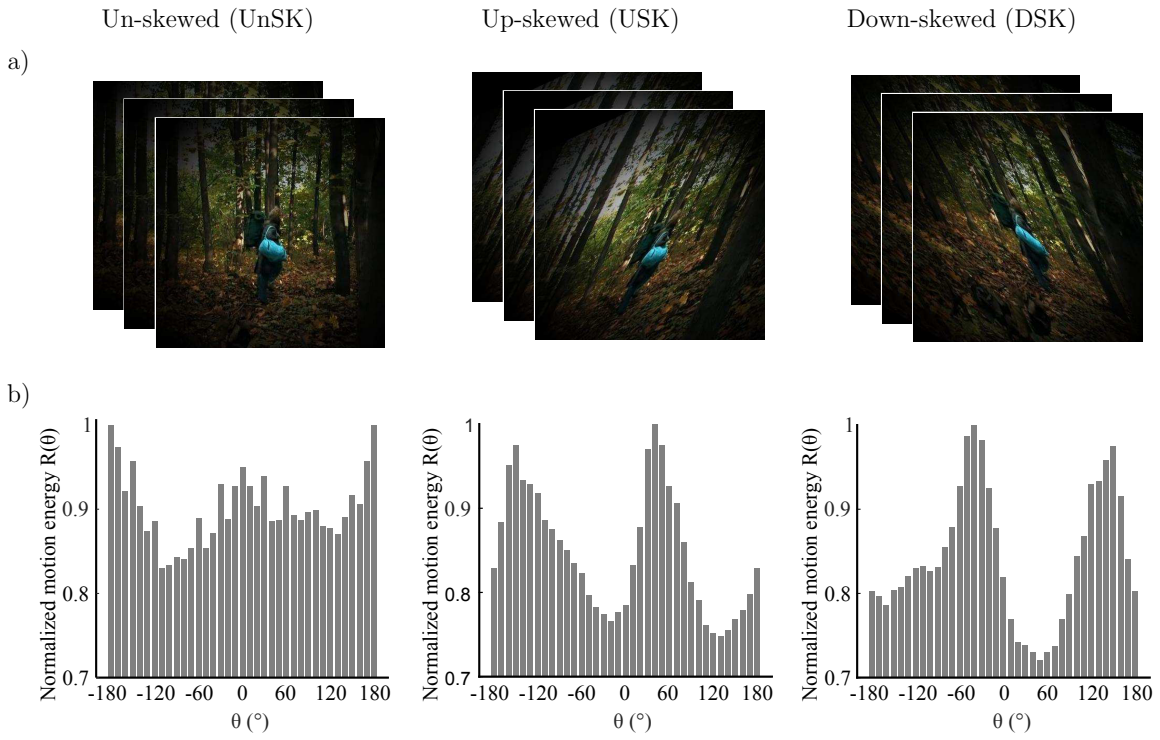

Figure 25: Illustration of the effect of image skew on motion direction statistics of natural image sequences. a) Examples of un-skewed (UnSK), up-skewed (USK) and down-skewed (DSK) natural images that are weighted by a circular shape Hanning window. b) Average motion energy from 12,000 natural image sequences as a function of motion direction (θ). Motion direction statistics of UnSK, USK and DSK natural image sequences was detected by correlation based Elaborated Reichardt detectors (ERDs)[Bayerl and Neumann, 2004; Reichardt, 1987]. Negative θ represents downward and positive θ represents up-ward motion directions.

6.3.2 Evaluation of skew induced MAE

MAE was tested after sequential exposure to DSK then USK natural image sequences. Adaptation aftereffects of each adapting skew direction were tested by the motion direction of a coherently moving random dot test stimuli that was perceived as horizontal, i.e. equally likely to be upward and downward in a method of constant stimulus procedure. From here on, we refer to this parameter as point of subjective equality (PSE).

Figure 26 illustrates the basic schematics of the three psychophysical experiments used to evaluate distortion induced adaptation. Experiment 1 and 2 were designed to test MAE after short and long timescales of skew exposure with randomized order of test stimuli motion direction. The results of these experiments were used to fit model parameters and to test prediction performances at different timescales. In experiment 3, MAE was tested after short skew exposure with sequentially increasing or decreasing order of test stimuli motion direction to introduce additional hysteresis effect, i.e. from down to up direction for the DSK adaptation and from up to down for the USK adaptation. Perceptual hysteresis occurs when motion direction of an input stimulus changes gradually, e.g. from up to down direction or vice versa, due to internal short term memory of the underling neural network as was previously demonstrated in computational findings [Bayerl and Neumann, 2004; Williams and Phillips, 1987]. Accordingly, the results of experiment 3 were used as an additional dataset to validate the models' predictions and in particular contribution of FB in the network short term dynamics. Detailed explanation of the psychophysical experiment procedures are included in the Methods section.

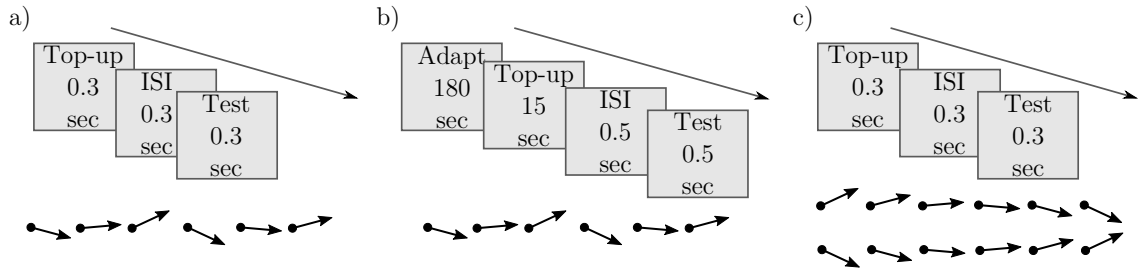

Figure 26: Basic illustration of MAE measurement experiments. a) Experiment 1: MAE after short skew exposure; each adapting skew top-up and test stimuli presentation lasted for 0.3 *seconds* separated by same duration of black screen presentation in the inter stimulus interval (ISI) period. b) Experiment 2: MAE after long skew exposure; prior 180 *seconds* of skew adaptation followed by 15 *seconds* of top-up, 0.5 *seconds* of ISI and 0.5 *seconds* of test stimuli presentation. c) Experiment 3: MAE after short skew exposure and hysteresis effect; each top-up,ISI and test stimuli presentation lasted for 0.3 *seconds*. The dot ended arrows represent if the order of the test stimuli between successive trials was randomized, in a and b, or sequential, in c.

6.3.3 Distortion induced MAE: Psychophysics

Figure 27 shows the psychometric curves of overall observers' responses recorded after skew exposure in the three psychophysical experiments. The percentage of upward responses is plotted as a function of test stimulus motion direction, θ. A negative θ value corresponds to a downward motion direction and a positive value to an upward one.

The shift in the PSEs of the opposite skew adaptation, i.e. $\Delta PSE = PSE_{USK} - PSE_{DSK}$, was significantly positive in all the three experiments (paired sample t-test, $p < 0.05$). After adaptation to up-skewed natural stimuli, observers perceived an upward motion direction as horizontal and vice versa. Thus, the PSE shifted to the direction of the adapting skew whereas the physical horizontal motion direction is perceived to be shifted in the opposite direction. Furthermore, in all the experiments, the PSEs from the two oppositely skewed stimuli were not symmetric about the physical 0° of motion direction albeit the amount of the skew in the adapting stimuli was equal in magnitude. This is illustrated by a significant bias in the sum of the PSEs, $\sum PSE = PSE_{USK} + PSE_{DSK}$, in all experiments towards the negative; paired sample t-test $p < 0.05$. The asymmetry conceivably reveals either the adaptation state induced by the first DSK exposure which was not recovered during the subsequent USK exposure or due to a relative difference in the strength of the DSK than the USK adapting signal, where both are not mutually exclusive.

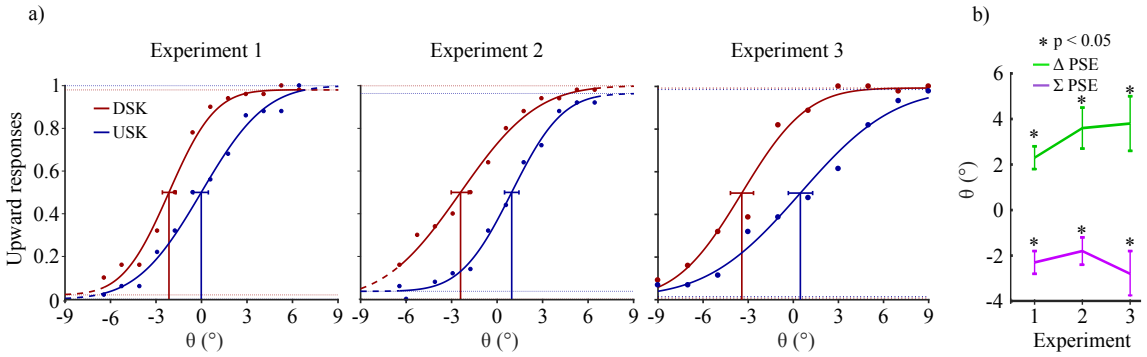

Figure 27: a) Psychometric functions of overall observers' responses in the three experiments. In each psychometric plot, the Gaussian fitted plot and the confidence intervals at PSE are respectively shown in red for the DSK adaptation aftereffects and in blue for the USK adaptation aftereffects. b) Overall observers' averages of ΔPSE and $\sum PSE$. The error bars show the standard errors of the averages.

Thus, multiple dynamic synapses within FF-FB circuitries explains adaptation at different time scales of skew exposure.

6.3.4 Model: dynamic synapses within a recurrent motion processing cortical circuit

Activity dependent short term synaptic depression is one potential source of neural response adjustments during adaptation [Abbott et al., 1997; Castellucci et al., 1970; Kohn, 2007; Regehr, 2012; Tetzlaff et al., 2012; Webster, 2015]. The strength of synaptic coupling between cells, i.e. synaptic efficacy, depends on the presynaptic vesicle occupancy which is the amount of releasable neurotransmitters [Hennig, 2013]. Repeated activation of the post synaptic cell by the presynaptic cell causes depletion of these vesicles and a concomitant reduction in postsynaptic response [Hawkins et al., 1993; Hennig, 2013; Zucker and Regehr, 2002]. If the excitation input is removed from the presynaptic neuron, the synaptic strength will slowly restore until the vesicles are fully replenished. Short term synaptic depression has been previously revealed in different cortical areas and its potential implications in various dynamics of recurrent cortical neural networks has been reported [Abbott et al., 1997; Tsodyks et al., 1998; van Rossum et al., 2008; York and Van Rossum, 2009]. The ubiquity of short term synaptic depression in several of cortical areas, reflects that it is a characteristic mechanism across cortical circuitries underlying neural response adjustments during adaptation. Such dynamic synaptic mechanism in motion processing cortical circuitry potentially underlies the psychophysically demonstrated distortion induced MAE. Wherein, during adaptation, exposure to distorted motion direction information decreases the synaptic strength between neurons selective to those directions. Subsequently, when test stimuli are presented before the synaptic strength is replenished, an aftereffect can be observed. Accordingly, such synapse specific gain control mechanism within a recurrent motion processing cortical circuitry is considered in our model to investigate response adjustments of motion processing neurons during exposure to motion information altered by distortions.

Our model extends a previously developed architecture for recurrent motion processing in V1 and MT areas comprising FF and FB recurrent streams [Bayerl and Neumann, 2004]. This model framework has been selected as it considers a characteristics feature of the cortical architecture, i.e. bidirectionally connected cortical areas, which would allow us to assess the relative contribution of the reciprocal streams for the adaptation process. Furthermore, this model has been shown to be able to predict data from neurophysiological recordings as well as behavioural studies [Bayerl and Neumann, 2004, 2007; Bouecke et al., 2011; Raudies and Neumann, 2010]. Direction tuned neural activation is described by a membrane potential of a single compartment cell model that depends on excitatory, modulatory and inhibitory synaptic inputs. As an extension, dynamic synaptic efficacies were considered in the FF and FB excitatory connections to introduce synaptic adaptation in the model.

A scheme for the basic architecture of the model in cascaded motion processing at different cortical areas is illustrated in Figure 28. The model starts with preprocessing of the input by LGN cells followed by motion direction signal detection by direction selective filters in V1 that are implemented as spatiotemporal correlation techniques (ERDs). The subsequent recurrent motion direction processing by direction selective cells within areas V1 and MT is the main component of the model where synaptic plasticity is implemented. In this stage, dynamic synapses within reciprocal FF and FB streams are taken into account to introduce plasticity. The dynamic synapse constitutes short-term synaptic adaptation as a consequence of vesicle depletion and replenishment that occur during the presence and absence of excitatory presynaptic signals, respectively. This is realized by dynamic synaptic efficacy parameters that weight the FF and FB excitatory inputs from V1 to MT and from MT to V1, respectively. As a final stage, a steady-state model of decision-making layer maps MT responses into 'upward' and 'downward' responses in order to account for the decision process employed in the psychophysical experiments. The computational modelling of the synaptic efficacies and neural activations is described in detail in the section 6.6.

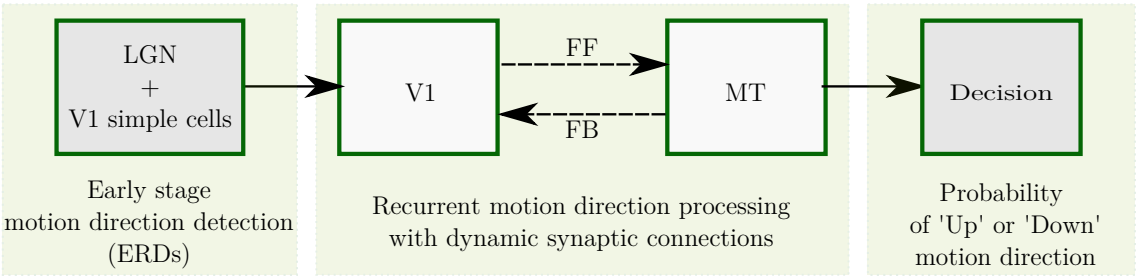

Figure 28: Overview of recurrent motion processing in cascaded model areas and their interactions. Motion is initially detected from image sequences in sequential early stage preprocessing by LGN and V1 simple cells which is realized by ERDs. Motion direction signals are subsequently processed in a recurrent loop of direction selective cells in V1 and MT connected by FF and FB streams. This stage is the core component of the model where synaptic plasticity is introduced within the FF and FB streams as highlighted by the broken lines. A steady-state model of decision-making finally maps MT responses into 'upward' and 'downward' responses.

Previous findings reported that adaptation at different timescales is mediated by multiple adaptive mechanisms which operate at distinct rates [Mesik et al., 2013]. Specifically, these findings suggested that a fast adaptive mechanism, which adapts and de-adapts fast, and a slow adaptive mechanism, which adapts and de-adapts slow, coexist in a cortical circuit to mediate adaptation at different timescales. In line with these findings, in our model variants, distinct fast and slow dynamic synapses tuned to different adaptation rates are considered. As explained in detail in the following paragraph, in the fast dynamic synapses, the rates of vesicle depletion and replenishment

were fitted to replicate MAE from milliseconds of skew exposure in experiment 1. In the slow dynamic synapses, the rates of vesicle depletion and replenishment were fitted to replicate MAE time scales of minutes of skew exposure in experiment 2 (see Methods section). To test if the synaptic dynamics in the recurrent FF-FB streams could underlie these findings, predictions of MAEs in the three psychophysical experiments were tested from five different model variants. As illustrated in Figure 29a, the model variants were defined by considering different complexity of the circuitry, either only FF or FF-FB, and different temporal rate dynamic synapses, either single or multiple dynamic synapses. Adaptation is commonly modeled as a reduction in input gain or changes in the strength of normalization within a single cortical area without recurrent connectivity. Using this approach as a baseline, model variant 1 and model variant 2 comprise a simple FF circuit with a dynamic synapse which changes the response gains of MT responses. The rates of the dynamic synapses in model variant 1 and model variant 2 were fast and slow which were fitted to replicate the psychophysical results of experiment 1 and experiment 2, respectively. To compare the recurrent FB effect, model variant 3 and 4 were defined by considering a FB circuit. Analogous to the first two model variants, model variant 3 and model variant 4 comprise either fast FF and slow FB dynamic synapses fitted to replicate psychophysical results of experiment 1 and experiment 2, respectively. With the presumption that FF mechanisms are faster than feedback mechanisms [Thiele, 2012; Roth and van Rossum, 2009; York and Van Rossum, 2009; Destexhe et al., 1998], fast dynamic synapses are considered in the FF stream and slow dynamic synapses are considered in the FB stream. In contrast to the above four model variants comprising single adaptive mechanism, model variant 5 was defined by considering dynamic synapses in both FF and FB circuits which operates at distinct timescales. The rates of its FF and FB dynamic synapses were taken from model variant 3 and model variant 4, respectively. The prediction performance of each model variant was validated with either experiment 1 or experiment 2 to which they were not fitted to and with an additional data set from experiment 3. Finally, the role of FF-FB interaction on neural response tuning properties has been investigated by comparing neural responses of model variant 1 and model variant 5 in the absence and presence of FB, respectively. For each model, the mathematical computation and exact values of the model parameters are provided in the section 6.6.

6.3.5 FF-FB functional role in adaptation at multiple time-scales

The human visual system optimally adapts to the changes in the natural environment which span different timescales. As suggested by previous studies, multiple adaptive mechanisms potentially underlie adaptation at different timescales [Bao and Engel, 2012; Bao et al., 2013]. However, if these multiple adaptive mechanisms correspond to

the dynamic synapses in the recurrent FF-FB streams of the cortical circuitry has not been previously assessed. To test the functional relevance of FF-FB circuits, specifically their synaptic dynamics for mediating MAE at different time-scales, we compared prediction performance of the first four model variants with dynamic synapses operating at a single rate to model variant 5 which entails different rate dynamic synapses in the FF and FB circuits.

A summarized prediction performance of each model variant is shown in Figure 29. The psychometric curves of model predictions together with the psychophysical results are presented in the Section 6.10. Model variants constituting a single adaptive mechanism, variant 1-4, does not predict $\Delta PSEs$ and $\sum PSEs$ at the time scales of adaptation other than they are fitted to. Model variant 1, comprising FF circuit with the fast dynamic synapse, does not predict any of the experiments and gives the largest prediction error. The fast synaptic mechanism of model variant 3 predicts only short adaptation MAEs in experiment 1 and 3 and not the MAEs from the long exposure in experiment 2. The slow dynamic synapses of model variants 3 and 4 predict the MAEs only from long exposure in experiment 2 but not from the short exposures in experiment 1 and 2. Model variant 5, comprising distinct fast and slow dynamic synapses in FF and FB streams, predicts all the three skew induced MAEs at the different time-scales. From the overall prediction, this model variant performed best. Furthermore, among the model variants with fast dynamic synapses, only those with FB circuit predicted experiment 3 albeit all were fitted to that specific adaptation timescales. This indicates FB is an integral part of the neural network underlying adaptation.

a)

	Circuit	Dynamic synapse	Experiment 1	2	3
Model 1	FF	fast FF	fitted	x	x
Model 2	FF	slow FF	x	fitted	x
Model 3	FF + FB	fast FF	fitted	x	✓
Model 4	FF + FB	slow FB	x	fitted	x
Model 5	FF + FB	fast FF + slow FB	✓	✓	✓

Prediction
✓ in psychophysical range
x not in psychophysical range

b)

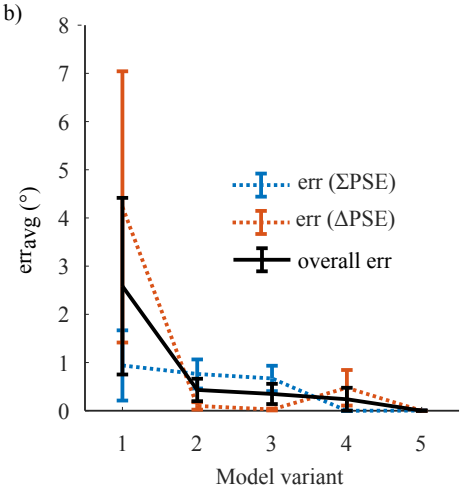

Figure 29: A summary on prediction performance of five model variants comprising dynamic synapses operating at either single or multiple rate in either only FF or FF-FB cortical circuitries. a) The experiments in which the model variants predict the $\Delta PSEs$ and $\sum PSEs$ within the range of psychophysical results or not. b) The prediction error, err_{avg}, which was defined as the averaged magnitude of the deviations of each model's predictions from the corresponding psychophysical ranges.

In sum, a FF-FB model with slow and fast adaptive mechanisms best predicts skew induced MAE at different time-scales which cannot fully be accounted by a single adaptive mechanisms in only FF or FF-FB circuit. Thus, the synaptic dynamics of FF-FB cortical circuitries tuned at different time-scales are relevant in mediating adaptation at different time scales during natural vision.

6.3.6 FF-FB functional role in neural response tuning

The input from the natural environment consists of uncertainties or noise. The visual system however adapts in an optimal manner by inferring relevant information from such uncertainties using prior knowledge of the environment [Kohn, 2007; Wark et al., 2009]. Since FB acts as such predictive signal from higher to lower cortical areas, it possibly plays a role in such optimal adaptation, but this has not been previously demonstrated. Here, to test the role of FF-FB interaction in neural response tuning during adaptation, we assessed responses of V1 and MT model units during and after adaptation in model variant 1 and 5, i.e. in the absence and presence of FB circuitry, respectively.

Figure 30 shows an example simulation of model units' responses in V1 and MT during adaptation to DSK stimuli for $0.3\,seconds$. In model variant 5, V1 and MT responses are similar and have a uni-modal response patterns with peaks at the salient information of the input. In model variant 1, i.e. when FB is eliminated, the response curves of V1 and MT model units have a different pattern and maxima. V1 response is bimodal and resembles the pattern of the noisy input statistics. Whereas, the MT response is uni modal with a maximum between the two modes of V1 response pattern. Thus, FB disambiguates salient motion information from the noisy input and results in similar response tuning in model area V1 and MT during adaptation.

An example simulation of V1 and MT model units' responses for $0\,^\circ$ test stimulus motion direction without and with prior DSK adaptation are illustrated in Figure 31. In model variant 5, exposure to DSK adapting stimuli shifted the response curves of both V1 and MT units towards the 'up' direction away from their preferred direction which was measured without prior adaptation. The FB dynamic synapse is slow, thus not depleted enough by such short exposure time-scale to induce adaptation effect in V1. The fast FF dynamic synapse tuned at short time-scale induces adaptation to the MT responses. The recurrent FB projection which modulates the V1 input matching to the adapted MT response induces the repulsive effect in V1. In model variant 1, however, the repulsive aftereffect is visible only in MT model units since the dynamic synapse in the FF circuit modulates only the input to MT. Furthermore, the repulsive effect in this variant is smaller than what is observed in model variant 5. This indicates compensatory adaptation effect of the V1 bimodal response pattern during

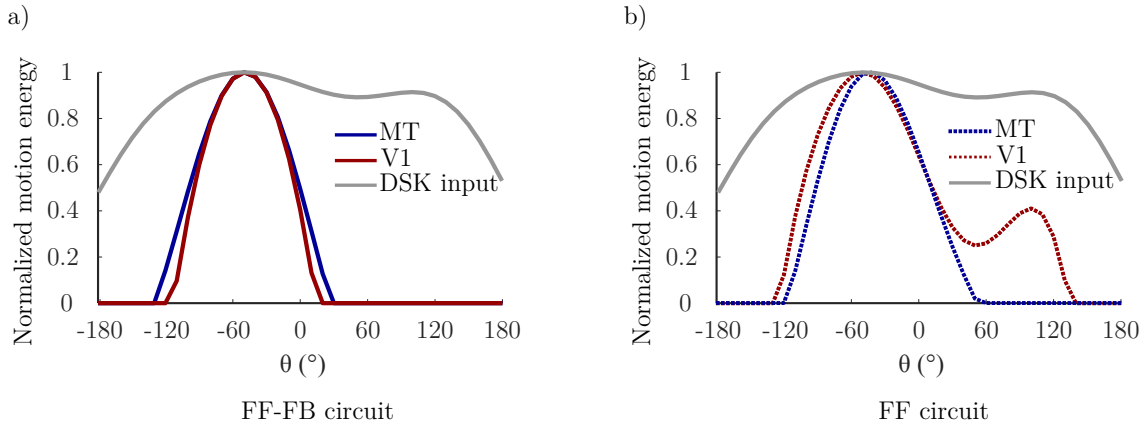

Figure 30: Contribution of FB in enhancing salient motion information: normalized response curves of V1 and MT model units after 0.3 *second* exposure to DSK adapting stimuli a) in model variant 5, i.e. FF-FB circuit and b) in model variant 1, i.e. only FF circuit.

DSK exposure in model variant 1. Thus, the inclusion of FB connections results in similar adaptation to a salient motion information in model area V1 and MT.

In sum, exposure to skewed natural image sequences results in repulsion of response curves in model areas V1 and MT. This neural response tuning conceivably underlies skew adaptation.

6.4 Discussion

Skew induced MAE and the underlying cortical processes were assessed with psychophysical experiments and model simulations. MAE was revealed at two time scales of skew exposures in both psychophysical results and model predictions. The observers' PSE, i.e. random dots' motion direction perceived as horizontal, shifted in the adapting skew direction. In other words, the physical horizontal motion direction of the test stimuli was perceived to be shifted away from the adapting skew direction. Thus, exposure to skewed natural stimuli induces adaptation in motion perception which is a candidate mechanism for habituation to distortions of optical elements.

A recurrent neural model of two stage motion direction processing with distinct dynamic synaptic mechanisms within FF and FB connections was suggested to explain the potential underlying mechanism of the observed MAE. Simulation results of the model replicated the psychophysically shown MAE at different time scales of skew exposure. Thus, multiple rate adaptive mechanisms within recurrent FF and FB cortical pathways explain adaptation to optical manipulations of the natural environment, e.g., through distortion by optical elements.

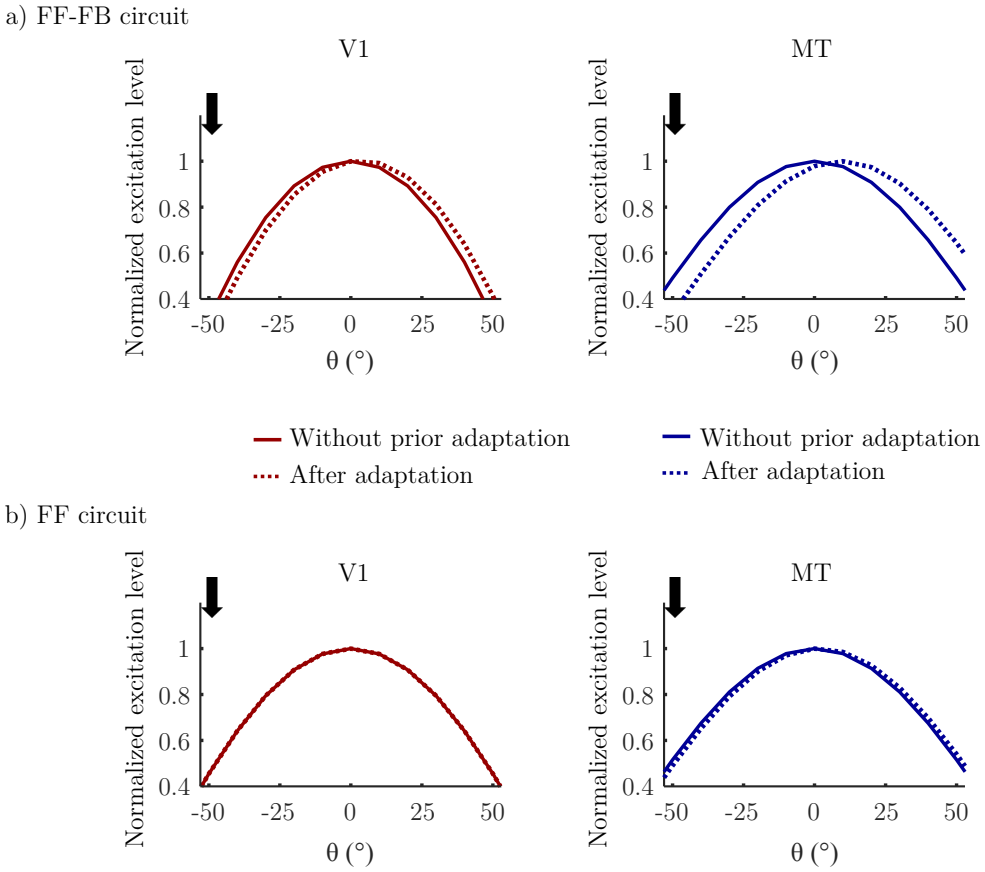

Figure 31: Adaptation effect comparison in a) Model variant 5 (FF-FB) and b) Model variant 1 (only FF). Normalized response curves of V1 and MT model units in for the test stimuli input at 0 ° motion direction without prior adaptation and after 0.3 *second* of DSK adaptation. The downward arrow indicates the dominant motion direction, at −50 °, in the adapting DSK stimuli.

6.4.1 Biological relevance of the suggested model

Unlike pure feedforward mechanisms considered in previous adaptation models[Clifford and Langley, 1996; van de Grind et al., 2003], motion information is processed in a cortical circuit formed by synaptic organization of FF and FB connections between different cortical areas [Mather et al., 2008; Rokszin et al., 2010; Sillito et al., 2006; Stuit, 2009]. A modulatory feedback re-entrant mechanism suggested in the present study has been reported in previous physiological investigations [Friston and Büchel, 2000; Hupe et al., 2001; Sillito et al., 2006]. Specifically, excitatory FB projection from MT combined with activity normalization by subsequent center surround competition was shown to affect activities of V1 cells.

One important aspect of top-down FB signal is the disambiguation of motion information via selective enhancement and propagation of salient signals [Bayerl and Neumann, 2004, 2007; Bouecke et al., 2011; Raudies and Neumann, 2010]. The motion direction signal from the adapting natural image sequences are highly ambiguous and

noisy as shown in Figure 25. In our model, these ambiguous signals are reduced and salient direction information is enhanced as a result of feedback and lateral competitive interactions. Figure 30 shows this disambiguation in activities of V1 and MT in the presence and absence of such FB mechanism. The FB functions as a predictive signal that enhances lower level input that matches 'expectations' or feature specificity of higher level responses [Grossberg, 1982; Ullman, 1995]. In this manner, only the input signal that is in resonance to the higher level MT response is enhanced. As a consequence, in line with physiological findings, FB disambiguates motion direction signal simultaneously in both V1 and MT areas [Pack et al., 2003]. Moreover, when FB connections are integrated into the model, similar adaptation induced response tuning occurs in both V1 and MT areas, consistent with physiological findings [Patterson et al., 2013], see Figure 31. If the FB pathway is eliminated, a repulsive shift adaptation effect would be visible only in MT model units since the FF dynamic synapses affect only the driving FF input stream from V1 to MT. Thus, synaptic adaptation within FF-FB connections reflects physiological plasticity in different visual areas during skew adaptation.

The model simulation results also align with Bayesian inference prediction frameworks of optimal adaptation processes which necessitate predictive prior information [Grzywacz and de Juan, 2003; Kording et al., 2007; Wark et al., 2009]. A comparable resemblance with such model can be derived by considering the receptive fields and dynamic synaptic strengths as adaptive likelihood functions and the feedback information as an adaptive prior information. However, in the present model, priors are dynamic over time and the likelihoods are not statistically independent. As FB allows predictive prior information from MT to modulate the likelihood of V1 responses, disambiguated motion signal will propagate though the network until a global consistent information in both areas is achieved. In line with the inference theory, this leads to optimal adaptation to a salient information by decreasing the risk of adapting to error signals. In this case, the suggested neural model can be treated as a neuronal implementation of Bayesian-like principles of adaptation.

Furthermore, the FB re-entrant mechanism is one way of integrating multiple adaptive mechanisms which control adaptation at different time-scales. Previous models assume motion adaptation to be a consequence of a single adaptive mechanism that operates at a specific time scale within a hierarchical bottom-up motion processing cortical circuit [Clifford and Langley, 1996; van de Grind et al., 2003]. However, recent psychophysical findings reported evidence on distinct multiple adaptation mechanisms operating at different time scales [Mesik et al., 2013]. In our model, we incorporated two different temporally tuned adaptive mechanisms, FF synapses tuned to short adaptation and the FB synapses to long adaptation. This enabled accurate prediction of skew

induced MAE at different time-scales. To examine if skew induced MAE could be explained by one of the single adaptive mechanisms, we compared prediction performance of our model with its variants which comprise only a single adaptive mechanism. The simulation comparison shows that the prediction performance critically depends on FF-FB recurrency with different adaptive mechanisms. Thus, multiple adaptive synapses within FF and FB streams of motion processing circuitry are candidate mechanisms for skew induced MAE operating at different time-scales.

The model employed in this investigation is detailed at a mesoscopic level of description regarding its structure and the computational elements. In particular, the state variable is defined by the mean activation (membrane potential) over a population of neurons equivalent to a cortical mini-column. Each mini-column represents a single feature selectivity at a specific spatial position. Different feature selectivities (motion direction, in our case) at one location comprise a model cortical column. The mean potential changes in such population are formally described by a first-order rate equation. The membrane time constant for individual cells in cortex varies for different types of neurons [Markram et al., 2004; Monier et al., 2008]. Since we here consider the dynamics of whole populations of neurons in mini-columns we have adjusted the time constants to a value higher than that of individual neurons. This accounts for the variation response times in the population and the exerted effects of inhibition on the excitatory units.

The components considered in the model are minimal in the sense that structural elements which do not contribute to the considered functionality are not included. Specifically, the model investigation emphasizes short-term synaptic adaptation, which is adopted here by a habituative mechanism [Castellucci et al., 1970], and feedback from activity representations at a higher stage (MT) to an earlier stage (V1). In contrast, lateral connections between columns in a spatial neighbourhood are not incorporated in the model, even though they are observed in anatomy. We argue that the adaptation of neuronal selectivity and its modulation by contextual feedback from higher stages are sufficient to explain motion adaptation in the experimental setting investigated here. Such feedback spreads over a larger spatial neighbourhood than lateral intracortical connections and also acts on a shorter timescale which is comparable with the feedforward delivery of signals. Since lateral connections seem not to make a major contribution to the contextual skew adaptation effects investigated here, we did not incorporate lateral connections in our model.

Overall, we believe that the proposed model and its selected granularity capture the most relevant details of neural response characteristics at the primary stages of cortical motion adaptation. The characteristics of the model dynamics have been investigated from a theoretical perspective to characterize steady-state solutions and

other temporal response properties [Brosch and Neumann, 2014]. These insights helped us to specify a stable configuration of a reference model network and to integrate the model extensions. In a nutshell, the short-term adaptation of synaptic connections explains the desensitization of units (groups of neurons in a mini-column) and the shift of direction tuning at the population level. This allowed us to establish a link to the mesoscopic neuronal model dynamics to the behavioural response characteristics of human subjects adapted to skewed input patterns as measured psychophysically.

6.4.2 Other potential neural correlates for distortion induced MAE

Substantial information has been revealed in classical adaptation studies by testing adaptation effects induced by artificial stimuli such as random dots and bars, albeit this might not always divulge visual performances observed in natural viewing conditions [David et al., 2004; Felsen and Dan, 2005; Ringach et al., 2002]. Natural image content is thereby an ideal stimulus to potently drive the visual system in its intended mode [Snow et al., 2017; Webster, 2015]. To enhance the ecological relevance of the investigation, the present study tests distortion induced motion adaptation when the visual system is exposed to stimuli that mimic the dynamics of the natural environment.

Adaptation aftereffects originate from response changes in neurons processing common features of adapting and test stimuli [Clifford et al., 2007; Webster, 2011, 2015]. Skew distortion of natural image sequences alters multiple features, e.g., motion direction statistics, orientation statistics and oblique magnification. Adaptation to such attribute rich stimuli might activate several cortical areas and could involve their coordinated responses [Habtegiorgis et al., 2017]. The present study assessed MAE induced by distortions of natural scenes and predicted response changes in direction selective neurons across cortical areas V1 and MT. Motion is dominantly processed in the dorsal visual pathway, albeit inputs from form processing areas might as well contribute to motion information processing, and thus to skew-induced MAE [Beck and Neumann, 2010; Edwards and Crane, 2007; Geisler, 1999; Pavan et al., 2013]. Our model's scope covers the role of FF-FB streams and their synaptic dynamics to adaptation within motion direction selective neurons in the dorsal visual pathway. However, FF and FB reciprocal streams considered in the present study are characteristic means of information flow between different cortical layers [Bastos et al., 2015; Felleman and Van, 1991]. Thus, the contributions revealed here might reflect a general adaptation mechanisms in other feature selective cortical areas as well.

6.5 Conclusion

The present study investigated skew adaptation mechanisms for image sequences from a psychophysical as well as a modelling perspective. Skew distortions, as simulated here with natural image sequences, typically occur for viewers wearing spectacles or experiencing distortions after changes in eyesight. The results obtained from the psychophysical investigations illustrate that skew exposure in milliseconds and minute's time-scales induces adaptation in motion perception. In the computational modelling investigation, a recurrent FF-FB model of motion detection and integration was employed and further elaborated to include synaptic adaptation mechanisms in the bottom-up and top-down connections. The model responses replicated psychophysical findings of adaptation effects after different time-scales of skew exposure. In the model, the FF-FB interactions and their synaptic dynamics had distinct roles in the computation wherein together they lead to such psychophysically plausible adaptation responses. Furthermore, the model's prediction on an additional hysteresis effect yielded similar results when tested psychophysically. This indicates analogous temporal dynamics of the neural networks in the suggested model and the human visual system underlying skew adaptation at multiple time-scales.

6.6 Methods

6.6.1 Psychophysics

Study approval The study was approved by the Ethics Committee of the Medical Faculty of the Eberhard Karls University of Tübingen and the University Hospital.

Observers 10 observers participated in experiment 1 and 2, among which six partook in both. 11 observers participated in experiment 3, eight of which also participated in experiment 1 and five of which in experiment 2. All observers aged between 18 to 40 years. All observers had normal or corrected to normal vision during the experiment and were naive about the purpose of the study. In adherence to the Declaration of Helsinki, informed written consent was collected from all observers before their participation in the study.

Set-up The psychophysical experiments were designed using PsychToolbox in Matlab (Mathworks, MA, USA) [Brainard, 1997]. Stimuli were displayed on a ViewPixx/3D monitor at a resolution of $1920 \times 1080\, pixels$ (with $0.271\, mm$ pixel pitch) and refresh rate of $100\, Hz$ in an otherwise darkened room. A chin and head rest was used to fix the viewing distance to $57\, cm$. Up and down keys of a keyboard were used to collect observer's responses during adaptation aftereffect measurements.

Stimuli 12,000 natural images, of size $1280 \times 720\, pixels$, were taken from an open source movie to prepare the skewed adapting stimuli [Baumann and Behnisch, 2010]. Each natural image was geometrically skewed at a shear angle of Ψ in a horizontal and vertical directions by remapping pixel positions of undistorted image, x and y, into new distorted pixel positions, x_d and y_d, as in equation 14.

$$\begin{bmatrix} x_d \\ y_d \end{bmatrix} = \begin{bmatrix} x + tan(\psi) \cdot y \\ tan(\psi) \cdot x + y \end{bmatrix} \tag{14}$$

The inner $650 \times 650\, pixels$ of each distorted image were used by cropping out the sheared edges. Each image was then filtered by a circular Hanning window, w [Harris, 1978].

$$w(r) = \cos^2(\frac{\pi}{N} \cdot r) \tag{15}$$

In equation 3, r is the radial distance of the pixel position from the center of the image and N was set to be equal to the image dimension, i.e. $650\, pixels$.

Up-skewed and down-skewed adapting image sequences (Figure 25a) were prepared by skewing 12,000 natural images at a shear angle of $\Psi = +25\,^\circ$ and $\Psi = -25\,^\circ$, respectively. During adaptation, these image sequences were rendered at a rate of 25 frames per second.

Test stimuli were dynamic random dots shown in a circular annulus (Figure 32). The diameter of the annulus had the same dimension as the adapting stimuli, i.e. $650\, pixels$, and always consists of 2000 dots. Each dot was circular and subtended a visual angle of 0.14°. The dots move coherently at a speed of $3^\circ/seconds$. The motion direction of the test stimuli was either diagonally up or diagonally down at an angle of θ from the horizontal (equation 16). For a specific motion direction, θ, the position of the dots, x_1 and y_1 was updated to x_2 and y_2 in the subsequent frame using equation 4. Positive θ corresponds to upward motion and negative to downward motion.

$$\begin{bmatrix} x_2 \\ y_2 \end{bmatrix} = \begin{bmatrix} cos(\theta) \cdot x_1 \\ sin(\theta) \cdot y_1 \end{bmatrix} \tag{16}$$

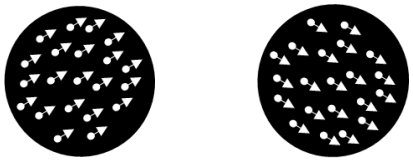

Up-motion Down-motion

Figure 32: Illustration of moving random dot test stimuli.

Procedure Before taking part in the psychophysical experiment, observers were informed about the procedure and trained on how to respond to the test stimuli using a keyboard. Viewing was monocular.

The schematic of the experimental procedure for the three psychophysical experiments is shown in Figure 33. In all the three experiments, adaptation was tested to the oppositely skewed image sequences alternately, first to the down-skewed then to the up-skewed natural image sequences. The adaptation aftereffect was tested after each adaptation using the method of constant stimuli.

In experiment 1, adaptation was tested after short exposure to skewed image sequences in a top-up procedure. Each top-up and test stimulus presentation was separated by inter stimulus interval (ISI) with blank screen, each lasting for duration of $0.3\,seconds$. In experiment 2, skewed adapting image sequence was shown first for $3\,minutes$ and then for $15\,seconds$ after each test stimulus presentation to top-up the adaptation. Test stimuli were presented for $0.5\,seconds$. ISI between each top-up and test stimulus presentation had $0.5\,seconds$ duration. In both experiments, the motion direction of the test stimuli was in a randomized order. After each test stimulus presentation, observers had to report whether the motion direction of the random dot stimuli was diagonally up or diagonally down by pressing the up or the down key of a keyboard, respectively. In experiment 1 and experiment 2, twelve motion directions were used for the test stimuli, from $-6.6\,^\circ$ to $6.6\,^\circ$ in step size of $1.2\,^\circ$. Five responses were recorded for each test stimulus motion direction. In total, 60 responses were recorded to compute the psychometric curves of each adapting skew direction.

In experiment 3, we utilized a neural hysteresis phenomena to validate our models' prediction. We tested the possible interaction between adaptation from short exposure to the skewed stimuli and hysteresis effect from sequentially changing motion direction of our test stimuli. The order of the test stimuli direction was from down ($-13\,^\circ$) to up ($13\,^\circ$), for the DSK adaptation, and from up ($13\,^\circ$) to down ($-13\,^\circ$), for the USK adaptation, in step size of $2\,^\circ$. Thus, any possible hysteresis effect of the test stimuli sequence is expected to induce an MAE larger than the one measured in experiment 1 with a randomised order of the test stimuli motion direction. Each top-up and test stimulus presentation was separated by ISI with blank screen, each lasting for a duration of $0.3\,seconds$. As in experiment 1 and 2, observers had to report the motion direction of the test stimuli by using the up or down key of a keyboard. Four responses were recorded per each test stimulus in four cycles. In total, 56 responses were recorded to compute the psychometric curves of DSK and USK MAEs.

Data analysis In all experiments, two psychometric curves of motion direction perception were separately computed from the responses which were recorded after ex-

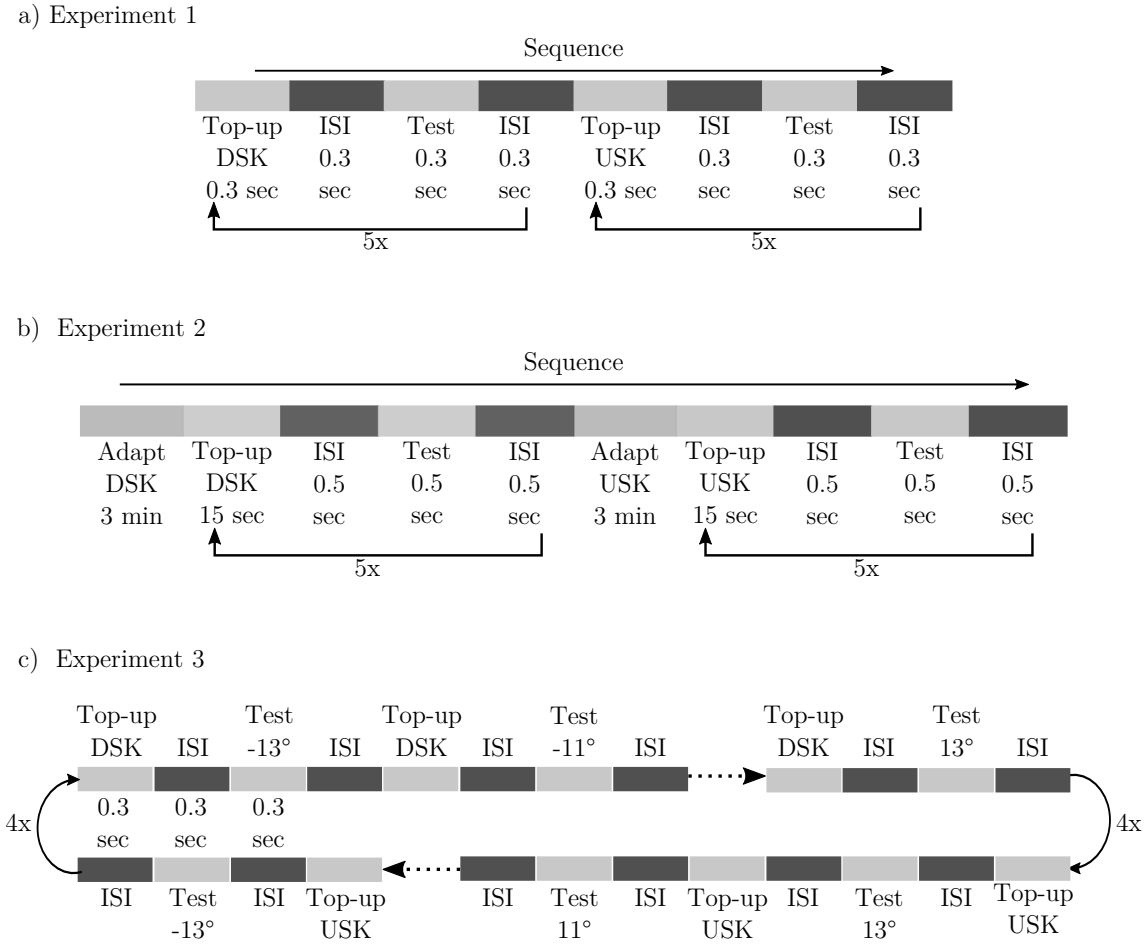

Figure 33: Detailed illustration of psychophysical procedures followed in experiment 1(a), experiment 2(b) and experiment 3(c).

posure to up- and down- skewed natural stimuli. In each psychometric function, the percentage of upward responses as a function of motion direction of the test stimuli was fitted with a cumulative Gaussian using the Psignifit 4.0 software (asymptotes set free but assumed to be equal) [Schutt et al., 2016]. The point of subjective equality (PSE), i.e. the motion direction at 50 percent of upward responses indicated the motion direction that was perceived as horizontal. The size of the magnitude of the adaptation aftereffect, ΔPSE, was evaluated as the difference between the PSE of the USK and DSK adaptations. The sum of the USK and DSK PSEs, $\sum PSE$, was also used to quantify any direction bias of the adaptation aftereffect from the temporal ordering of the up- and down-skew exposure. The overall aftereffect was computed by averaging the $\Delta PSEs$ and $\sum PSEs$ from all the observers. A paired sample t-test was conducted to evaluate the significance of the average effects.

6.6.2 Modelling

Our model focuses on motion direction tuned mechanisms in the dorsal pathway of the visual cortex, specifically V1 and MT. Motion direction processing in areas V1 and MT is modeled together with a population response readout decision layer. We suggest a dynamic short-term synaptic plasticity mechanism within FF and FB pathways between V1 and MT units to realize motion direction adaptation.

Our model extends a previously developed architecture for motion processing in areas V1 and MT [Bayerl and Neumann, 2004]. This model has been shown to be biologically plausible as it enabled prediction of data from neurophysiological recordings as well as behavioral studies [Bayerl and Neumann, 2004, 2007; Bouecke et al., 2011; Raudies and Neumann, 2010]. Here, we outline the basic features of the model and then describe the extension made to explain visual plasticity in motion perception. The readers are referred to the previous papers for detailed description of calculations, motivation and biological plausibility of the model.

The input to the recurrent motion processing V1 and MT model units is an average motion direction signal, R_θ, of either the random dot test stimuli or the adapting image sequences. For the random dot test stimulus, R_θ was a Gaussian signal centered at the corresponding test stimuli motion direction and width of 15°. For the adapting image sequences, R_θ was computed by spatiotemporal correlation technique as described in detail in Section 10.2. For each image sequence, the local motion signal, $R_{x,t,\rho,\theta}$ as a function of speed and direction at each spatial location x and sample time t, is initially detected by using modified Elaborated Reichardt detectors (ERDs) [Bayerl and Neumann, 2004; Reichardt, 1987] which comprise sequential preprocessing by LGN cells, orientation selective cells and cells which compute motion energy from consecutive frames. Since the focus of this study is on direction processing and also to ease the computational load, the population response $R_{x,t,\rho,\theta}$ is simplified to $R_{x,\theta}$ by integrating over speed and time. Subsequently, direction selective V1 cells filter normalized motion direction signal, $R^{norm}_{x,\theta}$, at each location with center-surround spatial normalization. For easing the computational load in the subsequent recurrent motion direction processing stage by V1 and MT units, $R^{norm}_{x,\theta}$ is spatially integrated by inserting an average pool layer just before the recurrent stage and the input signal is simplified to only direction domain R_θ. Thus, in the recurrent stage, only motion direction processing by direction selective V1 and MT cells will be considered irrespective of their spatial, temporal and speed preferences.

Model units for direction tuned cells in area V1 and MT process motion direction information in a recurrent manner via FF and FB connections. The FF connection drives the input from bottom to up cortical layers and the FB modulation enhances the lower level input matching to the higher level responses. The FF and FB excitatory connec-

tions are defined by two weighting factors; i.e. constant synaptic Gaussian weights (G) and dynamic synaptic efficacies (y). The synaptic weights can be considered as the receptive field structures and the efficacies as a probability of the presynaptic neuron to activate the post synaptic neuron depending on transmitter release.

In a nutshell, as illustrated in Figure 34, motion processing in each model area constitutes three sequential stages; FF motion direction filtering, input signal enhancement with FB modulation and activity normalization with pool inhibition.

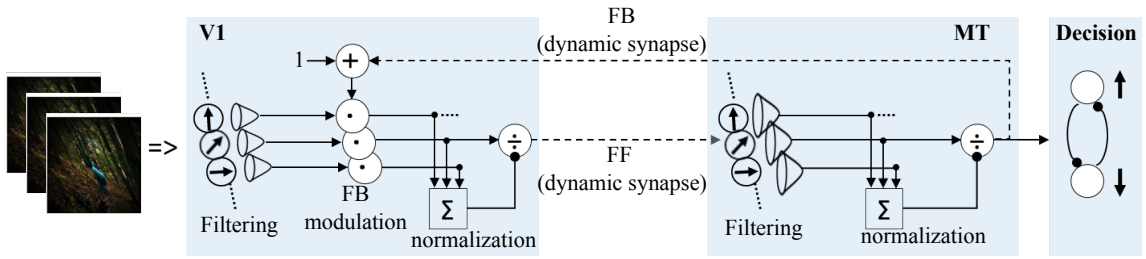

Figure 34: Details of motion processing in each model area. Motion is initially detected from image sequences by ERDs [Bayerl and Neumann, 2004; Reichardt, 1987], and subsequently processed in a recurrent loop in model areas V1 and MT. A steady-state model of decision-making layer is integrated to map MT responses into 'upward' and 'downward' motion perception decision process employed in the psychophysical experiments.

Assuming fast processes in filtering and modulating stages, the response dynamics of each model unit can be simplified to a single equation (equation 17).

$$\tau . \frac{d}{d_t} v^{V1|MT} = -v^{V1|MT} + (1 - v^{V1|MT}) \cdot I_{ex}^{V1|MT} - (1 + v^{V1|MT}) \cdot I_{inh}^{V1|MT} \tag{17}$$

$$I_{ex}^{V1} = (G_{c,V1}^{\theta} * R_{\theta}) \cdot (1 + \lambda \cdot I_{mod}) \tag{18}$$

$$I_{ex}^{MT} = y^{FF} \cdot (G_{c,MT}^{\theta} * v^{V1}) \tag{19}$$

$$I_{mod}^{V1} = y^{FB} \cdot v^{MT} \tag{20}$$

$$I_{inh}^{V1|MT} = \frac{1}{n} \cdot \sum_{\theta} I_{ex}^{V1|MT} \tag{21}$$

y^{FF} and y^{FB} are the dynamic synaptic efficacies in the FF and FB connections. v^{V1} and v^{MT} denote membrane potentials of each model unit in area V1 and MT, respectively. The membrane time constant, $\tau = 30\, milliseconds$, was set equal in both V1 and MT model units for simplification. I_{ex}, I_{mod} and I_{inh} are excitatory, modulatory and inhibitory inputs for each model unit. Since the focus of the model is only in the two stages, V1-MT, we only consider FB modulation from MT to V1. Thus, possible modulation input to area MT from higher areas, like MST and attention, would be set

to zero in our model. R_θ is the driving FF inputs for model area V1 and represents the aforementioned motion direction statistics of either the adapting image sequences or the moving random dot test stimuli. $G^{\theta}_{c,v1}$ and $G^{\theta}_{c,MT}$ are the direction filtering receptive fields of V1 and MT units. For simplicity, they are assumed to be the same and implemented as a Gaussian kernel with directional width of $\sigma^{\theta}_{c,V1} = \sigma^{\theta}_{c,MT} = 45°$, respectively. $n = 37$ represents the number of direction tuned cells in each model area and was selected randomly. Thus, with these assumptions similar input filtering and normalization processes are modelled. '$*$' and '$\cdot$' are the convolution and scalar multiplication operators, respectively. $\lambda = 20$ is the FB strength which was adjusted to enhance the main signal over the noise, see Figure 30.

The model was extended by incorporating dynamic synaptic efficacies in the FF and FB excitatory connections to introduce synaptic adaptation in the network. Neural models of synaptic adaptation have been proposed by several researchers [Carpenter and Grossberg, 1987; Tetzlaff et al., 2012; Wang, 1993]. The suggested mechanisms share common principles but also incorporate further details which depend on the particular aim of the modelling scope that is covered in addition. Here, the synaptic efficacy is described as the neurotransmitter occupancy of the presynaptic vesicle, ranging between zero and one. Previously proposed gating mechanism is considered to model the FF and FB dynamic efficacies by a first order differential equation of the form in equation 22 and 23, respectively [Carpenter and Grossberg, 1987; Hennig, 2013].

$$\tau_{syn} \cdot \frac{d}{dt} y^{FF}(t) = \alpha^{FF} \cdot (1 - y^{FF}(t)) - \beta^{FF} \cdot y^{FF}(t) \cdot v^{V1}(t) \tag{22}$$

$$\tau_{syn} \cdot \frac{d}{dt} y^{FB}(t) = \alpha^{FB} \cdot (1 - y^{FB}(t)) - \beta^{FB} \cdot y^{FB}(t) \cdot v^{MT}(t) \tag{23}$$

$\tau_{syn} = 1$ is the time constant of the gating mechanism; $\alpha^{FF} = 1.2$,$\beta^{FF} = 10$ are FF synaptic efficacy parameters which are fitted to replicate psychophysical results of short adaptation in experiment 1, and $\alpha^{FB} = 0.04$, $\beta^{FB} = 1.2$ are FB synaptic efficacy parameters which are fitted to replicate the psychophysical results of long adaptation in experiment 2. The first term of the gating function comprises two simultaneous processes with the amount of transmitter production (α) and its inhibition $-\alpha.y(t)$). Expressed differently, this term represents a tonic drive α to replenish the release pool with transmitter by an amount that is proportional to the unexcited vesicles (reserve pool), $1 - y(t)$. The second term denotes the transmitter release depending on the strength of presynaptic signal, v^{v1} (for the FF synapse) and v^{MT} (for the FB synapse), and the vesicle occupancy, $y(t)$. This term depletes the presynaptic vesicle occupancy at a rate of β and regulates the strength of the temporal adaptation to form an activity-gated input. In simple terms, the synaptic strength decreases from

1 towards equilibrium state of $\alpha/(\alpha+\beta)$ at a rate proportional to $-\beta$ during continuous presynaptic excitation and restores to 1 at a rate proportional to α when the presynaptic input is off. Thus, neural responses decrease during adaptation due to the depletion of presynaptic strength and adaptation aftereffects would occur if test stimuli are presented before the depleted synaptic strength fully recovers.

Decision making In order to account for the decision process employed in the psychophysical experiments, e.g. decision-making on up or down motion direction of the test stimuli, we included a related mechanism in the model. It contains competitive steady-state responses of two output units, each representing a possible upward or downward button press motor actions. A soft-max function is used as an action selection rule to determine the probability of upward (P_{up}) or downward (P_{down}) output unit to win the competition between the two actions based on their values as shown in equation 24.

$$P_{up} = \frac{exp(\frac{I^{ex}_{up}}{temp})}{exp(\frac{I^{ex}_{up}}{temp}) + exp(\frac{I^{ex}_{down}}{temp})} \qquad P_{down} = \frac{exp(\frac{I^{ex}_{down}}{temp})}{exp(\frac{I^{ex}_{up}}{temp}) + exp(\frac{I^{ex}_{down}}{temp})} \tag{24}$$

$$I^{ex}_{up} = G^{\theta}_{up}.v^{MT} \qquad I^{ex}_{down} = G^{\theta}_{down}.v^{MT} \tag{25}$$

I^{ex}_{up} and I^{ex}_{Down} are excitatory inputs to the two motor units and are weighted sum MT responses. G^{θ}_{up} and G^{θ}_{down} are Gaussian weights in the direction domain with width of $45\,^{\circ}$ and their maximum centered at $90\,^{\circ}$ and $-90\,^{\circ}$, respectively. They can be considered as two direction channels tuned to the two directions, up and down. *temp* is a temperature parameter [Sutton and Barto, 1998] and here, it is adjusted to replicate the slope of the psychometric curves of psychophysical results. A detailed neural implementation of such decision making process is out of the scope of the paper, though it has been previously suggested [Grossberg and Pilly, 2008; Raudies and Neumann, 2010].

Simulation procedure Identical procedures as in the real psychophysical experiments were followed in the model simulations. During adaptation, the input to the recurrent stage was the motion direction statistics, R_{θ}, of the corresponding skewed natural image sequence. During the test phase, a direction signal centered at the corresponding test stimuli motion direction and with Gaussian noise of width $15\,^{\circ}$ is fed to the recurrent motion processing stage. Figure 25 shows the input R_{θ} for the adapting image sequences.

From the output stage of the model, at each motion direction of the test stimulus, P_{up} corresponds to the observers' percentage of upward responses in the psychophysical measurement. P_{up} as a function of the test stimuli motion direction was then fitted with

a cumulative Gaussian using Psignifit 4.0 software (asymptotes set free but assumed to be equal) [Schutt et al., 2016]. The point of subjective equality (PSE), i.e. the motion direction at 50 percent of upward responses indicated the motion direction that was perceived as horizontal by the model.

Other variants of the model Five variants of the suggested model were defined by considering specific connections and dynamic synapses using the feedback strength λ, and the synaptic constants α and β as free parameters. The FB strength λ is used to turn on or off the FB connection and the rates α and β determine the dynamics of the synaptic efficacies in the corresponding directions as follows:

- Model 1: Only FF connection with fast dynamic synapse ($\lambda = 0$, $\alpha_{FF} = 0.0005$, $\beta_{FF} = 9$, $temp = 0.00001$) fitted to replicate MAE of short adaptation in experiment 1.
- Model 2: Only FF connection with slow dynamic synapse ($\lambda = 0$, $\alpha_{FF} = 0.5$, $\beta_{FF} = 10$, $temp = 0.001$) fitted to replicate MAE of long adaptation in experiment 2.
- Model 3: FF-FB connection with only fast FF dynamic synapse ($\lambda = 20$, $\alpha_{FF} = 1$, $\beta_{FF} = 10$, $\alpha_{FB} = \beta_{FB} = 0$, $temp = 0.001$) fitted to replicate MAE of short adaptation in experiment 1.
- Model 4: FF-FB connection with only slow FB dynamic synapse ($\lambda = 20$, $\alpha_{FF} = \beta_{FF} = 0$, $\alpha_{FB} = 0.04$, $\beta_{FB} = 1.2$, $temp = 0.001$) fitted to replicate MAE of long adaptation in experiment 2.
- Model 5: FF-FB connection with only slow FB dynamic synapse ($\lambda = 20$, $\alpha_{FF} = 1$, $\beta_{FF} = 10$, $\alpha_{FB} = 0.04$, $\beta_{FB} = 1.2$, $temp = 0.001$); bringing together the fitted values of Model variant 3 and 4.

6.7 Acknowledgements

We acknowledge support by Deutsche Forschungsgemeinschaft and Open Access Publishing Fund of University of Tübingen. Funding was received from Eberhard-Karls-University Tübingen (ZUK 63) as part of the German Excellence initiative from the Federal Ministry of Education and Research (BMBF). This work was done in an industry on campus cooperation between the University of Tübingen and Carl Zeiss Vision International GmbH. S.W.H is scientist at the University Tübingen; K.R and S.W are employed by Carl Zeiss Vision International GmbH and are scientists at the University Tübingen. H.N. acknowledges funding by the Baden-Württemberg foundation in the "Neurorobotik" program (project VA-MORPH, no. NEU012).

6.8 Author contributions statement

All authors designed the study. S.W.H conducted the experiment and wrote the manuscript. S.W.H and K.R designed the experiments and analysed the data. S.W.H, C.J and H.N developed the model. All authors interpreted the data, contributed intellectual content to the manuscript, and approved the final submission.

6.9 Additional information

The authors declare that the research was conducted in the absence of any commercial or financial relationships that could be construed as a potential conflict of interest.

6.10 Supporting data

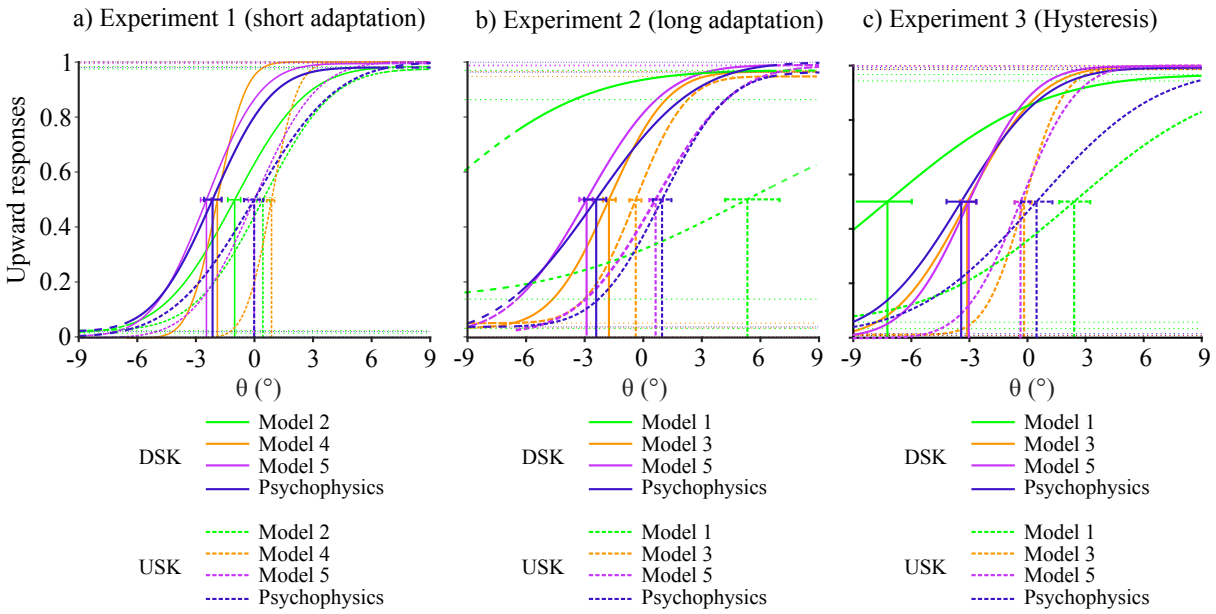

Figure 35: Predictions of model variants.

7 Summary

This work investigated how visual adaptation partakes in the habituation process to distortions of optical elements like PALs. Visual adaptation in response to distortion induced changes and the underlying neural mechanisms were probed with psychophysics and neurocomputational modelling approaches in a systematic way as recapitulated below.

On the study presented in section 3, we investigated whether or not exposure to distorted natural stimuli induces adaptation in form perception and traced the cortical level of the neural plasticity. The psychophysical results depicted that exposure to skewed natural image sequences resulted in a shift in form perception indicating adaptation aftereffect. In addition, partial retinal position invariance of the skew adaptation aftereffect was found during fixation; i.e. aftereffects occurred at adapted and non-adapted retinal locations. Visual aftereffects at non-adapted retinal locations reveal distortion encoding by neurons in higher cortical areas which entail large RF sizes. Visual adaptation in form perception thereby compensates skew induced alterations in form features of the natural environment, and it is mediated by coordinated plasticity of neural mechanisms in higher and lower cortical layers.

In section 4, we evaluated the reference frames of the distortion encoding neural mechanisms by testing how adaptation is transferred across saccades. After adaptation, a saccade was made to a new fixation and aftereffects were tested at different spatial locations in the visual field. Adaptation aftereffects were found only at retinotopically and spatiotopically matching locations. Thus, distortion is encoded by neural mechanisms entailing retinotopic and spatiotopic reference frames. The results divulge important visual mechanisms underlying habituation to optical elements that contain spatially varying distortions along their surface, e.g. PALs. While wearing these lenses, eye movements change the retinal location of the distortions disrupting retinotopic encoding. A robust adaptation is yet achieved regardless of such saccade induced retinal shifts due to spatiotopic mechanisms which encode the distortions relative to some extra retinal reference point, such as the head center. Thus, during habituation to spectacles, the visual system learns to adapt to both the local distortion profiles as well as their spatial layout in extra retinal reference frame. This explains why habituated PAL wearers need to readapt again to new glass designs entailing a different spatial layout of the distortions, albeit the local distortion profiles are similar to their old glasses. Thereby, retinotopic as well as spatiotopic reference frames are used during habituation to distortions of the natural environment.

In section 5, we tested if visual experience to the distortions in a long term facilitates the ability of fast adaptation underlying the change in perceptual performances

during the habituation process. Fast adaptation was quantified by the size of an aftereffect after a brief exposure to distorted natural scenes. Facilitation was investigated by testing if extended exposure to skew increases the magnitude of subsequent fast adaptations when distortions are reapplied. A possible facilitation of fast adaptation was examined for 30 minute and one hour of extended skew exposures. A facilitation effect was obtained only after the one hour extended exposure. This facilitation was further retained long-term wherein a larger aftereffect was replicated after two months of previous skew exposure. This makes it evident that the visual system uses accumulated distortion information in early days of PAL wearers to enable fast adaptation when they become habituated. Furthermore, the long term retention of the facilitation effect explains the fact why people do not need a long re-adaptation time when they re-wear their habituated glasses after a long period of break. Thus, extended exposure to distorted natural scenes facilitates adaptation whose long-term memory might enable fast and efficient re-adaptation when necessary.

In section 6, we investigated two main research questions in two parts. In the first part, we explored if adaptation to altered motion statistics of the natural environment contributes to the habituation process using psychophysics. Shift in motion perception was observed after exposure to skewed natural image sequences indicating an adaptation aftereffect. Thus, the results revealed that visual adaptation to distortion induced alteration of motion direction statistics is indeed an integral part of the habituation processes to PALs. In the second part, we evaluated how recurrent FF-FB interactions within the cortical hierarchy play a role in the process of distortion induced motion adaptation. A neural model of motion processing cortical circuit was developed for this purpose. Specifically, the role of recurrent interactions within motion direction tuned V1 and MT cells were investigated. Such interactions are representative for different hierarchically organized cortical areas selective for other features as well. A dynamic short term synaptic depression was considered within the reciprocal streams to introduce plasticity in the network. Simulation results illustrated that recurrent FF-FB interactions are essential for neurons to extract a salient signal from the broadband natural input and adapt to it. The aftereffects from adaptation to such a salient signal replicated the psychophysical MAEs. Whereas a simplified model variant, wherein FB is eliminated, could not compute a salient signal and failed to predict psychophysical results. Furthermore, the synaptic dynamics of the reciprocal streams are critical in mediating adaptation at different timescales. Dynamic synapses in the FF and FB streams operating at distinct rates predict psychophysical MAEs at different timescales of skew exposure. Such prediction was not accounted for by other model variants comprising single rate dynamic synapses. Thus, FF-FB cortical interactions and their synaptic dynamics play a significant role to efficiently compute relevant dis-

tortion induced changes from the natural input and to mediate adaptation at different timescales.

In sum, the results elucidate that visual adaptation is an integral component of habituation to PALs and has important practical implications. Particularly, the outcomes from the investigation of experience dependent long-term dynamics of adaptation shed light on the capability of facilitating habituation by a visual training paradigm. Such paradigm can be developed by using content rich stimuli to trigger multi-level cortical plasticity and by taking into account the spatial layout of distortions to facilitate spatiotopic neural mechanisms which partake in adaptation to PALs. Furthermore, the suggested biologically plausible model can be used as an objective predictor of how spectacle wearers adapt to the local distortion profiles of different PAL designs.

Future studies would further benefit to propose an efficient solution for facilitating habituation to PALs. This study mainly investigated adaptation to local distortions of PALs. Adaptation should further be assessed with simultaneous presentation of different distortion profiles as they appear in PALs. Furthermore, future work should look into how distortion induced changes in optic flow or motion information affect the ability of guiding oneself through the environment and how adaptation plays a role in compensating for them. This needs to be done by emulating the exact spatial distribution of distortions in PALs and by using VR set-ups to maintain the reference frames of distortion encodings. The model can as well be extended in a way to predict these behavioral studies. A suitable model could incorporate how the self-motion direction is computed from the motion signals and how a robust adaptation is achieved irrespective of eye movements. The outcomes of the model would not only be applicable to predict perceptual responses of PAL wearer's, but also leads to an efficient algorithm for a robust artificial sensory system, e.g. for a freely moving robot.

In conclusion, a targeted combination of psychophysical and neurocomputational modelling results of this work provides a seminal example for stability of the human visual system, applicable to any natural or artificial sensory system.

8 Zusammenfassung

Diese Arbeit untersucht, inwieweit visuelle Adaptation an einen Habituationsprozess an Verzerrungen, erzeugt von optischen Elementen wie Gleitsichtgläsern (PAL), beteiligt ist. Die visuelle Adaptation an verzerrungsinduzierte Veränderungen von Bildinhalten und die zugrunde liegenden neuronalen Mechanismen wurden mit psychophysikalischen und neuronalen Modellierungsansätzen systematisch untersucht.

In der Studie, welche im Abschnitt 3 behandelt wird, wurde untersucht, ob die Darbietung von verzerrten, natürlichen Reizen eine Anpassung der Formwahrnehmung induziert. Außerdem wurde die kortikale Ebene untersucht, in der die neuronale Plastizität stattfindet. Die psychophysikalischen Ergebnisse zeigten, dass die Darbietung von verzerrten, natürlichen Bildsequenzen zu einer Verschiebung der Formwahrnehmung führt, welche auf einen Adaptationseffekt hindeutet. Zusätzlich wurde während der Fixation eine partielle Invarianz gegenüber der retinalen Position der Adaptation festgestellt indem die Nachwirkungen an adaptierten und nicht adaptierten Stellen der Netzhaut auftraten. Diese visuelle Adaptation an nicht adaptierten Stellen der Netzhaut zeigt eine Verzerrungskodierung durch Neuronen in höheren kortikalen Bereichen, die große rezeptive Felder aufweisen. Die visuelle Adaption der Formwahrnehmung kompensiert dabei eine Formveränderung der natürlichen Umgebung durch Verzeichung und wird durch eine koordinierte Plastizität der neuronalen Mechanismen in höheren und niedrigeren kortikalen Schichten erzeugt.

Im Abschnitt 4 wird eine Analyse des Bezugssystems des neuronalen Mechanismus beschrieben, in dem Verzerrungen kodiert werden. Es wurde untersucht, wie die Adaptation transsakkadisch übertragen wird. Nach Adaptation wurde eine Sakkade zu einem Fixationstarget durchgeführt und anschließend der Adaptationsnacheffekt an verschiedenen räumlichen Stellen im Gesichtsfeld getestet. Nacheffekte wurden nur an retinotopen und spatiotopen Netzhautorten gefunden. Die neuronale Repräsentation der Verzerrung ist daher mit retinotopen und spatiotopen Bezugsrahmen kodiert. Diese Ergebnisse zeigen Mechanismen auf, die der Gewöhnung an optische Elemente zugrunde liegen, die räumlich variierende Verzerrungen entlang ihrer Oberfläche enthalten, z.B. PALs. Während des Tragens von PALs verändern Augenbewegungen die retinale Lage der Verzerrungen und stören die retinotope Adaptation. Eine robuste Anpassung wird jedoch unabhängig von solchen sakkaden-induzierten Netzhautverschiebungen durch spatiotope Mechanismen erreicht, die die Verzerrungen relativ zu einem zusätzlichen Referenzpunkt, wie z.B. dem Kopfzentrum, kodieren. So lernt das Sehsystem während der Gewöhnung an die Brille, sich sowohl an die lokalen Verzerrungsprofile als auch an deren räumliche Anordnung in einem zusätzlichen Netzhautbezugssystem anzupassen. Dies erklärt, warum sich gewöhnte PAL-Träger wieder an neue Glasdesigns anpassen

müssen, die eine andere räumliche Anordnung der Verzerrungen mit sich bringen, obwohl die lokalen Verzerrungsprofile ihren alten Gläsern ähnlich sind. Dabei werden sowohl retinotope als auch spatiotope Bezugsrahmen während der Gewöhnung zur Verzerrung der natürlichen Umgebung verwendet.

Im Abschnitt 5 wurde getestet, ob langfristige Adaptation an Verzerrungen die Fähigkeit zur kurzfristigen Adaptation verbessert. Die schnelle Anpassung wurde durch die Größe eines Nacheffekts nach einer kurzen Darstellung verzerrter, natürlicher Szenen quantifiziert. Die Verbesserung der Adaptation wurde untersucht, indem getestet wurde, ob eine längere Exposition an Verzeichnungen die Nacheffekte bei erneuter Anwendung von Verzerrungen erhöht. Eine mögliche Erleichterung der schnellen Anpassung wurde jeweils nach 30 Minuten und einer Stunde Langzeitadaptation untersucht. Ein Erleichterungseffekt wurde erst nach der einstündigen Adaptation erzielt. Dieser Erleichterungseffekt wurde auch langfristig beibehalten, wobei ein größerer Nacheffekt zwei Monate nach der Langzeitadaptation repliziert wurde. Dies macht deutlich, dass das visuelle System die akkumulierte Adaptation an Verzeichnungen während der Gewöhnung der PAL-Träger nutzt, um eine schnelle Anpassung nach Gewöhnung zu ermöglichen. Darüber hinaus erklärt die langfristige Beibehaltung des Erleichterungseffektes, warum Menschen keine lange Wiederanpassungszeit benötigen, wenn sie ihre gewohnte Brille nach einer langen Pause wieder tragen. So erleichtert eine längere Exposition von verzeichneten Bildinhalten die Anpassung, sie ermöglicht bei Bedarf eine schnelle und effiziente Wiederanpassung.

Im Abschnitt 6 wurden zwei Hauptfragen untersucht. Im ersten Teil wurde mittels Psychophysik der Frage auf den Grund gegangen, ob die Anpassung an durch Verzeichnung veränderte Bewegungsstatistiken der natürlichen Umgebung zum Gewöhnungsprozess beiträgt. Eine Verschiebung in der Bewegungswahrnehmung, die auf einen Anpassungseffekt hindeutet, wurde nach der Darbietung verzeichneter Bildsequenzen beobachtet. So zeigten die Ergebnisse, dass die visuelle Anpassung an verzerrungsbedingte Änderungen der Bewegungsrichtungsstatistik tatsächlich ein integraler Bestandteil des Gewöhnungsprozesses an PALs ist. Im zweiten Teil dieses Abschnitts wurde untersucht, wie wiederkehrende Interaktionen innerhalb hierarchischer Schichten des visuellen Systems eine Rolle bei der Anpassung an die veränderte Bewegungsstatistik der verzerrten natürlichen Umgebung spielen. Zu diesem Zweck wurde ein kortikales Modell eines neuronalen Bewegungsverarbeitungskreises im dorsalen Pfad des visuellen Systems entwickelt. Hierbei wurde eine wiederkehrende Wechselwirkung von V1- und MT-Zellen, die Bewegungsrichtung verarbeiten, untersucht. Das Modell ist repräsentativ für verschiedene hierarchisch organisierte kortikale Bereiche, die auch für die Verarbeitung anderer Bildmerkmale verantwortlich sind. Innerhalb der reziproken Ströme wurde eine dynamische, kurzzeitige synaptische Depression als präsynaptischen Anregung be-

trachtet, um somit eine Plastizität in das Netzwerk einzuführen. Somit konnte gezeigt werden, dass vorwärts und rückwärts gerichtete neuronale Verarbeitung eine wichtige Rolle bei der Adaptation an verzeichnete Bildsequenzen spielt. Insbesondere die reziproken Interaktionen ermöglichen es den Neuronen, ein dominantes Signal aus dem breitbandigen natürlichen Input zu extrahieren und sich daran anzupassen. Die Nacheffekte (MAE) an ein solches Signal replizierten im Modell die psychophysikalischen Ergebnisse. Darüber hinaus zeigte sich, dass die synaptische Dynamik zwischen den reziproken Pfaden auch eine kritische Wirkung bei der Vermittlung der Adaptation zu unterschiedlichen Zeitpunkten hat. Insbesondere dynamische Synapsen in den Vorwärts- und Rückwärtspfaden, die unterschiedlich schnell arbeiten, replizierten MAEs zu unterschiedlichen Zeitpunkten nach der Verzeichnungsexposition. So spielt die reziproke Interaktion von vorwärts- und rückwärts gerichteten Signalen innerhalb des hierarchischen Kortex eine wichtige Rolle, um relevante verzerrungsinduzierte Veränderungen in natürlichen Bildinhalten effizient zu berechnen und die Adaptation zu unterschiedlichen Zeitpunkten zu vermitteln.

Insgesamt verdeutlichen die Ergebnisse, dass die visuelle Adaptation ein integraler Bestandteil der Gewöhnung an PALs ist und somit praktische Auswirkungen hat. Insbesondere die Ergebnisse aus der Untersuchung der erfahrungsabhängigen Langzeitdynamik der Anpassung geben Aufschluss über die Möglichkeit, Gewöhnung durch ein visuelles Training zu erleichtern. Ein Trainingsparadigma kann entwickelt werden, indem man inhaltsreiche Stimuli zur Auslösung von mehrstufige kortikale Plastizität und unter Berücksichtigung der räumlichen Anordnung von Verzerrungen zur Erleichterung spatiotope neuronaler Mechanismen, die an der Anpassung an PALs beteiligt sind, verwendet. Darüber hinaus kann das vorgeschlagene biologisch plausible Modell als objektiver Prädiktor verwendet werden um zu untersuchen wie sich Brillenträger an die lokalen Verzerrungsprofile verschiedener PAL-Designs anpassen.

Zukünftige Studien würden weiter dazu beitragen, eine effiziente Lösung zur Erleichterung der Gewöhnung an PALs zu finden. Diese Studie untersuchte hauptsächlich die Anpassung an lokale Verzerrungen von PALs. Die Anpassung sollte ferner bei gleichzeitiger Darstellung verschiedener Verzerrungsprofile, wie sie in PALs auftreten, bewertet werden. Darüber hinaus sollte in Zukunft untersucht werden, wie sich verzerrungsinduzierte Veränderungen des optischen Flusses oder der Bewegungsinformation die Fähigkeit beeinflussen, sich selbst durch die Umwelt zu bewegen, und wie Adaptation eine Rolle spielt, um diesen Einfluss zu kompensieren. Dies kann durch Imitation der genauen räumlichen Verteilung von Verzerrungen in PALs und durch die Verwendung von Virtuelle-Reality-Setups geschehen, um die Bezugsrahmen der Verzerrungskodierungen beizubehalten. Das erstellte Modell kann erweitert werden, um Ergebnisse solcher Verhaltensstudien vorherzugesagt, um die Anwendungsrelevanz in verschiedenen

Bereichen zu erhöhen. Ein geeignetes Modell könnte beinhalten, wie aus den Bewegungssignalen die Eigenbewegungsrichtung berechnet wird und wie eine robuste Anpassung unabhängig von Augenbewegungen erreicht wird. Die Ergebnisse des Modells wären nicht nur für die Vorhersage der Wahrnehmungsreaktionen von PAL-Trägern anwendbar, sondern führen auch zu einem effizienten Algorithmus für ein robustes künstliches Sensorsystem, z.B. für einen frei beweglichen Roboter.

Zusammenfassend lässt sich sagen, dass eine gezielte Kombination von psychophysikalischen und Modellierungsergebnissen dieser Arbeit ein wegweisendes Beispiel für die Stabilität des menschlichen Sehsystems darstellt, das auf jedes natürliche oder künstliche sensorische System anwendbar ist.

9 References

Abbott, L. F., Varela, J. A., Sen, K., and Nelson, S. B. (1997). Synaptic depression and cortical gain control. *Science*, 275(5297):220–224.

Abrams, J., Nizam, A., and Carrasco, M. (2012). Isoeccentric locations are not equivalent: The extent of the vertical meridian asymmetry. *Vision Research*, 52(1):70–78.

Adams, W. J., Banks, M. S., and van Ee, R. (2001). Adaptation to three-dimensional distortions in human vision. *Nature Neuroscience*, 4(11):1063–1064.

Afraz, S.-R. and Cavanagh, P. (2008). Retinotopy of the face aftereffect. *Vision Research*, 48(1):42–54.

Aller, T. A. (2013). Clinical management of progressive myopia. *Eye*, 28:147.

Alvarez, T. L., Kim, E. H., and Granger-Donetti, B. (2017). Adaptation to Progressive Additive Lenses: Potential Factors to Consider. *Scientific Reports*, 7(1):2529.

Andersen, R. A. (1997). Multimodal integration for the representation of space in the posterior parietal cortex. *Philosophical Transactions of the Royal Society of London Series B-Biological Sciences*, 352(1360):1421–1428.

Andersen, R. A., Essick, G. K., and Siegel, R. M. (1985). Encoding of Spatial Location by Posterior Parietal Neurons. *Science*, 230(4724):456–458.

Angelucci, A. and Bullier, J. (2003). Reaching beyond the classical receptive field of v1 neurons: horizontal or feedback axons? *Journal of Physiology-Paris*, 97(2-3):141–154.

Angelucci, A., Levitt, J. B., Walton, E. J., Hupe, J.-M., Bullier, J., and Lund, J. S. (2002). Circuits for local and global signal integration in primary visual cortex. *Journal of Neuroscience*, 22(19):8633–8646.

Apps, M. A. J. and Tsakiris, M. (2014). The free-energy self: a predictive coding account of self-recognition. *Neuroscience & Biobehavioral Reviews*, 41:85–97.

Backus, B. T., Banks, M. S., van Ee, R., and Crowell, J. A. (1999). Horizontal and vertical disparity, eye position, and stereoscopic slant perception. *Vision Research*, 39(6):1143–1170.

Ball, K. and Sekuler, R. (1987). Direction-specific improvement in motion discrimination. *Vision Research*, 27(6):953–965.

Bao, M. and Engel, S. A. (2012). Distinct mechanism for long-term contrast adaptation. *Proceedings of the National Academy of Sciences*, 109(15):5898–5903.

Bao, M., Fast, E., Mesik, J., and Engel, S. (2013). Distinct mechanisms control contrast adaptation over different timescales. *Journal of Vision*, 13(10):14.

Barbero, S. and Portilla, J. (2015). Geometrical interpretation of dioptric blurring and magnification in ophthalmic lenses. *Optics Express*, 23(10):13185–13199.

Barlow, H. B. and Olshausen, B. A. (2004). Convergent evidence for the visual analysis of optic flow through anisotropic attenuation of high spatial frequencies. *Journal of vision*, 4(6):1.

Barrett, J. (2004). Side effects of virtual environments: A review of the literature. Technical report.

Bashiri, A., Ghazisaeedi, M., and Shahmoradi, L. (2017). The opportunities of virtual reality in the rehabilitation of children with attention deficit hyperactivity disorder: a literature review. *Korean J Pediatr*, 60(11):337–343.

Bastos, A., Vezoli, J., Bosman, C., Schoffelen, J.-M., Oostenveld, R., Dowdall, J., De Weerd, P., Kennedy, H., and Fries, P. (2015). Visual Areas Exert Feedforward and Feedback Influences through Distinct Frequency Channels. *Neuron*, 85(2):390–401.

Baumann, T. and Behnisch, H. (2010). Valkaama.

Bayerl, P. and Neumann, H. (2004). Disambiguating visual motion through contextual feedback modulation. *Neural Computation*, 16(10):2041–2066.

Bayerl, P. and Neumann, H. (2007). Disambiguating visual motion by form-motion interaction—A computational model. *International Journal of Computer Vision*, 72(1):27–45.

Beck, C. and Neumann, H. (2010). Interactions of motion and form in visual cortex–a neural model. *Journal of Physiology-Paris*, 104(1):61–70.

Belmore, S. C. and Shevell, S. K. (2008). Very-long-term chromatic adaptation: Test of gain theory and a new method. *Visual Neuroscience*, 25(03):411–414.

Belmore, S. C. and Shevell, S. K. (2011). Very-long-term and short-term chromatic adaptation: are their influences cumulative? *Vision Research*, 51(3):362–366.

Berkley, M. A., Debruyn, B., and Orban, G. (1994). Illusory, motion, and luminance-defined contours interact in the human visual system. *Vision Research*, 34(2):209–216.

Betsch, B. Y., Einhäuser, W., Körding, K. P., and König, P. (2004). The world from a cat's perspective–statistics of natural videos. *Biological Cybernetics*, 90(1):41–50.

Bex, P. J., Dakin, S. C., and Mareschal, I. (2005). Critical band masking in optic flow. *Network: Computation in Neural Systems*, 16(2-3):261–284.

Bex, P. J. and Makous, W. (2002). Spatial frequency, phase, and the contrast of natural images. *JOSA A*, 19(6):1096–1106.

Bex, P. J., Mareschal, I., and Dakin, S. C. (2007). Contrast gain control in natural scenes. *Journal of Vision*, 7(11):12.

Bex, P. J., Solomon, S. G., and Dakin, S. C. (2009). Contrast sensitivity in natural scenes depends on edge as well as spatial frequency structure. *Journal of Vision*, 9(10):1.

Billock, V. A., de Guzman, G. C., and Kelso, J. A. S. (2001). Fractal time and 1/f spectra in dynamic images and human vision. *Physica D: Nonlinear Phenomena*, 148(1):136–146.

Blake, R. and He, S. (2005). *Adaptation as a Tool for Probing the Neural Correlates of Visual Awareness: Progress and Precautions*. Oxford University Press, United States.

Blakemore, C. t. and Campbell, F. W. (1969). On the existence of neurones in the human visual system selectively sensitive to the orientation and size of retinal images. *The Journal of physiology*, 203(1):237–260.

Bouecke, J. D., Tlapale, E., Kornprobst, P., and Neumann, H. (2011). Neural mechanisms of motion detection, integration, and segregation: from biology to artificial image processing systems. *EURASIP J. Adv. Signal Process*, 2011:1–22.

Boynton, G. M. and Hegdé, J. (2004). Visual cortex: The continuing puzzle of area V2. *Current Biology*, 14(13):R523–R524.

Brainard, D. H. (1997). The psychophysics toolbox. *Spatial Vision*, 10:433–436.

Brosch, T. and Neumann, H. (2014). Computing with a canonical neural circuits model with pool normalization and modulating feedback. *Neural computation*, 26(12):2735–2789.

Burr, D. C. and Morrone, M. C. (2011). Spatiotopic coding and remapping in humans. *Philosophical Transactions of the Royal Society B-Biological Sciences*, 366(1564):504–515.

Carpenter, G. A. and Grossberg, S. (1987). Adaptation and transmitter gating in vertebrate photoreceptors. *Advances in Psychology*, 43:273–310.

Castellucci, V., Pinsker, H., Kupfermann, I., and Kandel, E. R. (1970). Neuronal mechanisms of habituation and dishabituation of the gill-withdrawal reflex in Aplysia. *Science*, 167(3926):1745–1748.

Clifford, C. W. and Langley, K. (1996). Psychophysics of motion adaptation parallels insect electrophysiology. *Curr Biol*, 6(10):1340–1342.

Clifford, C. W. G., Webster, M. A., Stanley, G. B., Stocker, A. A., Kohn, A., Sharpee, T. O., and Schwartz, O. (2007). Visual adaptation: neural, psychological and computational aspects. *Vision Research*, 47(25):3125–3131.

Clifford, C. W. G., Wenderoth, P., and Spehar, B. (2000). A functional angle on some after-effects in cortical vision. *Proceedings of the Royal Society of London. Series B: Biological Sciences*, 267(1454):1705–1710.

Contreras, A. and Ackland, P. (2017). Spectacle coverage report. *Int. Agency for Prev. Blind*.

Cornelissen, F. W., Peters, E. M., and Palmer, J. (2002). The Eyelink Toolbox: eye tracking with MATLAB and the Psychophysics Toolbox. *Behavior Research Methods, Instruments, & Computers*, 34(4):613–617.

Crespi, S., Biagi, L., D'Avossa, G., Burr, D. C., Tosetti, M., and Morrone, M. C. (2011). Spatiotopic Coding of BOLD Signal in Human Visual Cortex Depends on Spatial Attention. *PloS One*, 6(7).

Dakin, S. C., Williams, C. B., and Hess, R. F. (1999). The interaction of first-and second-order cues to orientation. *Vision Research*, 39(17):2867–2884.

David, S. V., Vinje, W. E., and Gallant, J. L. (2004). Natural stimulus statistics alter the receptive field structure of v1 neurons. *The Journal of Neuroscience*, 24(31):6991–7006.

D'Avossa, G., Tosetti, M., Crespi, S., Biagi, L., Burr, D. C., and Morrone, M. C. (2007). Spatiotopic selectivity of BOLD responses to visual motion in human area MT. *Nature Neuroscience*, 10(2):249–255.

Dekel, R. and Sagi, D. (2015). Tilt aftereffect due to adaptation to natural stimuli. *Vision Research*, 117:91–99.

Delahunt, P. B., Webster, M. A., Ma, L., and Werner, J. S. (2004). Long-term renormalization of chromatic mechanisms following cataract surgery. *Visual Neuroscience*, 21(03):301–307.

DeSouza, J. F. X., Dukelow, S. P., and Vilis, T. (2002). Eye position signals modulate early dorsal and ventral visual areas. *Cerebral Cortex*, 12(9):991–997.

Destexhe, A., Mainen, Z. F., and Sejnowski, T. J. (1998). Kinetic models of synaptic transmission. *Methods in neuronal modeling*, 2:1–25.

Dickinson, J. E., Almeida, R. A., Bell, J., and Badcock, D. R. (2010). Global shape aftereffects have a local substrate: A tilt aftereffect field. *Journal of Vision*, 10(13):5.

Dickinson, J. E. and Badcock, D. R. (2013). On the hierarchical inheritance of aftereffects in the visual system. *Frontiers in Psychology*, 4(472).

Dong, D. W. and Atick, J. J. (1995). Statistics of natural time-varying images. *Network: Computation in Neural Systems*, 6(3):345–358.

Duhamel, J. R., Bremmer, F., BenHamed, S., and Graf, W. (1997). Spatial invariance of visual receptive fields in parietal cortex neurons. *Nature*, 389(6653):845–848.

Duhamel, J.-R., Colby, C. L., and Goldberg, M. E. (1992). The updating of the representation of visual space in parietal cortex by intended eye movements. *Science*, 255(5040):90.

Eckert, M. P. and Zeil, J. (2001). Towards an ecology of motion vision. In *Motion Vision*, pages 333–369. Springer.

Edwards, M. and Crane, M. F. (2007). Motion streaks improve motion detection. *Vision Research*, 47(6):828–833.

Ehrenstein, W. H. and Ehrenstein, A. (1999). Psychophysical methods. In *Modern techniques in neuroscience research*, pages 1211–1241. Springer.

Eisner, A. and Enoch, J. M. (1982). Some effects of 1 week's monocular exposure to long-wavelength stimuli. *Perception & psychophysics*, 31(2):169–174.

Engel, S. A., Wilkins, A. J., Mand, S., Helwig, N. E., and Allen, P. M. (2016). Habitual wearers of colored lenses adapt more rapidly to the color changes the lenses produce. *Vision Research*, 125:41–48.

Epstein, W. (1972). Adaptation to uniocular image magnification: Is the underlying shift proprioceptive? *Perception & Psychophysics*, 11(1):89–91.

Ezzati, A., Golzar, A., and Afraz, A. S. R. (2008). Topography of the motion aftereffect with and without eye movements. *Journal of Vision*, 8(14).

Fahle, M. (2002). Perceptual learning: gain without pain? *Nature Neuroscience*, 5(10).

Fang, F., Murray, S. O., Kersten, D., and He, S. (2005). Orientation-tuned fMRI adaptation in human visual cortex. *Journal of Neurophysiology*, 94(6):4188–4195.

Fannin, T. E. and Grosvenor, T. (1987). Aniseikonia. In *Clinical optics*, pages 329–331. Butterworth-Heinemann, Stoneham, Massachusetts, 1st edition.

Fannin, T. E. and Grosvenor, T. (2013). *Clinical optics*. Butterworth-Heinemann.

Farell, B. and Pelli, D. G. (1999). Psychophysical methods, or how to measure a threshold and why. *Vision research: A practical guide to laboratory methods*, 5:129–136.

Felleman, D. J. and Van, D. C. E. (1991). Distributed hierarchical processing in the primate cerebral cortex. *Cerebral cortex (New York, NY: 1991)*, 1(1):1–47.

Felsen, G. and Dan, Y. (2005). A natural approach to studying vision. *Nature Neuroscience*, 8(12):1643–1646.

Field, D. J. (1987). Relations between the statistics of natural images and the response properties of cortical cells. *JOSA A*, 4(12):2379–2394.

Filangieri, C. and Li, A. (2009). Three-dimensional shape from second-order orientation flows. *Vision Research*, 49(11):1465–1471.

Fiorentini, A. and Berardi, N. (1981). Learning in grating waveform discrimination: Specificity for orientation and spatial frequency. *Vision Research*, 21(7):1149–1158.

Friston, K. J. and Büchel, C. (2000). Attentional modulation of effective connectivity from V2 to V5/MT in humans. *Proceedings of the National Academy of Sciences*, 97(13):7591–7596.

Gallant, J. L., Connor, C. E., and Van Essen, D. C. (1998). Neural activity in areas V1, V2 and V4 during free viewing of natural scenes compared to controlled viewing. *Neuroreport*, 9(9):2153–2158.

Galletti, C., Battaglini, P. P., and Fattori, P. (1993). Parietal neurons encoding spatial locations in craniotopic coordinates. *Experimental Brain Research*, 96(2):221–229.

Gardner, J. L., Merriam, E. P., Movshon, J. A., and Heeger, D. J. (2008). Maps of visual space in human occipital cortex are retinotopic, not spatiotopic. *Journal of Neuroscience*, 28(15):3988–3999.

Gattass, R., Nascimento-Silva, S., Soares, J. G. M., Lima, B., Jansen, A. K., Diogo, A. C. M., Farias, M. F., Marcondes, M., Botelho, E. P., Mariani, O. S., and Others (2005). Cortical visual areas in monkeys: location, topography, connections, columns, plasticity and cortical dynamics. *Philosophical Transactions of the Royal Society of London B: Biological Sciences*, 360(1456):709–731.

Gegenfurtner, K. R., Kiper, D. C., and Levitt, J. B. (1997). Functional properties of neurons in macaque area V3. *Journal of Neurophysiology*, 77(4):1906–1923.

Geisler, W. S. (1999). Motion streaks provide a spatial code for motion direction. *Nature*, 400(6739):65–69.

Geisler, W. S. (2008). Visual perception and the statistical properties of natural scenes. *Annual Review of Psychology*, 59:167–192.

Gibson, E. J. (1969). Principles of perceptual learning and development.

Gibson, J. J. (1966). The senses considered as perceptual systems.

Golomb, J. D. and Kanwisher, N. (2012a). Higher level visual cortex represents retinotopic, not spatiotopic, object location. *Cerebral Cortex*, 22(12):2794–2810.

Golomb, J. D. and Kanwisher, N. (2012b). Retinotopic memory is more precise than spatiotopic memory. *Proceedings of the National Academy of Sciences of the United States of America*, 109(5):1796–1801.

Groh, J. M., Trause, A. S., Underhill, A. M., Clark, K. R., and Inati, S. (2001). Eye position influences auditory responses in primate inferior colliculus. *Neuron*, 29(2):509–518.

Grossberg, S. (1982). How does a brain build a cognitive code? In *Studies of mind and brain*, pages 1–52. Springer.

Grossberg, S. and Pilly, P. K. (2008). Temporal dynamics of decision-making during motion perception in the visual cortex. *Vision research*, 48(12):1345–1373.

Grzywacz, N. M. and de Juan, J. (2003). Sensory adaptation as Kalman filtering: theory and illustration with contrast adaptation. *Network: Computation in Neural Systems*, 14(3):465–482.

Habtegiorgis, S. W., Rifai, K., Lappe, M., and Wahl, S. (2017). Adaptation to Skew Distortions of Natural Scenes and Retinal Specificity of Its Aftereffects. *Frontiers in Psychology*, 8:1158.

Habtegiorgis, S. W., Rifai, K., and Wahl, S. (2018). Transsaccadic transfer of distortion adaptation in a natural environment. *Journal of vision*, 18(1):13–13.

Harris, F. J. (1978). On the use of windows for harmonic analysis with the discrete Fourier transform. *Proceedings of the IEEE*, 66(1):51–83.

Hawkins, R. D., Kandel, E. R., and Siegelbaum, S. A. (1993). Learning to modulate transmitter release: themes and variations in synaptic plasticity. *Annual Review of Neuroscience*, 16(1):625–665.

Hegdé, J. and Van Essen, D. C. (2000). Selectivity for complex shapes in primate visual area V2. *Journal of Neuroscience*, 20(5):61–66.

Helson, H. (1964). *Adaptation-level theory*. Harper & Row, Oxford, England.

Hennig, M. H. (2013). Theoretical models of synaptic short term plasticity. *Frontiers in Computational Neuroscience*, 7.

Holden, B. A., Fricke, T. R., Ho, S., and al., E. (2008). Global vision impairment due to uncorrected presbyopia. *Archives of Ophthalmology*, 126(12):1731–1739.

Howe, P. D. L., Pinto, Y., and Horowitz, T. S. (2010). The coordinate systems used in visual tracking. *Vision Research*, 50(23):2375–2380.

Hubel, D. H. and Wiesel, T. N. (1968). Receptive fields and functional architecture of monkey striate cortex. *Journal of Physiology*, 195(1):215–243.

Hupe, J.-M., James, A. C., Girard, P., Lomber, S. G., Payne, B. R., and Bullier, J. (2001). Feedback connections act on the early part of the responses in monkey visual cortex. *Journal of Neurophysiology*, 85(1):134–145.

Ito, M. and Komatsu, H. (2004). Representation of angles embedded within contour stimuli in area V2 of macaque monkeys. *The Journal of Neuroscience*, 24(13):3313–3324.

Jay, M. F. and Sparks, D. L. (1984). Auditory receptive fields in primate superior colliculus shift with changes in eye position. *Nature*, 309(5966):345–347.

Johnson, L., Buckley, J. G., Scally, A. J., and Elliott, D. B. (2007). Multifocal spectacles increase variability in toe clearance and risk of tripping in the elderly. *Investigative Ophthalmology and Visual Science*, 48(4):1466–1471.

Kandel, E. R., Schwartz, J. H., Jessell, T. M., Siegelbaum, S. A., and Hudspeth, A. J. (2000). *Principles of neural science*, volume 4. McGraw-hill New York.

Karim, A. K. M. R. and Kojima, H. (2010). Thewhatandwhyof perceptual asymmetries in the visual domain. *Advances in Cognitive Psychology*, 6:103–115.

Karni, A. and Sagi, D. (1991). Where practice makes perfect in texture discrimination: evidence for primary visual cortex plasticity. *Proceedings of the National Academy of Sciences*, 88(11):4966–4970.

Kay, K. N. (2017). Principles for models of neural information processing. *Neuroimage*.

Kayser, C., Kording, K. P., and Konig, P. (2004). Processing of complex stimuli and natural scenes in the visual cortex. *Current Opinion in Neurobiology*, 14(4):468–473.

Kennedy, G. J., Orbach, H. S., and Loffler, G. (2006). Effects of global shape on angle discrimination. *Vision Research*, 46(8):1530–1539.

Kennedy, G. J., Orbach, H. S., and Loffler, G. (2008). Global shape versus local feature: An angle illusion. *Vision Research*, 48(11):1281–1289.

Keshner, E. A. (2004). Virtual reality and physical rehabilitation: a new toy or a new research and rehabilitation tool?

Kohn, A. (2007). Visual adaptation: physiology, mechanisms, and functional benefits. *Journal of Neurophysiology*, 97(5):3155–3164.

Kording, K. P., Tenenbaum, J. B., and Shadmehr, R. (2007). The dynamics of memory as a consequence of optimal adaptation to a changing body. *Nature Neuroscience*, 10(6):779–786.

Kusunoki, M. and Goldberg, M. E. (2003). The time course of perisaccadic receptive field shifts in the lateral intraparietal area of the monkey. *Journal of Neurophysiology*, 89(3):1519–1527.

Kwon, M., Legge, G. E., Fang, F., Cheong, A. M. Y., and He, S. (2009). Adaptive changes in visual cortex following prolonged contrast reduction. *Journal of Vision*, 9(2):20.

Lamme, V. A. F. and Roelfsema, P. R. (2000). The distinct modes of vision offered by feedforward and recurrent processing. *Trends in neurosciences*, 23(11):571–579.

Lamme, V. A. F., Super, H., and Spekreijse, H. (1998). Feedforward, horizontal, and feedback processing in the visual cortex. *Current opinion in neurobiology*, 8(4):529–535.

Laursen, A. M. and Rasmussen, J. B. (1975). Circle-ellipse discrimination in man and monkey. *Vision Research*, 15(2):173–174.

Laver, K., George, S., Thomas, S., Deutsch, J. E., and Crotty, M. (2012). Virtual reality for stroke rehabilitation. *Stroke*, 43(2):e20–e21.

Leopold, D. A., O'Toole, A. J., Vetter, T., and Blanz, V. (2001). Prototype-referenced shape encoding revealed by high-level aftereffects. *Nature Neuroscience*, 4(1):89–94.

Levinson, E. and Sekuler, R. (1976). Adaptation alters perceived direction of motion. *Vision research*.

Li, A., Tzen, B., Yadgarova, A., and Zaidi, Q. (2008). Neural basis of 3-D shape aftereffects. *Vision Research*, 48(2):244–252.

Livingstone, M. S. and Hubel, D. H. (1987). Psychophysical evidence for separate channels for the perception of form, color, movement, and depth. *Journal of Neuroscience*, 7(11):3416–3468.

Loffler, G. (2008). Perception of contours and shapes: Low and intermediate stage mechanisms. *Vision Research*, 48(20):2106–2127.

Markram, H., Toledo-Rodriguez, M., Wang, Y., Gupta, A., Silberberg, G., and Wu, C. (2004). Interneurons of the neocortical inhibitory system. *Nature reviews neuroscience*, 5(10):793.

Mather, G., Pavan, A., Bellacosa, R. M., and Casco, C. (2012). Psychophysical evidence for interactions between visual motion and form processing at the level of motion integrating receptive fields. *Neuropsychologia*, 50(1):153–159.

Mather, G., Pavan, A., Campana, G., and Casco, C. (2008). The motion aftereffect reloaded. *Trends in Cognitive Sciences*, 12(12):481–487.

Mather, G., Verstraten, F., and Anstis, S. M. (1998). *The motion aftereffect: A modern perspective*. Mit Press.

Mathot, S. and Theeuwes, J. (2013). A reinvestigation of the reference frame of the tilt-adaptation aftereffect. *Scientific Reports*, 3.

Matthews, N. and Welch, L. (2015). Left visual field attentional advantage in judging simultaneity and temporal order. *Journal of Vision*, 15(2):7.

Meister, D. J. and Fisher, S. W. (2008a). Progress in the spectacle correction of presbyopia. Part 1: Design and development of progressive lenses. *Clinical and experimental optometry*, 91(3):240–250.

Meister, D. J. and Fisher, S. W. (2008b). Progress in the spectacle correction of presbyopia. Part 2: Modern progressive lens technologies. *Clinical and experimental optometry*, 91(3):251–264.

Melcher, D. (2005). Spatiotopic Transfer of Visual-Form Adaptation across Saccadic Eye Movements. *Current Biology*, 15(19):1745–1748.

Melcher, D. (2007). Predictive remapping of visual features precedes saccadic eye movements. *Nature Neuroscience*, 10(7):903–907.

Melcher, D. and Morrone, M. C. (2003). Spatiotopic temporal integration of visual motion across saccadic eye movements. *Nature Neuroscience*, 6(8):877–881.

Meng, X., Mazzoni, P., and Qian, N. (2006). Cross-fixation transfer of motion aftereffects with expansion motion. *Vision Research*, 46(21):3681–3689.

Mesik, J., Bao, M., and Engel, S. A. (2013). Spontaneous recovery of motion and face aftereffects. *Vision research*, 89:72–78.

Monier, C., Fournier, J., and Frégnac, Y. (2008). In vitro and in vivo measures of evoked excitatory and inhibitory conductance dynamics in sensory cortices. *Journal of neuroscience methods*, 169(2):323–365.

Nageswaran, J. M., Richert, M., Dutt, N., and Krichmar, J. L. (2010). Towards reverse engineering the brain: Modeling abstractions and simulation frameworks. In *VLSI System on Chip Conference (VLSI-SoC), 2010 18th IEEE/IFIP*, pages 1–6. IEEE.

Nakamura, K. and Colby, C. L. (2002). Updating of the visual representation in monkey striate and extrastriate cortex during saccades. *Proceedings of the National Academy of Sciences*, 99(6):4026–4031.

Neitz, J., Carroll, J., Yamauchi, Y., Neitz, M., and Williams, D. R. (2002). Color perception is mediated by a plastic neural mechanism that is adjustable in adults. *Neuron*, 35(4):783–792.

Nishida, S., Motoyoshi, I., Andersen, R. A., and Shimojo, S. (2003). Gaze modulation of visual aftereffects. *Vision Research*, 43(6):639–649.

Pack, C. C., Livingstone, M. S., Duffy, K. R., and Born, R. T. (2003). End-stopping and the aperture problem: two-dimensional motion signals in macaque V1. *Neuron*, 39(4):671–680.

Parwaga, S., Buckley, D., and Duke, P. A. (2016). Tilt representation beyond the retinotopic level. *Journal of Vision*, 16(3).

Pasupathy, A. and Connor, C. E. (1999). Responses to contour features in macaque area V4. *Journal of Neurophysiology*, 82(5):2490–2502.

Pasupathy, A. and Connor, C. E. (2001). Shape representation in area V4: position-specific tuning for boundary conformation. *Journal of Neurophysiology*, 86(5):2505–2519.

Patterson, C. A., Duijnhouwer, J., Wissig, S. C., Krekelberg, B., and Kohn, A. (2013). Similar adaptation effects in primary visual cortex and area MT of the macaque monkey under matched stimulus conditions. *Journal of Neurophysiology*, 111(6):1203–1213.

Pavan, A., Marotti, R. B., and Mather, G. (2013). Motion-form interactions beyond the motion integration level: evidence for interactions between orientation and optic flow signals. *Journal of Vision*, 13(6):16.

Pelli, D. G. and Farell, B. (1995). Psychophysical methods. *Handbook of optics*, 3:3.1–3.12.

Pick, H. L. and Hay, J. C. (1966). Gaze-contingent adaptation to prismatic spectacles. *The American journal of psychology*, pages 443–450.

Poirier, F. J. A. M. and Frost, B. J. (2005). Global orientation aftereffect in multi-attribute displays: implications for the binding problem. *Vision Research*, 45(4):497–506.

Purves D Fitzpatrick D, Hall WC, LaMantia A-S, et al., A. G. J. (2008). *Neuroscience*. Sinauer Associates, Inc., M. A., USA, fourth edition edition.

Raudies, F. and Neumann, H. (2010). A model of neural mechanisms in monocular transparent motion perception. *Journal of Physiology-Paris*, 104(1):71–83.

Redding, G. M., Rossetti, Y., and Wallace, B. (2005). Applications of prism adaptation: a tutorial in theory and method. *Neuroscience & Biobehavioral Reviews*, 29(3):431–444.

Regan, D. and Hamstra, S. J. (1992). Shape discrimination and the judgement of perfect symmetry: Dissociation of shape from size. *Vision Research*, 32(10):1845–1864.

Regehr, W. G. (2012). Short-term presynaptic plasticity. *Cold Spring Harbor Perspectives in Biology*, 4(7):a005702.

Reichardt, W. (1987). Evaluation of optical motion information by movement detectors. *Journal of Comparative Physiology A: Neuroethology, Sensory, Neural, and Behavioral Physiology*, 161(4):533–547.

Ringach, D. L., Hawken, M. J., and Shapley, R. (2002). Receptive field structure of neurons in monkey primary visual cortex revealed by stimulation with natural image sequences. *Journal of Vision*, 2(1):2.

Roach, N. W., Webb, B. S., and McGraw, P. V. (2008). Adaptation to global structure induces spatially remote distortions of perceived orientation. *Journal of Vision*, 8(3):31.

Rokszin, A., Márkus, Z., Braunitzer, G., Berényi, A., Benedek, G., and Nagy, A. (2010). Visual pathways serving motion detection in the mammalian brain. *Sensors*, 10(4):3218–3242.

Roth, A. and van Rossum, M. C. (2009). Modeling synapses. *Computational modeling methods for neuroscientists*, 6:139–160.

Ruderman, D. L. and Bialek, W. (1994). Statistics of natural images: Scaling in the woods. *Physical Review Letters*, 73(6):814.

Sagi, D. and Tanne, D. (1994). Perceptual learning: learning to see. *Current Opinion in Neurobiology*, 4(2):195–199.

Salomon, R., Fernandez, N. B., Van Elk, M., Vachicouras, N., Sabatier, F., Tychinskaya, A., Llobera, J., and Blanke, O. (2016). Changing motor perception by sensorimotor conflicts and body ownership. *Scientific Reports*, 6:25847.

Saunders, D. R. and Woods, R. L. (2014). Direct measurement of the system latency of gaze-contingent displays. *Behavior Research Methods*, 46(2):439–447.

Sawides, L., Marcos, S., Ravikumar, S., Thibos, L., Bradley, A., and Webster, M. (2010). Adaptation to astigmatic blur. *Journal of Vision*, 10(12):22.

Schutt, H. H., Harmeling, S., Macke, J. H., and Wichmann, F. A. (2016). Painfree and accurate Bayesian estimation of psychometric functions for (potentially) overdispersed data. *Vision Research*, 122:105–123.

Sheedy, J. E. and Andre, B. J. (2013). Prescribing multifocal lenses. In *Duane's Clinical Ophthalmology*, volume 1, pages 6–12. Lippincott Williams & Wilkins, Philadelphia, PA.

Sheedy, J. E., Campbell, C., King-Smith, E., and Hayes, J. R. (2005). Progressive powered lenses: the Minkwitz theorem. *Optometry and Vision science*, 82(10):916–922.

Shih, S.-W., Hung, Y.-P., and Lin, W.-S. (1995). When should we consider lens distortion in camera calibration. *Pattern recognition*, 28(3):447–461.

Sillito, A. M., Cudeiro, J., and Jones, H. E. (2006). Always returning: feedback and sensory processing in visual cortex and thalamus. *Trends in Neurosciences*, 29(6):307–316.

Simoncelli, E. P. (2003). Vision and the statistics of the visual environment. *Current Opinion in Neurobiology*, 13(2):144–149.

Smith, L. N. and Smith, M. L. (2005). Automatic machine vision calibration using statistical and neural network methods. *Image and Vision Computing*, 23(10):887–899.

Smith, S., Clifford, C. W. G., and Wenderoth, P. (2001). Interaction between first-and second-order orientation channels revealed by the tilt illusion: psychophysics and computational modelling. *Vision Research*, 41(8):1057–1071.

Smithson, H. and Zaidi, Q. (2004). Colour constancy in context: Roles for local adaptation and levels of reference. *Journal of Vision*, 4(9):3.

Snow, M., Coen-Cagli, R., and Schwartz, O. (2017). Adaptation in the visual cortex: a case for probing neuronal populations with natural stimuli. *F1000Research*, 6.

Snowden, R., Snowden, R. J., Thompson, P., and Troscianko, T. (2012). Spatial vision. In *Basic vision: an introduction to visual perception*, chapter 4, pages 106–113. Oxford University Press.

Soechting, J. F. and Flanders, M. (1992). Moving in three-dimensional space: frames of reference, vectors, and coordinate systems. *Annual review of neuroscience*, 15(1):167–191.

Stricanne, B., Andersen, R. A., and Mazzoni, P. (1996). Eye-centered, head-centered, and intermediate coding of remembered sound locations in area LIP. *Journal of neurophysiology*, 76(3):2071–2076.

Stuit, S. M. (2009). *Motion processing, adaptation and aftereffects: A review.* PhD thesis.

Sutton, R. S. and Barto, A. G. (1998). *Reinforcement learning: An introduction*, volume 1. MIT press Cambridge.

Suzuki, S. and Cavanagh, P. (1998). A shape-contrast effect for briefly presented stimuli. *Journal of Experimental Psychology: Human Perception and Performance*, 24(5):1315.

Suzuki, S., Clifford, C., and Rhodes, G. (2005). High-level pattern coding revealed by brief shape aftereffects. *Fitting the mind to the world: Adaptation and after-effects in high-level vision*, pages 135–172.

Tetzlaff, C., Kolodziejski, C., Markelic, I., and Wörgötter, F. (2012). Time scales of memory, learning, and plasticity. *Biological Cybernetics*, 106(11-12):715–726.

Thiele, A. (2012). Nmda receptors figure it out. *Proceedings of the National Academy of Sciences*, 109(27):10749–10750.

Thompson, R. F. and Spencer, W. A. (1966). Habituation: a model phenomenon for the study of neuronal substrates of behavior. *Psychological Review*, 73(1):16.

Todorovic, A., van Ede, F., Maris, E., and de Lange, F. P. (2011). Prior expectation mediates neural adaptation to repeated sounds in the auditory cortex: an MEG study. *The Journal of Neuroscience*, 31(25):9118–9123.

Trommershäuser, J., Schneggenburger, R., Zippelius, A., and Neher, E. (2003). Heterogeneous presynaptic release probabilities: functional relevance for short-term plasticity. *Biophysical journal*, 84(3):1563–1579.

Trotter, Y. and Celebrini, S. (1999). Gaze direction controls response gain in primary visual-cortex neurons. *Nature*, 398(6724):239–242.

Tsodyks, M., Pawelzik, K., and Markram, H. (1998). Neural networks with dynamic synapses. *Neural computation*, 10(4):821–835.

Ullman, S. (1995). Sequence seeking and counter streams: a computational model for bidirectional information flow in the visual cortex. *Cerebral Cortex*, 5(1):1–11.

United Nations Population Division, D. o. E. and Affairs, S. (2015). World Population Ageing 2015. *United Nations*.

van Boxtel, J. J. A., Alais, D., and van Ee, R. (2008). Retinotopic and non-retinotopic stimulus encoding in binocular rivalry and the involvement of feedback. *Journal of Vision*, 8(5):17.

van de Grind, W. A., Lankheet, M. J., and Tao, R. (2003). A gain-control model relating nulling results to the duration of dynamic motion aftereffects. *Vision Res*, 43(2):117–133.

van der Schaaf, A. and van Hateren, J. H. (1996). Modelling the Power Spectra of Natural Images: Statistics and Information. *Vision Research*, 36(17):2759–2770.

Van Essen, D. C. and Anderson, C. H. (1995). Information processing strategies and pathways in the primate visual system. In Zornetzer SF Lau C, McKenna T, D. J. L., editor, *An introduction to neural and electronic networks*, volume 2, pages 45–76. Academic Press, Orlando (Florida).

Van Essen, D. C. and Maunsell, J. H. R. (1983). Hierarchical organization and functional streams in the visual cortex. *Trends in neurosciences*, 6:370–375.

van Hateren, J. H. and van der Schaaf, A. (1998). Independent component filters of natural images compared with simple cells in primary visual cortex. *Proceedings of the Royal Society of London B: Biological Sciences*, 265(1394):359–366.

van Rossum, M. C., van der Meer, M. A., Xiao, D., and Oram, M. W. (2008). Adaptive integration in the visual cortex by depressing recurrent cortical circuits. *Neural Computation*, 20(7):1847–1872.

Vinas, M., de Gracia, P., Dorronsoro, C., Sawides, L., Marin, G., Hernandez, M., and Marcos, S. (2013). Astigmatism impact on visual performance: meridional and adaptational effects. *Optometry and Vision Science*, 90(12):1430–1442.

Vinas, M., Sawides, L., de Gracia, P., and Marcos, S. (2012). Perceptual Adaptation to the Correction of Natural Astigmatism. *PloS One*, 7(9).

Vlaskamp, B. N. S., Filippini, H. R., and Banks, M. S. (2009). Image-size differences worsen stereopsis independent of eye position. *Journal of Vision*, 9(2):17.

Wadel, K., Neher, E., and Sakaba, T. (2007). The coupling between synaptic vesicles and ca2+ channels determines fast neurotransmitter release. *Neuron*, 53(4):563–575.

Wang, D. (1993). A neural model of synaptic plasticity underlying short-term and long-term habituation. *Adaptive Behavior*, 2(2):111–129.

Wark, B., Fairhall, A., and Rieke, F. (2009). Timescales of inference in visual adaptation. *Neuron*, 61(5):750–761.

Webster, M. A. (2011). Adaptation and visual coding. *Journal of Vision*, 11(5):3.

Webster, M. A. (2015). Visual adaptation. *Annual review of vision science*, 1:547–567.

Welch, R. B. (1969). Adaptation to prism-displaced vision: The importance of target-pointing. *Perception & Psychophysics*, 5(5):305–309.

Welch, R. B. (1978). *Perceptual modification: Adapting to altered sensory environments*. Academic Press, New York, NY.

Wexler, M., Panerai, F., Lamouret, I., and Droulez, J. (2001). Self-motion and the perception of stationary objects. *Nature*, 409(6816):85–88.

Wexler, M. and Van Boxtel, J. J. A. (2005). Depth perception by the active observer. *Trends in Cognitive Sciences*, 9(9):431–438.

Wilkinson, F., Wilson, H. R., and Habak, C. (1998). Detection and recognition of radial frequency patterns. *Vision Research*, 38(22):3555–3568.

Williams, D. and Phillips, G. (1987). Cooperative phenomena in the perception of motion direction. *JOSA A*, 4(5):878–885.

Wilson, H. R. and Wilkinson, F. (2002). Symmetry perception: A novel approach for biological shapes. *Vision Research*, 42(5):589–597.

Wölfel, M., Lou, X., and Schneggenburger, R. (2007). A mechanism intrinsic to the vesicle fusion machinery determines fast and slow transmitter release at a large cns synapse. *Journal of Neuroscience*, 27(12):3198–3210.

Wolpert, D. M. and Flanagan, J. R. (2001). Motor prediction. *Current Biology*, 11(18):R729–R732.

Yao, R., Heath, T., Davies, A., Forsyth, T., Mitchell, N., and Hoberman, P. (2014). Oculus vr best practices guide. *Oculus VR*, pages 27–39.

Yehezkel, O., Sagi, D., Sterkin, A., Belkin, M., and Polat, U. (2010). Learning to adapt: Dynamics of readaptation to geometrical distortions. *Vision Research*, 50(16):1550–1558.

York, L. C. and Van Rossum, M. C. (2009). Recurrent networks with short term synaptic depression. *Journal of computational neuroscience*, 27(3):607.

Zhao, C., Seriès, P., Hancock, P. J. B., and Bednar, J. A. (2011). Similar neural adaptation mechanisms underlying face gender and tilt aftereffects. *Vision Research*, 51(18):2021–2030.

Zhao, L. and Chubb, C. (2001). The size-tuning of the face-distortion after-effect. *Vision Research*, 41(23):2979–2994.

Zimmer, M. and Kovacs, G. (2011). Position specificity of adaptation-related face aftereffects. *Philosophical Transactions of the Royal Society B-Biological Sciences*, 366(1564):586–595.

Zimmermann, E., Morrone, M. C., Fink, G. R., and Burr, D. (2013). Spatiotopic neural representations develop slowly across saccades. *Current Biology*, 23(5):R193–R194.

Zimmermann, E., Weidner, R., Abdollahi, R. O., and Fink, G. R. (2016). Spatiotopic Adaptation in Visual Areas. *Journal of Neuroscience*, 36(37):9526–9534.

Zucker, R. S. and Regehr, W. G. (2002). Short-term synaptic plasticity. *Annual Review of Physiology*, 64(1):355–405.

10 Supplementary Materials

10.1 Computation of form statistics

Average orientation and spatial frequency distribution of the amplitude spectra from image sequences are computed to inspect distortion induced changes in contour orientations and spatial dimension symmetry statistics.

Each RGB image was converted to gray scale using 'rgb2gray' function in Matlab (Mathworks, MA, USA) and the DC component was removed by subtracting the mean image intensity from every pixel. Each $650 \times 650\, pixels$ image was then transformed to Fourier space by 'fft2' function in Matlab (Mathworks, MA, USA). The amplitude spectrum (A) of each image, expressed in cycles per image (cpi), was then calculated for integer values of spatial frequencies in the vertical and horizontal directions (u and v respectively). For the subsequent analysis, the amplitude spectrum was presented in polar coordinates with radial frequency ($f = \sqrt{u^2 + v^2}$) and orientation ($\psi = tan^{-1}(\frac{v}{u})$).

10.1.1 Spatial frequency statistics

To examine the spatial frequency distribution, the amplitude spectrum was averaged across all orientations within $\sqrt{2}\, cpi$ radial frequency bands.

$$A(f) = \frac{\sum_{\psi} A(\psi, f)}{n} \tag{26}$$

n is the number of points in each frequency bin f.

The amplitude spectra as a function of radial frequency was represented on a log-log scale and the slope was analysed after fitting by a linear polynomial function.

$$log_{10}A(f) = \zeta log_{10}f + c \tag{27}$$

To inspect the dimension symmetry, the spectral amplitude distribution over spatial frequencies was investigated for different orientations. Magnification of spatial dimension results in higher spectral amplitude distribution in low spatial frequencies. Thus, in orientations with longer dimensions, higher magnitude of slope (ζ) will be expected on spectral amplitude vs. spatial frequency log-log scale (equation 26). Accordingly, the oriented amplitude spectra vs. frequency was computed, as $A(f, \psi_i)$, in four orientations centered at $\psi_i = 0\,^\circ$, $45\,^\circ$, $-45\,^\circ$, $90\,^\circ$. In each orientation, the amplitude spectrum was averaged over orientations from $\psi_i - 22.5\,^\circ$ to $\psi_i + 22.5\,^\circ$ as in equation 26. Then, the oriented-slope value, $\zeta(\psi_i)$, was calculated using equation 27.

10.1.2 Orientation statistics

The weighted average of the spectral amplitude for each orientation, (ψ), was chosen as a metric to investigate orientation distribution of contours in each image. Consequently at each particular orientation, the amplitude spectrum was weighted by the corresponding spatial frequencies and the average over all spatial frequencies was computed.

$$A(\psi) = \frac{\sum_f f \times A(\psi, f)}{m} \tag{28}$$

m is the number of points in spectral domain in each orientation ψ

10.2 Computation of motion direction statistics

At each location, local motion direction was measured from input image sequences with correlation-based motion detection using modified elaborated Reichardt detectors (ERDs). This input stage consists of three steps.

- The first is center surround Gaussian filtering mimicking contrast detection by LGN cells.

$$r^{lgn}(x, y, t) = I(x, t) * (G_c(x) - G_s(x)) \tag{29}$$

  G_c and G_s are the center and surround isotropic Gaussian filters with width of $0.1\,^\circ$ and $0.3\,^\circ$ in space domain, respectively and r^{lgn} is LGN response at each location x and time t.

- The second step is static oriented contrast detection by orientation selective complex cells at a fixed frequency and independent of polarity. This is realized by oriented Gabor filter responses with shunting normalization.

$$r'_{x,t,\psi} = (r^{lgn} * G_{x_{odd}(\psi)})^2 + (r^{lgn} * G_{x_{even}(\psi)})^2 \tag{30}$$

$$r_{x,t,\psi} = \frac{r'_{x,t,\psi}}{0.01 + \sum_\psi r'_{x,t,\psi} * G_{surr}(x, y)} \tag{31}$$

  $G_{x_{odd}(\psi)}$ and $G_{x_{even}(\psi)}$ are sine and cosine Gabor filters, respectively, with isotropic width of $1\,^\circ$, spatial frequency of $1.57cpd$ and oriented at ψ. $r_{x,t,\psi}$ is the filter response normalized by the surround field G_{surr} of width $5\,^\circ$ at each location and time. Oriented contrasts were computed in eight orientations; $\psi = 0, 22.5\,^\circ ... 180\,^\circ$.

- The third step consists of responses of direction selective cells which compute orientation-independent motion energy between two consecutive frames. These mechanisms pool over responses of all orientation selective cells at different time

steps.

$$r^{+}_{x,t,\rho,\theta} = \sum_{\psi}(r_{x,t,\psi}.r_{x+\Delta x,t+\Delta t,\psi}) * G_c \tag{32}$$

$$r^{-}_{x,t,\rho,\theta} = \sum_{\psi}(r_{x+\Delta x,t,\psi}.r_{x,t+\Delta t,\psi}) * G_c \tag{33}$$

$$R_{x,t,\rho,\theta} = \frac{r^{+}_{x,t,\rho,\theta} - 0.5.r^{-}_{x,t,\rho,\theta}}{1 + \lfloor r^{-}_{x,t,\rho,\theta} \rfloor_{+}} \tag{34}$$

r^{+} and r^{-} are orientation independent responses of half-detectors for a specific velocity defined by a shift $\Delta x = (\rho(speed), \theta(direction))$between consecutive frames and pooled over small spatial neighborhood by isotropic Gaussian field (G_c) of width $1\,^{\circ}$. Thus, they can be considered as raw correlation outputs of complex cells. $R_{x,t,\theta}$ indicates the population response normalized by the opponent signal at each location and time. A $max(..., 0)$ non-linear operation is realized by a half wave rectification operator $\lfloor . \rfloor_{+}$.

We computed $\mathrm{R}_{x,t,\rho,\theta}$ for each natural image sequences used in the psychophysical experiments in five speed ranges, $\rho = 1, 2, 3, 4, 5\ dps$, and 36 direction ranges, $\theta = -180\,^{\circ}, 170\,^{\circ} \ldots 180\,^{\circ}$. Since the focus of the study is only motion direction, the population response was averaged in time and speed domain as in equation 35.

$$R_{x,\theta} = \sum_{t}\sum_{\rho} R_{x,t,\rho,\theta} \tag{35}$$

Subsequently, at each location, the signal is detected by direction selective V1 cells with center-surround shunting normalization mechanism as in equation 36.

$$R^{norm}_{x,\theta} = \frac{R_{x,\theta} * G^{x}_{c}}{0.01 + (\sum_{\theta} R_{x,\theta} * G^{x}_{s})^2} \tag{36}$$

$R^{norm}_{x,\theta}$ is the normalized direction signal at each location. G^{x}_{c} and G^{x}_{s} are the center and surround Gaussian fields with spatial width of $1\,^{\circ}$ and $5\,^{\circ}$, respectively.

For computational load purpose, we averaged the $R^{norm}_{x,\theta}$ in space domain by inserting an average pool layer just before the recurrent stage as in equation. Thus, the averaged population response, R_{θ}, for each adapting skewed natural image sequence represents the average motion direction statistics.

$$R_{\theta} = \frac{\sum_{x} R^{norm}_{x,\theta}}{n_x} \tag{37}$$

Where $n_x = 650 \times 650$ is the number of pixels in each image frame.

For all the simulations in this paper, R_{θ} is used as an input to the higher level model areas during exposure to skewed natural image sequences.

11 Publications, conference contributions and talks related to this work

11.1 Peer reviewed publications

Habtegiorgis, S.W., Rifai, K., Lappe, M., & Wahl, S. (2017). Adaptation to skew distortions of natural scenes and retinal specificity of its aftereffects. Frontiers in psychology, 8, 1158. doi: 10.3389/fpsyg.2017.01158.

Habtegiorgis, S.W., Rifai, K., & Wahl, S. (2018). Transsaccadic transfer of distortion adaptation in a natural environment. Journal of vision, 18(1), 13-13. doi: 10.1167/18.1.13.

Rifai, K., Hornauer, M., Buechinger, R., Schoen, R., Barraza-Bernal, M., **Habtegiorgis, S.W.**, ... Mappes, T. (2018). Efficiency of ocular UV protection by clear lenses. Biomedical Optics Express, 9(4), 1948–1963. http://doi.org/10.1364/BOE.9.001948

Habtegiorgis, S.W., Rifai, K., Lappe M., & Wahl, S. (2018). Experience dependent long-term facilitation of skew adaptation. Journal of vision,18(9):7, 1–11. doi: 10.1167/18.9.7.

Habtegiorgis, S.W., Jarvers, C., Rifai, K., Neumann H., & Wahl, S. (2019). The role of bottom-up and top-down cortical interactions in adaptation to natural scene statistics. Frontiers in neural circuits, 13, 9. doi: 10.3389/fncir.2019.00009.

11.2 Peer reviewed conference contributions

Habtegiorgis, S.W., Rifai, K., & Wahl, S. (2016). Prolonged exposure to image skews of dynamic natural scenes facilitates future adaptation performance. Journal of Vision, 16(12), 880-880. Vision Science Society. Florida(USA).

Habtegiorgis, S.W., Rifai, K., & Wahl, S. (2017). Adaptation to distortions of natural scenes is retained across saccades. Journal of Vision, 17(10), 884-884. Vision Science Society. Florida(USA).

Habtegiorgis, S.W., Jarvers, C., Rifai, K., Neumann H., & Wahl, S. (2017). Evaluation of a distortion induced motion aftereffect psychophysics and modelling. European Conference on Visual Perception. Berlin (Germany).

Habtegiorgis, S.W., Rifai, K., & Wahl, S. (2018). Interaction between form and motion processing partakes in habituation to distortions of the natural visual world. Vision Science Society. Florida(USA).

11.3 Peer reviewed talks

Habtegiorgis, S.W., Rifai, K., & Wahl, S. (2015). Monocular adaptation to spatially varying distortions. Talk given at Young Researcher Vision Camp. Leibertingen (Germany).

Wahl, S., **Habtegiorgis, S.W.**, Jarvers, C., Rifai, K., & Neumann H. (2018). Model investigation on contribution of feedback in distortion induced motion adaptation. Computational and Mathematical models in Vision Workshop. Florida(USA).

12 Statement of own contribution

12.1 Publication 1 - Adaptation to skew distortions of natural scenes and retinal specificity of its aftereffects

Habtegiorgis, S. W., Rifai, K., Lappe, M., & Wahl, S. (2017). Adaptation to skew distortions of natural scenes and retinal specificity of its aftereffects. Frontiers in psychology, 8, 1158. doi: 10.3389/fpsyg.2017.01158.

Contribution of the first author:
In this academic work, I contributed in the conception of the principal research question. I developed the investigation approaches, recruited participants and performed the experiments. I collected, analysed and interpreted the experimental data. I wrote the manuscript and improved it based on ideas from the co-authors.

Contribution of the co-authors:
The second author, Dr. Katharina Rifai, supported with idea on the development of the investigation methodology, contributed in data interpretation and reviewed the manuscript. The third author, Prof. Markus Lappe, contributed in data interpretation and reviewed the manuscript. The fourth author, Prof. Siegfried Wahl, coordinated and supervised the research, supported with ideas for the improvement of the manuscript and provided the research material.

12.2 Publication 2 - Transsaccadic transfer of distortion adaptation in a natural environment

Habtegiorgis, S. W., Rifai, K., & Wahl, S. (2018). Transsaccadic transfer of distortion adaptation in a natural environment. Journal of vision, 18(1), 13-13. doi: 10.1167/18.1.13.

Contribution of the first author:
In this academic work, I contributed in the conception of the principal research question. I developed the investigation approaches, recruited participants and performed the experiment. I collected, analysed and interpreted the experimental data. I wrote the manuscript and improved it based on ideas from the co-authors.

Contribution of the co-authors:
The second author, Dr. Katharina Rifai, contributed ideas for data interpretation and reviewed the manuscript. The third author, Prof. Siegfried Wahl, coordinated and supervised the research, supported with ideas for the improvement of the manuscript and provided the research material.

12.3 Publication 3 - Experience dependent long-term facilitation of skew adaptation. Journal of vision

Habtegiorgis, S. W., Rifai, K., Lappe M., & Wahl, S. (2018). Experience dependent long-term facilitation of skew adaptation. Journal of vision,18(9):7, 1–11. doi: 10.1167/18.9.7.

Contribution of the first author:
In this academic work, I contributed in the conception of the principal research question. I developed the investigation approaches, recruited participants and performed the experiment. I collected (with a HIWI student), analysed and interpreted the experimental data. I wrote the manuscript and improved it based on ideas from the co-authors.

Contribution of the co-authors:
The second author, Dr. Katharina Rifai, supported with idea for the development of the investigation methodology and data interpretation, and reviewed the manuscript. The third author, Prof. Markus Lappe, contributed in data interpretation and reviewed the manuscript. The fourth author, Prof. Siegfried Wahl, coordinated and supervised the research, supported with ideas for the improvement of the manuscript and provided the research material.

12.4 Publication 4 - The role of bottom-up and top-down cortical interactions in adaptation to natural scene statistics

Habtegiorgis, S. W., Jarvers, C., Rifai, K., Neumann H., & Wahl, S. (2019). The role of bottom-up and top-down cortical interactions in adaptation to natural scene statistics. Frontiers in neural circuits, 13, 9. doi: 10.3389/fncir.2019.00009.

Contribution of the first author:
In this academic work, I contributed in the conception of the principal research question. I developed the investigation approaches, recruited participants and performed the experiment. I collected, analysed and interpreted the experimental data. I developed the neural model, wrote the manuscript and improved it based on ideas from the co-authors.

Contribution of the co-authors:
The second author, Christian Jarvers, and the fourth author, Prof, Heiko Neumann, supported with idea for data interpretation and model development. The third author, Dr. Katharina Rifai, supported with idea for designing investigation methodology, data analysis and interpretation. The fifth author, Prof. Siegfried Wahl, coordinated and supervised the research, supported with idea for data interpretation and provided the research material. All co-authors reviewed the manuscript.

Acknowledgements

I would like to express my sincere gratitude for Prof. Siegfried Wahl for giving me the opportunity to work on my thesis in Zeiss Vision Science Lab and for his dedicated guidance and supervision which helped me to successfully achieve this work and to acquire key experiences in academics as well as industry.

I am also indebted for Dr. Katharina Rifai for her priceless immediate mentorship, for imparting her experiences on the subject matters, for her unwavering encouragement and guidance, and for her significant constructive criticisms which immensely contributed to the success of this research as well as for laying an important foundation for my career.

I would like to thank Prof. Felix Wichmann for allowing me to pursue my doctoral study under his supervision, for the insightful discussions and for introducing me to the bulk of the academic basis for much of the work.

I am also beholden for our collaboration partners, Prof. Markus Lappe, Prof. Heiko Neumann and Christian Jarvers, for the fruitful discussions and feedbacks.

My gratitude also extends for my colleagues and friends at the Zeiss Vision Science Lab for creating a conductive and a pleasant working environment, for the helpful discussions and for sharing their experiences which gave me different perspectives and endlessly enriched my professional and personal life.

I am also sincerely thankful for my life partner and my best friend Fisseha, for your enduring support and encouragement, for our inspirational discussions and for walking besides me during the most important moments. With out you, this would not be possible. You are 'the butter to my bread and the breath to my life'.

Finally, I want to thank my beloved family for believing in me, for showing me nothing is impossible, and for giving me your ears and helpful hands which helped me to successfully pass through the difficult parts.